

Washington University in St. Louis  
**Washington University Open Scholarship**

---

All Theses and Dissertations (ETDs)

---

January 2009

# Getting to the Point: Bridging the Gap between Simple and Complex Catalytic Systems using Temporal Analysis of Products (TAP)

Xiaolin Zheng

*Washington University in St. Louis*

Follow this and additional works at: <https://openscholarship.wustl.edu/etd>

---

## Recommended Citation

Zheng, Xiaolin, "Getting to the Point: Bridging the Gap between Simple and Complex Catalytic Systems using Temporal Analysis of Products (TAP)" (2009). *All Theses and Dissertations (ETDs)*. 402.  
<https://openscholarship.wustl.edu/etd/402>

This Dissertation is brought to you for free and open access by Washington University Open Scholarship. It has been accepted for inclusion in All Theses and Dissertations (ETDs) by an authorized administrator of Washington University Open Scholarship. For more information, please contact [digital@wumail.wustl.edu](mailto:digital@wumail.wustl.edu).

WASHINGTON UNIVERSITY IN ST. LOUIS  
School of Engineering and Applied Science  
Department of Energy, Environmental, and Chemical Engineering

Dissertation Examination Committee:

John T. Gleaves, Chair  
Muthanna Al-Dahhan  
Milorad Dudukovic  
Renato Feres  
Cynthia Lo  
Palghat Ramachandran  
Gregory S. Yablonsky

GETTING TO THE POINT: BRIDGING THE GAP BETWEEN SIMPLE AND  
COMPLEX CATALYTIC SYSTEMS USING TEMPORAL ANALYSIS OF  
PRODUCTS (TAP)

by

Xiaolin Zheng

A dissertation presented to the  
Graduate School of Arts and Sciences  
of Washington University in partial fulfillment of the  
requirements for the degree of

DOCTOR OF PHILOSOPHY

August 2009  
Saint Louis, Missouri

copyright by

Xiaolin Zheng

2009

## ABSTRACT OF THE DISSERTATION

Getting to the Point: Bridging the Gap between Simple and Complex Catalytic Systems  
using Temporal Analysis of Products (TAP)

by

Xiaolin Zheng

Doctor of Philosophy in Energy, Environmental, and Chemical Engineering

Washington University in St. Louis, 2009

Research Advisors: Professors John T. Gleaves and Gregory S. Yablonsky

One of the key issues in the field of catalysis is to relate the catalyst structure/composition to its activity/selectivity. One way to understand this relationship is to understand the individual role each catalyst component plays in the chemical reaction. Industrial catalysts can be extremely complex in structure and to understand their reaction kinetics, researchers often study simpler surfaces such as single crystals using surface science techniques. This introduces a well-known problem in the field of catalysis commonly referred to as the “pressure and materials gap.” Typically, industrial catalyst research is performed under process conditions, which means operating pressures of one atmosphere or higher. Under these conditions, it is difficult to extract intrinsic kinetic properties of the catalyst which are properties that are directly related to the

catalyst structure and composition. To find these intrinsic kinetic properties, scientists turn to surface science techniques using different types of spectroscopic tools to study reaction properties on single crystal surfaces under ultra-high vacuum (UHV) conditions. Experiments using single crystals and surface science techniques have helped establish that some crystal planes are more active and/or selective than others. Although surface science approaches are successful in obtaining fundamental information on a variety of catalytic reactions on the atomic level, current catalytic reactions are still carried out under atmospheric pressures or greater and on much more complex materials than single crystal surfaces.

This dissertation introduces a new approach to characterize catalysts that vary in compositional/structural complexity in order to understand their performance in a conventional reactor/reaction environment under both atmospheric pressure and ultra-high vacuum conditions. Experiments performed under both pressure regimes were carried out using the same apparatus, the Temporal Analysis of Products (TAP) reactor. The catalysts under investigation are bulk transition metals (Pt), transition metals deposited on metal oxide supports (Pt/SiO<sub>2</sub>), and mixed metal oxides (VPO). The catalysts are applied to two types of reaction systems, CO oxidation and selective oxidation of hydrocarbons. The goal of the experiments is to understand and distinguish the role of each component of the catalyst during chemical reaction. Using the TAP reactor, the number of active sites, reaction mechanisms, adsorption/desorption rate constants, and rates of reaction can be determined.

# Acknowledgments

I would like to thank my advisor, Professor John T. Gleaves, for his guidance and inspiring me to get excited about science, his patience as I mature both as a researcher and a person, and his support in helping me finish my degree. It has been a pleasure to work for you and I have learned so much.

I would like to thank my co-advisor, Professor Gregory S. Yablonsky, for his great help in developing my theoretical skills, his patience, and encouragement. I am truly blessed to be under the guidance of the “King of Chemical Kinetics.”

I thank Dr. Rebecca Fushimi for her help in modifying the TAP system and the data analysis software in order for me to finish my experiments.

I thank Professor Renato Feres for his help in the development of the theoretical models for the single particle experiments.

A special thanks to my parents, Guoqiang Zheng and Yumin Liu, who have sacrificed so much to give me the opportunities that I have today. I could not have done this without your constant love and support.

I thank Daniel Duplantier for always believing in me.

Finally, I thank the National Science Foundation GOALI Grant CTS-0432593 for making my research possible.

Xiaolin Zheng

*Washington University in St. Louis  
August 2009*

Dedicated to my parents.

# Contents

|   |      |
|---|------|
| <b>Abstract</b> .....                                   | ii   |
| <b>Acknowledgments</b> .....                            | iv   |
| <b>List of Figures</b> .....                            | viii |
| <b>Nomenclature</b> .....                               | xii  |
| <b>1 Introduction and Motivation</b> .....              | 1    |
| 1.1 Heterogeneous Catalysis.....                        | 1    |
| 1.2 The Study of Catalytic Systems.....                 | 6    |
| 1.2.1 Steady-State Experiments.....                     | 6    |
| 1.2.2 Non-Steady-State/Transient Experiments.....       | 8    |
| 1.2.3 Surface Science Experiments.....                  | 12   |
| 1.2.4 Pressure and Materials Gap.....                   | 15   |
| 1.2.5 Interrogative Kinetics.....                       | 16   |
| 1.3 Applications of Simple to Complex Catalysts.....    | 18   |
| 1.3.1 CO Oxidation on Platinum (Pt).....                | 18   |
| 1.3.2 Selective Oxidation of Hydrocarbons over VPO..... | 22   |
| <b>2 Objectives</b> .....                               | 30   |
| 2.1 Catalyst Structure/Activity Relationship.....       | 30   |
| 2.2 Bridging the “Pressure-Materials Gap”.....          | 32   |
| 2.3 Microreactor Characterization.....                  | 33   |
| <b>3 Experimental Description</b> .....                 | 36   |
| 3.1 The TAP Reactor.....                                | 36   |
| 3.1.1 Apparatus Description and Operation.....          | 37   |
| 3.1.2 The TAP Experiment.....                           | 42   |
| 3.1.3 Theory of TAP Microreactor Configurations.....    | 47   |
| 3.2 Catalyst Preparation and Surface Analysis.....      | 63   |
| 3.2.1 Pt Bulk Metal Particle.....                       | 63   |
| 3.2.2 Pt Foil.....                                      | 65   |
| 3.2.3 Supported Pt Catalysts.....                       | 66   |
| 3.2.4 VPO Catalysts.....                                | 71   |
| <b>4 CO Oxidation on Pt Catalysts</b> .....             | 73   |
| 4.1 Single Pt Bulk Particle TAP Experiments.....        | 73   |
| 4.1.1 Oxygen Uptake.....                                | 73   |
| 4.1.2 Reaction under Vacuum Conditions.....             | 75   |
| 4.1.3 Reaction at Atmospheric Pressures.....            | 80   |



|                   |   |            |
|-------------------|---|------------|
| 4.1.4             | Comparison of Results from Vacuum and Atmospheric Pressure Regimes .....    | 81         |
| 4.1.5             | Inert Experiments.....  | 84         |
| 4.1.6             | Surface Lifetimes of Reactive Species .....                                 | 85         |
| 4.2               | Probabilistic Single Particle Theoretical Model .....                       | 96         |
| 4.2.1             | Conversion Dependence on Catalyst Position .....                            | 98         |
| 4.2.2             | Comparison of Experimental Results to Probabilistic Theory .....            | 100        |
| 4.3               | Reaction on Pt Supported Catalysts .....                                    | 105        |
| 4.3.1             | TAP Vacuum Pulse Response Results.....                                      | 105        |
| 4.3.2             | Comparison with Pt Bulk Metal Particle .....                                | 108        |
| <b>5</b>          | <b>Selective Oxidation of Furan over VPO Catalysts.....</b>                 | <b>110</b> |
| 5.1               | Temperature Dependence of Product Yield and Reactant Conversion .....       | 111        |
| 5.2               | Characterization of VPO Catalyst State from Apparent Kinetic Constants..... | 119        |
| 5.3               | Deducing Mechanistic Detail from Real TAP Data .....                        | 124        |
| 5.4               | Observation of VPO Structure Sensitivity.....                               | 134        |
| <b>6</b>          | <b>Conclusions.....</b>   | <b>139</b> |
| <b>7</b>          | <b>Recommendations for Future Work.....</b>                                 | <b>144</b> |
| <b>Appendix A</b> | <b>Calibration of Pulse Valves.....</b>                                     | <b>150</b> |
| <b>References</b> | <b>.....</b>  | <b>155</b> |
| <b>Vita</b>       | <b>.....</b>  | <b>164</b> |

# List of Figures

|   |    |
|---|----|
| Figure 1.1: Catalytic cycle.....  | 3  |
| Figure 1.2: Schematic of catalyst development cycle (CDC) .....   | 4  |
| Figure 1.3: Reaction pathways for re-oxidation of VPO catalyst.....   | 29 |
| Figure 3.1: (A) Schematic of TAP-2 reactor system (B) The inlet pulse in a TAP pulse response experiment is represented by a delta function. (C) As the pulse travels through the microreactor, it broadens. The example curve compares an experimentally measured argon exit flow curve to the standard diffusion curve.....                 | 38 |
| Figure 3.2: TAP-3 Reactor System.....   | 39 |
| Figure 3.3: Typical TAP pulse response curve with inset showing the noise magnitude in the tail of the response. Signal to noise ratio is > 30,000 to 1 .....   | 41 |
| Figure 3.4: Conceptual comparison of key components of (A) molecular beam scattering experiment and (B) TAP experiment.....   | 43 |
| Figure 3.5: Scale drawing of a TAP “reaction zone” and packed bed microreactor containing a loading of nonporous spherical particles $\approx 250 \mu\text{m}$ in diameter .....  | 46 |
| Figure 3.6: (A) Standard diffusion curve showing key time characteristics and the criterion for Knudsen diffusion. (B) Comparison of standard diffusion curve with experimental inert gas curve over inert packed bed [23].....   | 53 |
| Figure 3.7: Comparison of diffusion + irreversible adsorption/reaction exit flow curves with the standard diffusion curve. (A) Standard diffusion exit flow curve, $\bar{k}_a = 0$ (B) Diffusion + irreversible adsorption/reaction curve, $\bar{k}_a = 3$ (C) Diffusion + irreversible adsorption/reaction curve, $\bar{k}_a = 10$ [23]..... | 55 |
| Figure 3.8: Comparison of standard diffusion and diffusion + reversible adsorption exit flow curves. (A) Standard diffusion exit flow curve, $\bar{k}_a = 0$ (B) Diffusion + reversible adsorption curve, $\bar{k}_a = 20, \bar{k}_d = 20$ (C) Diffusion + reversible adsorption curve, $\bar{k}_a = 20, \bar{k}_d = 5$ [23] .....            | 58 |
| Figure 3.9: Moment analysis in TAP experiments is the time weighted areas under the exit flow curves.....   | 61 |
| Figure 3.10: Comparison of non-uniformity versus conversion for the different PFR and TZTR. Different ratios of microreactor length to length of catalyst zone are given for the TZTR.....  | 63 |
| Figure 3.11: (A) Schematic of TAP microreactor single particle configuration. (B) Digital camera image comparing the Pt particle to a pencil point to demonstrate the actual size of the catalyst particle. (C) SEM   |    |

|   |    |
|---|----|
| image showing the entire polycrystalline Pt particle. The diameter of the particle is estimated to be 350 $\mu\text{m}$ . (D) High magnification (15,000X) SEM image of Pt particle surface, which shows the surface is nonporous .....   | 65 |
| Figure 3.12: (a)-(b) SEM images of mesoporous silica SBA-15 and unimodal porous silica (UPS), respectively. (c)-(d) TEM images of SBA-15 and UPS, respectively .....  | 68 |
| Figure 3.13: (a)-(b) SEM images of mesoporous silica SBA-15 after compression to form 400 $\mu\text{m}$ sized particles and impregnation with Pt at magnification of 20,000X and 80,000X, respectively. (c)-(d) SEM images of UPS after compression to form 400 $\mu\text{m}$ sized particles and impregnation with Pt at magnification of 10,000X and 80,000X, respectively .....  | 70 |
| Figure 3.14: SEM image of VPO particle. The image shows a characteristic layered structure.....   | 72 |
| Figure 4.1: Oxygen exit flow response curves obtained from single Pt particle oxygen uptake experiments at 50 $^{\circ}\text{C}$ .....  | 74 |
| Figure 4.2: Oxygen conversion per pulse found by taking the area under each of the exit flow pulse curves from Figure 4.1 .....   | 75 |
| Figure 4.3: Schematic of TAP single Pt particle pump-probe experiment .....   | 76 |
| Figure 4.4: Comparison of $\text{CO}_2$ produced during TAP vacuum pump-probe and atmospheric flow experiments for CO oxidation over single Pt particle with the same composition of reactants. (A) A typical set of pump-probe $\text{CO}_2$ responses ( $m/e = 44$ ) for reaction at 140, 170, and 350 $^{\circ}\text{C}$ . (B) $\text{CO}_2$ production observed from atmospheric flow experiment. (C) $\text{CO}_2$ production observed from vacuum pump-probe experiment. The black line (- $\blacktriangle$ -) represents the total $\text{CO}_2$ yield. The red (- $\bullet$ -) and blue lines (- $\blacklozenge$ -) represent the $\text{CO}_2$ yield on the oxygen pulse and CO pulse, respectively..... | 78 |
| Figure 4.5: $\text{CO}_2$ production observed in the inert microreactor with quartz packing only .....  | 85 |
| Figure 4.6: Pump-probe data showing $\text{CO}_2$ production as a function of temperature and pump-probe interval.....  | 87 |
| Figure 4.7: Normalized $\text{CO}_2$ production on the CO pulse calculated from the zeroth moment of the pulse response curve. $\text{CO}_2$ production is constant at 150 $^{\circ}\text{C}$ , and drops to $\approx 0.5$ times its value in 9 s at 350 $^{\circ}\text{C}$ ....  | 88 |
| Figure 4.8: Normalized $\text{CO}_2$ production on the $\text{O}_2$ pulse .....   | 91 |
| Figure 4.9: Total $\text{CO}_2$ yield/CO conversion from both $\text{O}_2$ and CO pulses added together .....   | 92 |
| Figure 4.10: Apparent constant calculated based on the data obtained from the CO pulse (Figure 4.7) as a function of time delay .....   | 93 |
| Figure 4.11: Apparent constant as a function of reaction temperature for different time delays .....  | 94 |
| Figure 4.12: Calculation of apparent constant “B” from the slopes of the linear relationship between $\ln(K)$ and time delay .....  | 95 |

|   |     |
|---|-----|
| Figure 4.13: Model of microreactor with catalyst (black dot) and inert quartz particles (light colored dots). The right open side of the figure indicates the microreactor outlet ..... | 97  |
| Figure 4.14: A typical molecular trajectory in the microreactor based on Brownian motion .....  | 98  |
| Figure 4.15: A square catalyst sample of side length 0.1 in R with active center at (x,y). The position $x_0$ denote the position for reactant gas injection into the space R .....     | 99  |
| Figure 4.16: Conversion dependence found as a function of the active catalyst center position (x,y) .....   | 100 |
| Figure 4.17: Comparison of experimental and theoretical values for CO <sub>2</sub> yield /CO conversion as a function of Pt foil position in microreactor .....                         | 102 |
| Figure 4.18: CO <sub>2</sub> yield/CO conversion when $x = 0.5$ (middle point along axis) and variable y .....  | 102 |
| Figure 4.19: CO <sub>2</sub> yield/CO conversion found for Pt nanoparticles deposited on SBA-15 SiO <sub>2</sub> support.....   | 106 |
| Figure 4.20: CO <sub>2</sub> yield/CO conversion found for Pt nanoparticles deposited on unimodal porous silica (UPS) support .....   | 106 |
| Figure 5.1: Molecular structures of furan and maleic anhydride.....   | 110 |
| Figure 5.2: Furan conversion as a function of pulse number for four different reactor temperatures.....   | 112 |
| Figure 5.3: MA yield as a function of pulse number for four different reactor temperatures.....   | 113 |
| Figure 5.4: CO <sub>2</sub> yield as a function of pulse number for four different reactor temperatures.....  | 113 |
| Figure 5.5: CO yield as a function of pulse number for four different reactor temperatures.....   | 114 |
| Figure 5.6: Selectivity of MA as a function of pulse number for four different reactor temperatures.....  | 114 |
| Figure 5.7: Selectivity of CO <sub>2</sub> as a function of pulse number for four different reactor temperatures.....   | 115 |
| Figure 5.8: Selectivity of CO as a function of pulse number for four different reactor temperatures.....  | 115 |
| Figure 5.9: MA yield obtained with VPO catalyst oxidized in an atmospheric flow of O <sub>2</sub> /Ar at 480 °C .....   | 119 |
| Figure 5.10: Apparent kinetic constant for furan versus catalyst oxidation degree...122   | 122 |
| Figure 5.11: Apparent kinetic constant for maleic anhydride versus catalyst oxidation degree.....   | 123 |
| Figure 5.12: Apparent kinetic constant for CO <sub>2</sub> versus catalyst oxidation degree ....  | 123 |
| Figure 5.13: Apparent kinetic constant for CO versus catalyst oxidation degree .....  | 124 |
| Figure 5.14: TAP pulse response 3-dimensional exit flow curves for the reactant furan obtained over thin bed of VPO catalysts at 400 °C .....   | 125 |
| Figure 5.15: TAP pulse response 3-dimensional exit flow curves for MA obtained over thin bed of VPO catalysts at 400 °C .....   | 126 |

|  |     |
|--|-----|
| Figure 5.16: TAP pulse response 3-dimensional exit flow curves for CO <sub>2</sub> obtained over thin bed of VPO catalysts at 400 °C .....   | 126 |
| Figure 5.17: TAP pulse response 3-dimension exit flow curves for CO obtained over thin bed of VPO catalysts at 400 °C.....   | 127 |
| Figure 5.18: Individual pulse response curves for furan plotted from the 3-D graph in Figure 5.14 obtained over thin bed of VPO catalysts at 400 °C. The inset shows the height normalized pulse curves for pulse 8 and 30.....  | 127 |
| Figure 5.19: Individual pulse response curves for MA plotted from the 3-D graph in Figure 5.15 obtained over thin bed of VPO catalysts at 400 °C. The inset shows the height normalized pulse curves for pulse 8 and 15.....   | 128 |
| Figure 5.20: Individual pulse response curves for CO <sub>2</sub> plotted from the 3-D graph in Figure 5.16 obtained over thin bed of VPO catalysts at 400 °C. The inset shows the height normalized pulse curves for pulse 1 and 15.....  | 129 |
| Figure 5.21: Individual pulse response curves for CO plotted from the 3-D graph in Figure 5.17 obtained over thin bed of VPO catalysts at 400 °C. The inset shows the height normalized pulse curves for pulse 1 and 15.....   | 130 |
| Figure 5.22: Graph of argon zeroth moment (M <sub>0</sub> ) plotted against the corresponding pulse number at 400 °C. This shows that the pulse valve is very consistent and each pulse contains approximately the same number of gas molecules sent into the microreactor ..... | 131 |
| Figure 5.23: 3-D plot of MA production obtained with smaller furan pulses at 400 °C. Each MA pulse response curve was collected during every other furan pulse sent into the TAP microreactor .....  | 137 |
| Figure 5.24: MA normalized zeroth moment found from the areas under the MA pulse response curves shown in Figure 5.23.....   | 138 |
| Figure A.1: Schematic of assembly used to calibrate pulse valves .....   | 151 |
| Figure A.2: Argon pulse response curves showing the pressure dependence on pulse valve operation .....   | 153 |
| Figure A.3: Argon pulse response curves at low pulse intensities in the Knudsen diffusion regime.....  | 154 |
| Figure A.4: Comparison of experimentally obtained argon pulse response curve and the standard diffusion curve.....   | 154 |

# Nomenclature

|                     |   |
|---------------------|---|
| $a_s$               | surface concentration of active sites (mol/cm <sup>2</sup> of catalyst)               |
| $A$                 | cross sectional area of the microreactor (cm <sup>2</sup> )                           |
| $\alpha$            | ratio of total number of active centers and number of molecules of gas A in the pulse |
| $C_A$               | concentration of gas A (mol/cm <sup>3</sup> )   |
| $\bar{C}_A$         | dimensionless concentration of gas A  |
| $D_e$               | effective Knudsen diffusivity (cm <sup>2</sup> /s)                                    |
| $D_{eA}$            | effective Knudsen diffusivity of gas A (cm <sup>2</sup> /s)                           |
| $\delta_z$          | delta function with respect to axial coordinate $z$                                   |
| $\delta_\zeta$      | delta function with respect to dimensionless axial coordinate $\zeta$                 |
| $\varepsilon_b$     | fractional voidage of the packed bed inside microreactor                              |
| $F_A$               | flow of gas A at microreactor outlet (mol/s)  |
| $\bar{F}_A$         | dimensionless flow of gas A at microreactor outlet                                    |
| $H_p$               | peak height of the normalized gas exit flow   |
| $k_a$               | adsorption rate constant (cm <sup>3</sup> /mol s)                                     |
| $k'_a$              | adsorption rate constant (s <sup>-1</sup> )   |
| $\bar{k}_a$         | dimensionless adsorption rate constant  |
| $k_{ads}$           | apparent adsorption constant (s <sup>-1</sup> )                                       |
| $k_d$               | desorption rate constant (s <sup>-1</sup> )   |
| $\bar{k}_d$         | dimensionless desorption rate constant  |
| $K_a$               | dimensionless modified kinetic constant of adsorption                                 |
| $L$                 | length of the microreactor (cm)   |
| $L_{II}$            | length of diffusion zone II (cm)  |
| $\Delta L$          | thickness of the catalytic zone (cm)  |
| $M$                 | molecular mass  |
| $N_{pA}$            | number of moles or molecules of gas A in the input pulse                              |
| $R$                 | universal gas constant  |
| $S_v$               | surface area of catalyst per volume of catalyst (cm <sup>-1</sup> )                   |
| $t$                 | time (s)  |
| $t_p$               | time at which the gas exit flow is at a maximum                                       |
| $\tau$              | dimensionless time  |
| $\tau_p$            | dimensionless time at which gas exit flow is at a maximum                             |
| $\tau_{res}^{conv}$ | residence time for convective flow in CSTR (s)  |

|                        |   |
|------------------------|---|
| $\tau_{res,cat}^{dif}$ | residence time for diffusion through the catalytic zone in thin-zone TAP microreactor (s) |
| $T$                    | temperature   |
| $\theta_A$             | fractional surface coverage   |
| $\bar{\theta}_A$       | pulse normalized surface concentration  |
| $V_{void}$             | void volume inside microreactor (cm <sup>3</sup> )  |
| $X$                    | conversion  |
| $z$                    | axial coordinate (cm)   |
| $\zeta$                | dimensionless axial coordinate  |

# Chapter 1

## Introduction and Motivation

### 1.1 Heterogeneous Catalysis

Catalysis is the key to chemical transformations. Wilhelm Ostwald first introduced the definition for catalysts in 1895, which stated “catalysts are substances which change the velocity of a reaction without modification of the energy factors of the reaction [1].” Catalysts control the rates at which chemical bonds are formed and broken, and make possible the efficient transformation of raw materials into desired products with minimal input of energy. In addition to accelerating the rate of reactions, catalysts can also influence the selectivity of chemical reactions. Selectivity is the measure of the percentage of reactants converted to useful products. Often times in industry, selectivity is favored more over the catalytic activity.

Catalysts are extremely valuable to the production industry by enabling reaction chemistries for a variety of processes and products including chemicals, petroleum products, pharmaceuticals, rubber and plastics, and environmental protection through the prevention of harmful emissions in automobiles, among many others. Also, enzymes,



nature's catalysts, are responsible for essentially all biological reactions. Catalysts have been successfully used in the chemical industry for more than 100 years, and approximately 90 percent of all chemicals produced in newly developed processes require the aid of catalysts [2]. One of the important things to realize is that everyone is directly or indirectly involved in some aspect of catalysis in their everyday life.

The field of catalysis is generally separated into two categories, homogeneous and heterogeneous (solid-state) catalysis. Heterogeneous catalysis is more widely practiced and dominates 90 percent of industrial chemical processes. Therefore, it will be the focus of this dissertation. Heterogeneously catalyzed reactions are composed of purely chemical and purely physical reaction steps. In order for the catalytic process to take place, the reactants must be transported to the active centers on the catalyst surface by diffusion. Adsorption of the reactants occurs on the catalyst surface via chemical adsorption (chemisorption) or physical adsorption (physisorption). The chemical reaction occurs on the catalyst surface at an active site when reactants interact to form a product. Desorption of the product from the catalyst surface then takes place, and the products through diffusion are transported away from the catalyst surface and into the gas phase. The steps described in the catalytic reaction process are illustrated in Figure 1.1.

Catalysis is a cyclic process in which reactants are bound to one state of the catalyst, and the products are released from another state, regenerating the initial catalytic state. The cycle then repeats again as more reactants are introduced. It was previously assumed that

the catalyst remained unchanged during the course of the reaction; however, it is now known that the catalyst is involved in chemical bonding with the reactants during the catalytic process. Owing to competing reactions on the catalyst surface, the catalyst can undergo chemical changes and over time its activity decreases resulting in catalyst deactivation. Because of this, catalysts have to be regenerated or eventually be replaced.

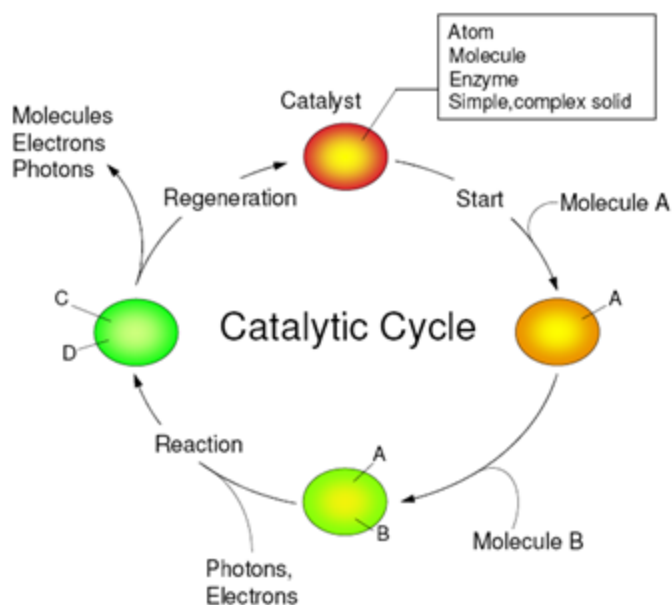


**Figure 1.1** Catalytic cycle.

Although the field of catalysis has been established many decades ago, the catalyst development process is not an easy process. Catalyst development for realistic, industrial processes still relies mainly on empirical and trial and error methods with many years of research before a catalyst can be commercialized. Figure 1.2 shows a simple schematic of the Catalyst Development Cycle (CDC) that can be expected in catalyst research. In the first step of the CDC, candidate materials are selected to be tested as catalysts. In

step two, the materials are synthesized. In steps three and four, the materials are tested for catalyst activity and selectivity, and characterized structurally. The CDC includes a decision path which can be reached through steps three and four. This path represents a key cycle in the CDC, and provides crucial performance information used to determine if the cycle can be exited. The output of one CDC cycle may result in postulating new starting materials to serve as the catalyst, the addition or alteration of one or more components to the already existing catalyst, a new catalyst preparation method, or in very few cases, a finalized catalyst will emerge. Generally, a large number of iterations, often involving the preparation and modification of thousands or tens-of-thousands of catalyst samples, precede the finalization of a new catalyst formulation.

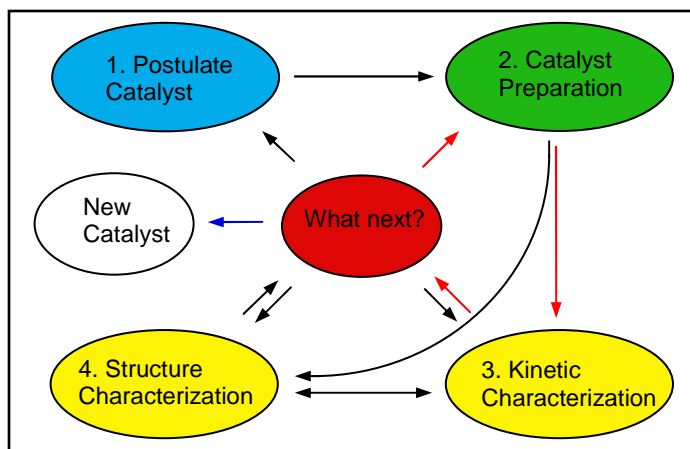


**Figure 1.2** Schematic of catalyst development cycle (CDC).

Since most catalysts involve multi-component compositions, the number of possible combinations and structures can be staggering, and years of iteration still may not produce a commercially viable catalyst. Two general strategies have been proposed in an

effort to accelerate the rate of catalyst invention when fundamental guidance or previous data is either absent or has failed to produce a viable catalyst candidate. The first strategy is focused on decreasing the CDC cycle time by decreasing the time it takes to synthesize and evaluate the performance of new catalyst samples. The second strategy is focused on making the CDC more efficient by increasing the quantity and quality of information obtained in each cycle. The catalyst development and characterization approach proposed in this dissertation will be a combination of the above two strategies by decreasing the time to evaluate the performance of the catalyst samples and increasing the quantity and quality of the information obtained from the kinetic characterization. The ultimate goal in heterogeneous catalysis is to understand and relate how the composition of the catalyst affects its kinetic performance. The following section will detail types of experiments used in industry and academia to study heterogeneous catalytic systems. In order to make the catalyst development process more efficient, it is necessary to combine through an integrated multi-scale approach the development of novel reactors, characterization of molecular level kinetics, characterization of particle and reactor kinetic/transport processes, and bridging the gap between the molecular level and process reactor scales.

## **1.2 The Study of Catalytic Systems**

### **1.2.1 Steady-State Experiments**

Steady-state experiments are typically used to study practical catalysts at reaction or process conditions in conventional industrial type reactors such as the continuously stirred tank reactor (CSTR) or the plug flow reactor (PFR). Temkin originally proposed the idea of the CSTR in 1950 for the purposes of extracting kinetic information from industrial heterogeneous catalytic reactions with the assumption of no concentration or temperature gradients [3]. The CSTR achieves uniformity and perfect mixing in the catalyst zone by a combination of steady, continuous flow of reactants and products simultaneously, and turbulent flow within the stirred tank. Due to the well-mixed nature of the CSTR, temperature and composition of the reaction mixture are assumed to be uniform in all parts of the vessel and are the same as the exit flow. The transport in and out of the CSTR is assumed to be purely convective flow. Although the CSTR is a simple and relevant technique for steady-state kinetic studies [4], there are several limitations to this method. The first is that a CSTR typically operates at low conversions, especially for highly exothermic reactions. The second limitation is the unreliability of non-steady-state kinetic information provided by CSTR experiments. This unreliability is caused by the non-uniformity of CSTR hydrodynamics in the non-steady-state regime [5]. In fact for such a regime, it is difficult to even estimate non-uniformity in the catalyst zone under working conditions.

Similar to the CSTR, traditional PFR experiments only provide kinetic information related to the rate-determining step(s) of a complex catalytic reaction, and do not provide detailed mechanistic information. Modifications to the CSTR and PFR were made in order to perform non-steady-state experiments on the systems to gain insight into more detailed catalyst kinetic information. Non-steady-state experiments in the CSTR were proposed by Bennett [6] using Eigen's relaxation model [7]. However, to greater success was the modification of the traditional PFR into the "differential PFR," which was introduced more than 40 years ago by Kobayashi and Kobayashi [8]. A PFR experiment can provide a wealth of non-steady-state kinetic information using step-response or wave propagation techniques. In the differential PFR, the catalyst zone is made very thin to minimize any concentration gradients and keep the catalyst zone uniform (conversion is also made small). By doing this, the differential PFR approximates the transport factors (convective flows) in the reactor in a linear fashion, and the reaction rate is calculated as a function of the spatial average reactant concentration in the catalyst zone. Non-uniformity in a differential PFR is mostly a result of reaction. In order to maintain a reasonable uniformity within the catalyst zone, the differential PFR should not be operated at conversions higher than 15-20 percent [9].

An issue with performing CSTR and PFR experiments is that there is no technique that can be used to directly monitor the catalyst surface composition. In situ catalyst characterization using spectroscopic techniques can be used, however, under reaction conditions, the catalyst structure and composition is constantly changing when exposed to

the reactant gas making the process difficult and insufficient. Therefore, in order to directly relate the intrinsic catalyst kinetic properties to its structure and composition, there is a need to utilize non-steady-state kinetic tools to study catalytic systems.

### **1.2.2 Non-Steady-State/Transient Experiments**

In comparison to steady-state experiments, transient experiments have the potential to provide intrinsic reaction kinetics, provide detailed information on the individual mechanistic steps of a reaction, and obtain kinetic information in a much faster way. Also, many real-life catalytic processes are transient in nature where the catalysts experience a cyclic exposure to different conditions. For example, some common cyclic catalytic processes include fluid catalytic cracking [10], selective oxidation of butane to maleic anhydride [11, 12], oxidative propane dehydrogenation [13], lean-rich cycles for NO<sub>x</sub> release-reduction in diesel exhaust [14], and the treatment of exhaust gas in the start-up and shut down of automobile engines [15, 16].

Non-steady-state or transient experiments are characterized by introducing a transient into a reacting system by rapidly changing one or more of the state variables, such as concentration, (partial-) pressure, temperature, or flow rate, and following the temporal response of the system. In transient experiments, three elements need to be considered, a stimulus or transient, a reaction system, and an analysis system to follow the time dependent response. There are typically three types of stimuli, a step function, a pulse, and a time dependent function. The most well known of the three stimuli is the step

function which can be found in batch reactor operation, the pulse injection can be found in chromatography with the injection of a reactant into an inert flow through a reactor, and the time dependent functions comprise of linear or periodical programmed changes such as in cases where the temperature or concentration is varied. Some common analysis techniques to detect the response of the reaction system are mass spectrometry (MS) which is preferred for labeled components and/or rapid changes, gas chromatography (GC) for when different isomers are present, spectroscopy (IR, Raman, UV-vis), or a combination technique such as a differential scanning calorimetry (DSC) with the GC [17, 18].

There are two main types of reactor systems used for transient kinetic studies, the (semi-) batch reactor and the fixed-bed tubular reactor. The (semi-) batch reactor is typically used for liquid-solid and gas-liquid-solid reactions. The catalyst may be suspended in the liquid phase, fixed in a packed bed, or fixed on a structured support [19]. The (semi-) batch reactor is operated at atmospheric to high pressures. The data obtained is usually in terms of the concentration versus time for the different components, at fixed pressure, temperature, and initial concentration. For kinetic studies, multiple experimental runs are needed to explore the concentration, pressure, and temperature space. One of the benefits of (semi-) batch operation is the abundant amount of data points obtained over a wide range of conversions using discrete sampling, GC, and HPLC analysis. Some drawbacks to (semi-) batch operation are the time resolution, which is limited to minutes due to the large reactor volume, and catalyst deactivation tends to go unnoticed. The deactivation



problem can be fixed if multiple experimental runs are performed with the same catalyst sample [18].

Fixed-bed tubular reactors are mostly used for gas-solid reactions, although it has been used in liquid-solid and gas-liquid-solid reactions as well. The time resolution for these reactors is on the order of 0.1 to 1 s for gas phase operation and no better than 10 s for liquid phase operation. The data obtained from fixed-bed reactors depends on whether the reactor is operated under transient or steady-state operation. Although transient techniques imply non-steady-state, it can be applied to steady-state operation of a catalytic reaction system as well. Steady-state operation simply means that the reacting system is not disturbed by the stimulus. An example of a transient technique under steady-state operation is the Steady-State Isotopic Transient Kinetic Analysis (SSITKA) [20, 21]. In this experiment, an isotopically labeled species is introduced into the reacting system via a step change or a pulse injection. The total concentrations of reactants, products, and intermediates do not change, only their isotopic composition changes. Also, the catalyst does not undergo any change in conditions. For transient operation, the data obtained from fixed-bed reactors at a certain fixed space time, temperature, and pressure gives the temporal evolution of the exit composition under varying operating conditions. For steady-state operation as in the case of SSITKA, the data obtained is the temporal evolution of the isotopic composition and the composition at the reactor exit which is the same as the given inlet concentration. With careful data analysis, reaction mechanisms, rate constants of elementary steps, concentration profiles

of surface species along the reactor bed, kinetics, diffusion, and titration of surface species and surface sites can all be obtained in fixed-bed reactor experiments. Also, catalyst deactivation can be directly monitored [18].

One type of fixed-bed tubular reactor that will be the focus of this dissertation is the Temporal Analysis of Products (TAP) reactor system [22, 23]. The TAP experiment is a transient vacuum pulse response experiment capable of providing precise kinetic data for the elementary reaction steps of a complex catalytic mechanism. Under ultra-high vacuum conditions, transport through the reactor bed is dominated by Knudsen diffusion, thus excluding all gas-phase reactions. The TAP system has been used to study a variety of important heterogeneous catalytic reactions and transport in porous catalytic materials [24]. The standard TAP microreactor has been used with a variety of materials (metals, bulk and supported metal oxides, porous materials), and different catalyst geometries (particles, foils, wires, grids, fibers, gauzes, crystals). Fundamental studies using the TAP system have elucidated details of reaction mechanisms of hydrocarbon cracking and reforming reactions [25], the hydrogenation of acrolein using supported silver catalysts [26], oxidation reactions, and environmental catalysis. Using the TAP "pump-probe" experiment and isotopic reactants, important insights have been obtained into the role of adsorbed and lattice species in the oxidative dehydrogenation of propane [27, 28], oxidative coupling of methane [29], production of syngas from methane [30], ammoxidation of propane [31], toluene [32], and *n*-butane [33], and ammonia oxidation [34]. The TAP experiment has also been applied to environmental problems, including

soot oxidation [35], SCR of toxic  $\text{NO}_x$  gas from automobiles [36], testing catalysts for the storage of  $\text{NO}_x$  [37],  $\text{N}_2\text{O}$  abatement [38], VOC oxidation [39], and CO oxidation [40-43]. Detailed reaction kinetic theory has been developed over the years to obtain intrinsic kinetic parameters based on a moment analysis of transient response data. Reactor transport properties have also been studied extensively taking into account how catalyst position, temperature, and diffusion coefficients affect gas molecule transport behavior. TAP theoretical studies have led to practical microreactor configurations, the most recent being the single particle reactor [43] in which concentration and temperature gradients in the catalyst bed are assumed to be negligible. A detailed discussion of the TAP apparatus and experiments will be discussed in Chapter 3.

### **1.2.3 Surface Science Experiments**

There are many advantages to studying heterogeneous catalysis using surface science techniques at ultra-high vacuum (UHV) conditions such as the availability of a variety of modern surface spectroscopies to detect and visibly monitor structural and compositional changes on the single crystal surfaces during the course of reaction and to identify any relevant surface species. Typically, surface science techniques use temperature programmed desorption (TPD) or molecular beam scattering experiments to find catalyst kinetic parameters or relate structure sensitivity to catalyst activity. TPD experiments typically start with a reactant gas or a mixture of gases already adsorbed onto a cold single crystal. The single crystal surface is then heated at a controlled programmed rate. The reactant gases that are adsorbed onto the single crystal surface will start to react as

the surface is heated and a mass spectrometer measures the amount of product that desorb off the surface. In molecular beam scattering experiments, a beam of atoms or molecules is directed at a single crystal surface and the scattered beam is analyzed. The reactant beam is modulated so that the reactant and product beams can be differentiated in time.

One example of a common surface science techniques used for single crystal studies is Auger electron spectroscopy (AES). AES determines the composition of the surface layers of a sample by measuring the energy of electrons emitted from that surface when it is irradiated with electrons of energy in the range 2–50 keV. The electrons emitted from the surface will have energies characteristic of the element from which they were emitted from, and sometimes this information can be used to find the bonding state of those surface atoms [44]. Pt single crystal studies using AES have found that certain Pt single crystal surface orientations exhibit surface structure transformations during the course of reaction (CO oxidation) under isothermal and low pressure conditions. For example, studies have shown that clean Pt(100) and Pt(110) single crystal surfaces exhibit changes in surface atom orientations and this reconstruction of the surface stops only when a critical CO coverage is reached. The switch between surface reconstructions also changes the Pt single crystal activity from a state of low activity to a state of high activity on the non-reconstructed surface. The difference in activity between the reconstructed and non-reconstructed single crystal surface phases is a result of different oxygen sticking coefficients [45]. Similar experiments performed on the Pt(111) single crystal surface show no surface structural changes under the influence of gas interaction [46]. The

reason for this could be that the Pt(111) surface is much more densely packed with atoms on its surface than the Pt(100) or Pt(110) so there is less space on the surface for any atom reconstruction to take place. From these results, it is hypothesized that on polycrystalline and supported catalysts, activity and catalytic behavior during reaction conditions is a result of the synchronization between various parts of the surface. However, whether specific catalytic activity is associated with catalyst surface atoms, bulk structure, surface micro-facets, particle sizes, or support interactions is still difficult to determine.

One criticism of surface science techniques has been that it is not applicable to real catalytic reaction conditions which are typically carried out under atmospheric (or higher) pressures and with far more complex surfaces than single crystals. This is commonly referred to as the so-called “pressure and materials gap.” In past years, attempts to bridge the “pressure and materials gap” has been in progress by combining in a single apparatus the ability to measure kinetics on a single crystal under both UHV and elevated pressures [47]. In these combined UHV/high-pressure studies, a well-defined single crystal plane is used to model a site or set of sites that are existent on a practical high surface area catalyst. The combined methods has allowed for the direct comparison of reaction rates measured on single crystal surfaces to those measured on more practical catalysts as well as detailed catalyst structure sensitivity studies and effects of promoters/inhibitors on catalytic activity [48].

## 1.2.4 Pressure and Materials Gap

Two general experimental approaches using different forms of catalytic materials are used in heterogeneous catalysis research. The "model catalyst" approach employing materials with well-defined surfaces, such as metal single crystals, provides a direct method of linking surface structure to elementary steps in a catalytic process. A well-known example is the measurement of sticking coefficients on different crystal planes of noble metals [49, 50]. The second approach, which can be called the "practical catalyst" approach, is the basis for most industrial catalyst development. Practical catalysts include supported metals, mixed metal oxides, and zeolites. The "practical catalyst" approach involves the systematic synthesis, testing, and characterization of numerous catalyst samples. In general, practical catalysts have complex ill-defined surfaces, and the active surface structure cannot be directly identified. Also, the measurement of catalytic activity under process conditions does not provide a direct link between structure and activity. In addition, the composition of a practical catalyst can change under the influence of the reaction medium resulting in a change in its properties. Consequently, practical catalyst development is hampered by a lack of fundamental information on the composition and structure of the catalytic phase or catalytic site.

Information from model catalyst studies is intended to provide guidance in the development of practical catalytic materials. However, the application of fundamental information has not been straightforward, since there is a significant "gap" between the conditions of "real world" catalytic processes, and those of model reaction studies.

Bonzel [51] was the first to discuss the problem and coined the term "pressure gap" to emphasize the  $10^{12}$  difference in reactant pressures. Practical and model catalyst experiments are also separated by a "materials gap" arising from the differences in structural and compositional complexity of catalyst samples. The materials gap presents a significant problem since the interplay of bulk and surface and the complex interactions of different constituents in practical catalysts are not easily reducible to a set of simple individual interactions. It is questionable whether results obtained at vacuum conditions on a set of well-defined uniform surfaces can be extrapolated to practical materials operating at atmospheric pressures, unless the uniform and practical samples can be directly compared experimentally.

### **1.2.5 Interrogative Kinetics**

Interrogative kinetics [23] is a kinetic approach utilized by the TAP reactor system that attempts to systematically probe a variety of different states of the catalyst surface, and to understand how one state evolves into another state. There are two types of experiments in interrogative kinetics which are performed in sequence to reveal complex reaction mechanisms and structure-activity relationships. The first experiment is the 'state-defining' experiment which provides kinetic information (i.e. rate parameters of adsorption and desorption) that can characterize the catalytic state but does not perturb the state of the catalyst. The second experiment following the 'state-defining' experiment is the 'state-altering' experiment which changes the catalyst composition in a controlled manner. To complete the sequence, another 'state-defining' experiment is

performed to characterize the new state of the catalyst. For example, the surface kinetic properties (conversion, selectivity, activation energy, reaction rate constants, adsorption/desorption behavior, number of active sites, oxidation state) of a selective oxidation catalyst such as vanadyl pyrophosphate (VPO) can be measured using interrogative kinetics by incrementally probing the catalyst surface from an oxidized to a reduced catalytic state.

Interrogative kinetics is based on the application of high-speed transient TAP pulse response experiments in conjunction with traditional kinetic experiments such as steady-state experiments, TPD, and step-transient experiments. The interrogative kinetics approach uses a series of kinetic measurements to probe the kinetic characteristics of a catalyst surface, and then monitors how these kinetic characteristics change as a function of changing reaction conditions such as temperature, pressure, surface coverage, and reactant composition. By performing multiple experiments on a single catalyst sample, the kinetic characteristics can be used to understand the structure of the catalytic sites as well as construct a model of the reaction mechanism. In addition to serving as an experimental methodology, interrogative kinetics also provides a special theoretical analysis of the kinetic information. The theory provides for the fast interpretation of kinetic data, distinguishes between different reaction mechanisms and kinetic cases, and rapid extraction of kinetic parameters using a moment-based analysis technique.



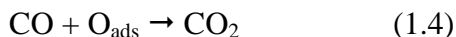
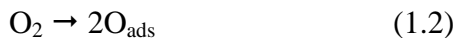
## 1.3 Applications of Simple to Complex Catalysts

Two types of catalytic systems will be explored in detail in this dissertation. The first system consists of a simple catalyst, a single platinum (Pt) particle, subjected to the CO oxidation reaction. The second catalytic system that will be studied is the selective oxidation of hydrocarbons (furan) on a much more complex real industrial catalyst, vanadyl pyrophosphate (VPO) which is a mixed metal oxide. The goal of this project is to create an experimental methodology using the TAP reactor to understand the catalyst development and characterization process in a much simpler manner. Also, the work presented in this dissertation provides for new advances in microreactor design, understanding transport processes in the reactor bed, and bridging the gap between surface science and industrial research.

### 1.3.1 CO Oxidation on Platinum (Pt)

The CO oxidation reaction is a model reaction because it is fairly simple and widely used in both research and industry. The CO oxidation reaction represents one of the key steps in the overall reaction of  $2\text{NO} + 2\text{CO} \rightarrow \text{N}_2 + 2\text{CO}_2$  which is one of the major pathways for the conversion of NO to  $\text{N}_2$  in automobile three-way catalytic converters. Also, the CO oxidation reaction is an ideal reaction to demonstrate the relationship between UHV and high-pressure kinetic studies. Many of the mechanistic steps of the CO oxidation reaction such as reactant adsorption/desorption, surface reaction, and product desorption has been studied in detail using UHV surface science techniques and many of the reaction parameters found can be directly applied to kinetics at high pressures [52].

There is debate as to the exact reaction mechanism for the CO oxidation reaction. In a review by Engel and Ertl [53], the individual reaction steps for the reaction are listed below:



The individual reaction steps are made on the assumption that all oxygen adsorbs irreversibly and dissociatively on the platinum surface, which is valid for all platinum group metals at temperatures above 100 K [54]. Recombination and desorption of adsorbed oxygen atoms only take place at temperatures above 700 K [53]. Equation 1.3 shows reaction of the Langmuir-Hinshelwood mechanism, which involves the adsorption of both CO and atomic oxygen on the catalyst surface. The product, CO<sub>2</sub>, is formed when reactants, CO and oxygen, are in the chemisorbed state. Under both atmospheric pressure and high vacuum conditions, CO predominantly covers the catalyst surface and the reaction rate is determined by the rate at which CO desorbs off the surface. Oxygen adsorption is limited to available sites where CO has desorbed. As reaction temperature increases, the reaction rate increases also allowing for more available sites for oxygen adsorption due to the higher CO desorption rate. Equations 1.4 and 1.5 are of the Eley-Rideal mechanism, which states that CO<sub>2</sub> is formed from gas-phase oxygen or CO striking surface adsorbed CO or oxygen, respectively. In the review by Engel and Ertl

[53], it is assumed that the only relevant reaction model for CO oxidation over platinum under steady-state conditions is the Langmuir-Hinshelwood mechanism. Therefore, only the reaction steps indicated by Equations 1.1-1.3 are relevant. However, in a study by Bonzel and Ku [55], they state that at temperatures greater than 473 K, the CO<sub>2</sub> production rate is not inhibited by a high CO surface coverage, possibly indicating an Eley-Rideal reaction mechanism.

It is generally accepted that the CO oxidation reaction proceeds by the Langmuir-Hinshelwood mechanism [53, 56]. CO<sub>2</sub> formation occurs via the reaction of chemisorbed CO with adsorbed atomic oxygen. When both species are in low concentrations on the Pt surface, the activation energy for the CO oxidation reaction is approximated to be 96.4 kJ/mol (24.1 kcal/mol). For high oxygen concentrations on the Pt surface, the activation energy decreases to 46.8 kJ/mol (11.7 kcal/mol). This data is found for a Pt(111) single crystal surface [57, 58].

There is a vast amount of information in the literature regarding CO oxidation studies on different types of platinum materials such as Pt metal, nanoparticles, supported Pt catalysts, and Pt single crystals under both UHV and high-pressure conditions. Although the CO oxidation reaction is quite simple compared to other heterogeneously catalyzed reactions, there are many aspects of the reaction that are complex such as size dependence of Pt particles on catalytic activity [59], temperature hysteresis [60], island formation [61], kinetic oscillations [62], and the role of subsurface oxygen [63], just to

name a few. For example, in the case of temperature hysteresis, it was found that with two samples of Pt deposited on  $\text{Al}_2\text{O}_3$  with a weight percent of 0.5% and 0.6% Pt, the width of the hysteresis loop depends on the activity of the catalyst. The catalyst with the lower activity, 0.5% Pt on  $\text{Al}_2\text{O}_3$ , exhibited a smaller hysteresis loop width. However, when the catalyst is changed to a Pt foil, no temperature hysteresis was observed. One of the reasons why temperature hysteresis was not observed with the Pt foil is that Pt foil is a bulk metal that exhibits good heat conductivity, favoring intense energy dissipation. As a result, the overheating of active centers on the Pt foil is minimal, and the conversions on the ascending and descending branches of the curve coincide closely as the same average temperature [60]. For Pt supported catalysts, the support may play a role in the reaction causing temperature hysteresis. From surface science studies on single crystals, it was found that kinetic oscillations occur in CO oxidation due to the periodic structural changes of the substrate, which change the oxygen sticking coefficient and cause oscillations in the reaction rate. CO adsorption is rather insensitive to the structure of a Pt surface; however, the oxygen sticking coefficient can vary over several orders of magnitude [62]. Using surface science techniques such as Low Energy Electron Diffraction (LEED) and Fourier Transform Infrared Spectroscopy (FTIR) on single crystal surfaces, it was found that oxygen and CO atoms adsorbed on Pt surfaces form islands. LEED results indicate that oxygen adatoms form islands for degrees of surface coverage greater than 10%, and CO adatoms form islands when it is adsorbed on surfaces containing adsorbed oxygen. FTIR measurements found that large CO islands formed at room temperature and at pressures up to 1 bar.  $\text{CO}_2$  formation will occur at the

boundaries of the CO and oxygen islands as the CO and oxygen come into contact with each other on the Pt surface. The surface mobility of adsorbed oxygen adatoms is much lower than adsorbed CO because of the strong Pt-O bond. Adsorbed CO molecules move within an essentially fixed matrix of oxygen atoms. Taking Pt(111) surface as an example, the activation energy for CO surface diffusion is approximately 50 kJ/mol. This rate is very slow compared to other similar surfaces for CO diffusion such as Rh(111) and Ru(001). The slow surface migration explains the formation of CO surface islands. At high reaction temperatures, the CO islands are no longer present on Pt surfaces due to a higher CO surface diffusion rate [61]. The above examples show that even though CO oxidation is considered one of the simpler reactions in heterogeneous catalysis, many factors need to be understood completely in order to develop a commercial catalyst. Using the TAP reactor system, we can find the surface lifetimes of both CO and oxygen on the catalyst surface, support effects, catalyst activity, and selectivity for the CO oxidation reaction using both a single Pt bulk metal particle and supported Pt catalysts. From these experimental results, we can deduce what the mechanism for CO oxidation may be on Pt and its individual mechanistic steps.

### **1.3.2 Selective Oxidation of Hydrocarbons over VPO**

Selective heterogeneous oxidation catalysis is one of the most vital areas in the chemical industry because it produces approximately 25% of the most important industrial organic chemicals and intermediates used in the manufacture of industrial products and consumer goods. Some examples of the products include intermediates such as acrolein, acrylic

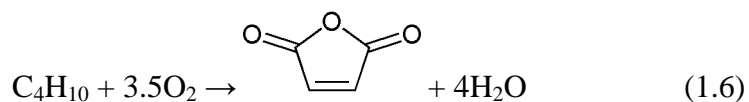
acid, acrylonitrile, methacrylic acid, MTBE, maleic anhydride, phthalic anhydride, ethylene, and propylene oxide. Efforts are continuously being made to make selective oxidation processes and catalysts more efficient and environmentally friendly. Grasselli [64], through his own personal experience working with selective oxidation systems for nearly 50 years, introduced seven fundamental principles that are useful in understanding the behavior of metal oxide catalysts used in selective oxidation processes. The seven principles are the role of lattice oxygen, metal-oxygen bond strength, host structure, redox, multi-functionality of active sites, site isolation, and phase cooperation. The first principle states that lattice oxygen from the metal oxide catalyst might serve as a more versatile and more selective oxidizing agent than gaseous  $O_2$ . The idea is to utilize the metal oxide catalyst as a reactant, and then re-oxidizing the catalyst at a later stage in the process. The metal/lattice oxygen bond strength is also important in selective oxidation catalysis. If the metal-oxygen bond is too strong, no reaction will occur. If the metal-oxygen bond is too weak, then over oxidation will occur which can lead to undesired waste products. The metal-oxygen bond should be of intermediate strength under reaction conditions. The best metal oxide catalysts with intermediate metal-oxygen bond strength are typically covalent and amphoteric in nature such as molybdates, antimonates, and vanadates. The third principle is the host structure of the metal oxide catalyst. The host structure must be pliable enough to contain the desired amount of lattice oxygen, accommodate the reduction of the catalyst without structural collapse, facilitate rapid electron transfer, vacancy, and lattice oxygen diffusion. Examples of materials that would serve as good host structures would be scheelites, fluorites, rutiles,

and perovskites. Metal oxides used in selective oxidation processes must also exhibit redox properties to replenish the removed surface lattice oxygen by gaseous O<sub>2</sub>. The lattice oxygen from the bulk of the metal oxide fills an anion vacancy on the surface while the vacancy moves to another site, where it is ultimately filled by O<sub>2</sub> in the gas phase completing the redox cycle. Regeneration of the reduced metal oxide must be faster than its reduction for the system to function as a catalyst. The fifth principle states that active sites on selective oxidation catalysts are generally multi-functional and multi-metallic (mixed metal oxide). The active sites can perform various functions in the catalytic reaction such as chemisorption of the reactant(s), abstraction and insertion of certain species from and to the substrate, or desorption of the product(s). The site isolation principle states that the reactive surface lattice oxygen must be spatially isolated from each other in defined groupings on the catalyst surface in order to achieve selectivity. The number of oxygen atoms in each grouping would determine the reaction channel through the stoichiometry requirements imposed on the reaction by the availability or lack of oxygen atoms at the reaction site. The final principle, phase cooperation, states that sometimes it is necessary to design a catalyst with two or more phases of the host structure in order for the catalyst to carry out the necessary functions for the catalytic reaction. The phases must communicate with each other and work together to carry out the reaction.

One selective oxidation reaction that demonstrates some of the above principles proposed by Grasselli is the selective oxidation of *n*-butane to maleic anhydride (MA) using VPO

catalysts. Maleic anhydride is an important intermediate used for the production of unsaturated polyester resins, agricultural chemicals, lubricating oil additives, and pharmaceuticals [65, 66]. The *n*-butane to MA process is currently the only industrially practiced heterogeneous selective oxidation reaction involving an alkane. The selective conversion of alkanes to oxygenates has great practical significance because alkanes are lower-cost feedstocks than their olefin counterparts, and are currently under utilized. A fundamental understanding of the function of VPO catalysts for the *n*-butane to MA process would be an important tool for developing new classes of catalytic materials for alkane oxidation [12, 23, 67, 68].

The *n*-butane to MA reaction performs a 14-electron oxidation involving the abstraction of 8 hydrogen atoms and insertion of 3 oxygen atoms (Equation 1.6).



A key unanswered question in the selective oxidation of *n*-butane to MA over VPO catalysts is the nature of the active-selective phase or phases. Although there is evidence to suggest that  $(\text{VO})_2\text{P}_2\text{O}_7$  is an essential element in active-selective VPO catalysts, it is still unclear how the  $(\text{VO})_2\text{P}_2\text{O}_7$  lattice supplies the 7 oxygen atoms needed to convert *n*-butane to MA. One theory is that the oxidation primarily involves the oxygen adspecies that are adsorbed at vanadium surface sites, and relatively little oxidation is from the bulk lattice oxygen of the VPO. This theory is based on studies measuring the amount of active oxygen on  $(\text{VO})_2\text{P}_2\text{O}_7$ , which indicate a close correspondence between the amount

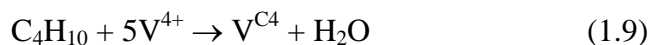
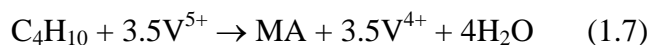


of active oxygen and the number of surface vanadium atoms [69]. Other studies measuring the redox properties of supported VPO catalysts indicate that the amount of active oxygen can exceed the amount of surface oxygen [70]. Researchers have also proposed that other crystalline phases are involved in the supply of active-selective oxygen in the VPO system with vanadium in the +5, +4, and +3 oxidation state [71]. Previous TAP reactor studies on the VPO system show that oxygen adspecies are not the only source of active-selective oxygen [67]. Also, the selectivity and activity of the catalyst was found to be strongly dependent on the oxygen pre-treatment conditions. For example, VPO that was exposed to 10 min oxygen pre-treatment showed significant increases in selectivity than VPO that was only exposed to 5 min of oxygen pre-treatment.

An important feature of the VPO system is the facile formation and inter-conversion under catalytic conditions of the  $V^{4+}$  pyrophosphate  $(VO)_2P_2O_7$  phase and  $V^{5+}$  phase phosphates  $VOPO_4$  ( $\alpha_I$ ,  $\alpha_{II}$ ,  $\beta$ ,  $\gamma$ ,  $\delta$ ). Studies show that the  $(VO)_2P_2O_7$  samples exhibiting predominantly the (100) face can be topotactically transformed into  $\delta$ - $VOPO_4$  and back again to the  $V^{4+}$  phase at reaction temperatures [72, 73]. Active and selective VPO catalysts typically have a mean oxidation state of vanadium slightly higher than 4.0 and a phosphorus to vanadium ratio (P/V) slightly higher than 1.0. These characteristics are mostly associated with the  $(VO)_2P_2O_7$  phase. Other studies have also indicated that the active phase may be composed of mostly the  $V^{4+}$   $(VO)_2P_2O_7$  phase with some  $VOPO_4$  ( $V^{5+}$ ) phase. The formation rate of maleic anhydride is said to be strongly dependent on

the surface distribution and location of the  $V^{5+}$  sites, and the sites must be isolated in order to decrease the yield of the by-product,  $CO_2$  [12, 66].

The mechanism for the selective oxidation of *n*-butane to maleic anhydride over VPO catalysts can be partly explained by the Mars-Van Krevelen mechanism because it involves the participation of lattice oxygen. In order for the *n*-butane to MA reaction to proceed, there must be enough oxygen present in the system. According to some authors, there are two types of oxygen species in the selective oxidation reaction of *n*-butane to MA. The first type is bulk oxygen species, which is involved in the *n*-butane/1,3-butadiene oxidative dehydrogenation and for oxygen insertion in the MA cycle. The second type is adsorbed and activated oxygen species that is responsible for oxidation to CO and  $CO_2$ , and for the oxidation of furan to MA [66]. Patience and Lorences [11] proposed the following general mechanism describing the re-oxidation mechanism for the conversion of *n*-butane to MA.



The mechanism assumes that butane reacts with 3.5 oxidized sites to form MA, and MA can also react with 2 oxidized sites to form  $CO_x$  (carbon oxides) and water (Equations 1.7 and 1.8). This assumption predicts that a lower selectivity may result for catalysts that are highly oxidized. In other words, there is an optimal oxidation state for the VPO catalyst in order to achieve maximum activity and selectivity. In Equation 1.9, butane chemisorbs to the surface of a reduced site to form a vanadium-carbon complex ( $V^{C4}$ )

accompanied by the evolution of one molecule of water. The  $V^{C4}$  complex effectively passivates four adjacent  $V^{4+}$  sites. For catalyst re-activation, molecular oxygen is assumed to react with a reduced site to form an oxidized site, and 5.5 moles of oxygen are required to oxidize the vanadium-carbon complex. This oxidation results in the formation of four moles of  $CO_x$  and water, and frees five  $V^{4+}$  sites (Equations 1.10 and 1.11).



Figure 1.3 shows a general schematic of the mechanism proposed by Patience and Lorences. The figure shows that oxygen reacts with  $V^{4+}$  to form  $V^{5+}$  or butane may react with  $V^{4+}$  to form a vanadium-carbon complex. This schematic shows two possible routes for the re-oxidation of the vanadium-carbon complex. In the first route, it was assumed that  $V^{5+}$  sites were responsible for supplying oxygen to the vanadium-carbon complex. In the second route, it is assumed that molecular oxygen reacts directly with the vanadium-carbon complex to form carbon oxides and water. In the first route, carbon oxide formation occurs first followed by the re-oxidation of  $V^{4+}$  to  $V^{5+}$ . In the second route,  $V^{4+}$  is the first to be oxidized followed by the formation of the vanadium-carbon complex and carbon oxides [11]. The activation energy for the selective oxidation of *n*-butane to MA over VPO catalysts found under steady-state conditions range from 11 to 27 kcal/mol [12, 74]. Transient kinetic studies under vacuum conditions found that the activation energy for *n*-butane conversion to MA in the absence of gas phase oxygen

depends on the catalyst surface oxidation state. The activation energy was found to be lower for more highly oxidized VPO samples. It was also reported that the combined rate of MA formation and desorption was faster on more oxidized VPO surfaces [12, 67].

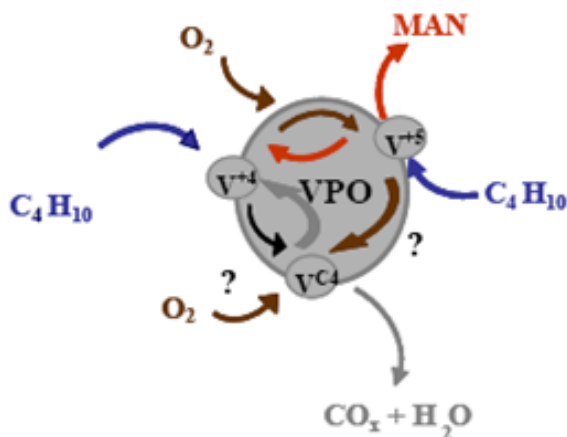


**Figure 1.3** Reaction pathways for re-oxidation of VPO catalyst.

The selective oxidation of *n*-butane to MA is a very complex reaction. In this dissertation, the conversion of furan (an intermediate in the *n*-butane to MA reaction) to MA will be used to explore the kinetics of the VPO catalyst under transient conditions using the TAP reactor system. Experiments probing the catalyst surface under reduced and oxidized conditions at different reaction temperatures will give insight into the kinetic mechanism of the reaction, rate constants, activation energy, conversion, selectivity, and oxidation degree of the catalyst.

# Chapter 2

## Objectives

### 2.1 Catalyst Structure/Activity Relationship

There are three main objectives that is the motivation behind the choice of experiments presented in this dissertation. The first objective is to better understand how catalyst surface structure and composition is related to or affect its kinetic performance. In ongoing catalysis research, it is hypothesized that some chemical reactions are sensitive or insensitive to certain catalyst structural compositions. In more complex multi-faceted industrial catalysts, the question often resides in whether higher catalytic activity and selectivity is associated with the bulk metal structure or is it actually a result of the surface metal atoms. By studying two types of catalytic systems of varying complexity, we can first try to understand a relatively simple catalytic system, CO oxidation on Pt, and see how activity is related to the transition metal. For example, by performing experiments using a single particle of a single component polycrystalline bulk Pt metal catalyst, initial studies are obtained in the TAP reactor to understand bulk structural

properties to the CO oxidation reaction. Once we have shown that it is possible to obtain kinetics from the single particle Pt bulk metal catalyst in the TAP reactor, similar experiments can be repeated using much more complex catalytic materials such as the addition of an inert oxide support or real industrial catalysts such as mixed metal oxides. By performing stepwise experiments with catalysts increasing in structural and compositional complexity, we can understand the role of each catalyst component in the chemical reaction. Also, one of the advantages of using a single catalyst particle is that any kinetic information obtained can be solely related to the composition of that one catalyst particle. Altering the composition of the single particle in a controlled manner and relating the kinetic change can give important insight into the structure/activity relationship of catalysts.

The TAP reactor system is an ideal catalyst characterization tool to monitor the relationship between catalyst structure/composition and its performance because it allows the catalyst to be studied under transient conditions where the composition of the catalyst can be systematically altered and probed for performance. Using the TAP “Interrogative Kinetics” experimental approach, a variety of catalyst surface states can be probed in a controlled manner to determine how one catalyst state can evolve into another. Each TAP reactant pulse can give information on the activity, selectivity, adsorption/desorption rate parameters, number of active sites, and oxidation/reduction degree of the catalyst and correlate this information to the composition of the catalyst surface as it is incrementally altered. Understanding the structure/activity relationship of

a catalytic system and creating a methodology to study this relationship in an efficient and fruitful manner is an important step in the development and optimization of new catalytic technologies, and simplifying the catalyst development cycle.

## **2.2 Bridging the “Pressure-Materials Gap”**

The second objective of this dissertation is to develop an initial methodology using the TAP reactor system to bridge the so-called “pressure and materials gap” [51]. By using the single component polycrystalline Pt particle, experiments ranging from atmospheric pressure to UHV conditions can be performed in a single apparatus, the TAP reactor, to understand how catalyst surface coverage changes with changing reaction pressures. It is predicted that as the reaction pressure is lowered, the reactant surface coverage tends to decrease as well. In the case of CO oxidation, there would be less coverage of CO overpowering oxygen adsorption as pressure is lowered. Studying real catalytic materials in a conventional reactor under both process and UHV conditions allows the researcher to understand how the catalyst behaves at the industrial level as well as gain insight into more fundamental kinetic information such as reaction mechanisms and rate parameters under transient, non-steady-state conditions (molecular scale). This well-defined experimental procedure uses an alternate method to traditional spectroscopic surface science techniques that study single crystals, which are not realistic industrial catalytic materials, to understand kinetic interactions during chemical reaction on real catalysts.

## 2.3 Microreactor Characterization

The third and final objective is to better understand and characterize gas transport in the TAP microreactor bed and minimize concentration and temperature gradients within the catalyst (active) zone. In kinetic catalyst characterization, it is important to have a nearly uniform reactant gas concentration and catalyst composition profile within the catalytically active zone in a reactor. The biggest problem in this field is to maintain high uniformity in the catalyst zone even in the high conversion domain. Uniformity enables us to relate the observed rate of chemical transformation to the spatial average of reactant composition within the catalytically active zone. This ensures that the same catalytic performance is achieved throughout the catalyst bed. Spatial uniformity also provides the kinetic data for revealing important characteristics between catalyst surface structure and composition to its performance. Qualitatively, non-uniformity can be estimated as the difference between inlet and outlet concentrations of the working catalyst zone divided by the absolute value of the average catalyst zone concentration. Therefore, uniformity in the catalyst bed is greatest when the spatial concentration difference is very small compared to the maximum reactant concentration value. It can be described by the equation  $(C_{\max}-C_{\min})/C_{\max}$ . Typically uniformity ranges between 0 and 1, with values closer to 0 corresponding to greater uniformity in the catalyst zone [9].

The thin-zone TAP microreactor (TZTR), proposed by Shekhtman and Yablonsky in 1999 [9, 75-77], is an improvement in the TAP microreactor configuration to achieve



greater uniformity in the catalyst zone. Under typical TAP working conditions ( $10^{-8}$ - $10^{-9}$  torr); transport in the microreactor is dominated by Knudsen diffusion, which is mainly driven by a gas concentration gradient. The magnitude of the gas concentration gradient is dependent on the microreactor length and the vacuum boundary condition at the microreactor outlet. Under the conditions of catalytic reaction, the gas concentration gradient causes a surface concentration gradient inside the microreactor. When the length of the catalyst bed is significant compared to the whole length of the microreactor, catalyst composition non-uniformity is generated within the catalyst bed [9, 75]. Throughout TAP history there have been multiple theoretical configurations of the reactor to compensate and minimize the presence of the concentration gradient in the catalyst bed by minimizing the length of the catalyst zone [22, 23]. In the TZTR, the thickness of the catalyst zone was made very small in comparison to the whole length of the microreactor. TZTR in some extent is similar to the differential PFR, although the transport regime in a TZTR (diffusional flow) is very different from the transport regime in a differential PFR regime (convective flow). Non-uniformity in the TZTR can be attributed to two factors: the applied concentration gradient, which drives diffusion and is present even when no reaction occurs, and chemical reaction, which changes the concentration profile in the catalyst zone [9, 76]. The TZTR for a wide range of conversions (up to 75%), provides a non-uniformity level not higher than 20%. However, at very high conversions (higher than 80%), even the TZTR cannot guarantee uniformity in the catalyst zone. So the next logical progression from the TZTR would be to make the catalyst zone even smaller to increase uniformity and conversion.

By transitioning to the single particle microreactor configuration, non-uniformity in the catalyst composition and temperature profiles within the microreactor bed can be assumed to be negligible because there is only one catalyst particle. A single particle can also be moved to different axial and radial positions and the influence of catalyst position on kinetic characteristics can be explored. Also, kinetic information obtained can be used to model the microreactor from a 3-dimensional standpoint.

# Chapter 3

## Experimental Description

### 3.1 The TAP Reactor

The TAP (Temporal Analysis of Products) reactor system was first patented by the Monsanto Company in 1986 as a novel device for studying the kinetics and mechanisms of heterogeneous catalyzed gas phase reactions by using a transient response technique with submillisecond time resolution [78]. Two years later in 1988, open literature publications by Monsanto catalyst scientists described how the TAP reactor system was used to elucidate the mechanisms for several heterogeneous catalytic reactions having commercial significance [22, 79]. Particular reactions that were studied included *n*-butane oxidation to maleic anhydride over vanadium-phosphorus oxide (VPO) catalysts, propylene oxidation to acrolein over bismuth-molybdates, methanol ammoxidation to HCN over  $\text{MnPO}_x$  and  $\text{FeMoO}_x$ , and ethylene epoxidation over silver metal [80, 81]. In 1989, Monsanto granted an exclusive license to manufacture and sell a commercial version of the TAP reactor to Autoclave Engineers of Erie, PA. Later in that same year, DuPont became the first chemical company in the United States to purchase a TAP reactor from Autoclave Engineers for the newly established Corporate Catalysis Center in

Central Research and Development [79]. Later, the TAP-1 system was redesigned and simplified and eventually developed into the TAP-2 reactor system [23], which was commercialized by Mithra Technologies. The TAP-3 system retains the basic design of the TAP-2, but is a fully automated instrument that can be operated either locally or remotely via the Internet.

### **3.1.1 Apparatus Description and Operation**

Figure 3.1 presents a simplified schematic of a TAP-2 reactor system, and Figure 3.2 shows a photograph of the newest TAP-3 reactor system. The TAP-3 reactor is comprised of 1) a pulse-valve manifold assembly that supplies gas reactants for pulsed and flow experiments at user defined temperatures and pressures, 2) a microreactor assembly that can be operated isothermally or in a temperature programmed mode, 3) a mass spectrometer detector contained in a high-throughput ultrahigh-vacuum system, and 4) a computer based control and data acquisition system.

The pulse-valve manifold contains one continuous flow valve and four high-speed pulse valves that are arranged to minimize the dead volume between the valves and the microreactor. The four pulse valves can be triggered simultaneously or in a programmed alternating sequence. Pulse intervals can be varied from microseconds to minutes. Switching between feeds is accomplished electronically and can occur almost instantaneously. The continuous flow valve is connected to a separate manifold containing four flow controllers. The flow controllers and pulse valves can be operated simultaneously.

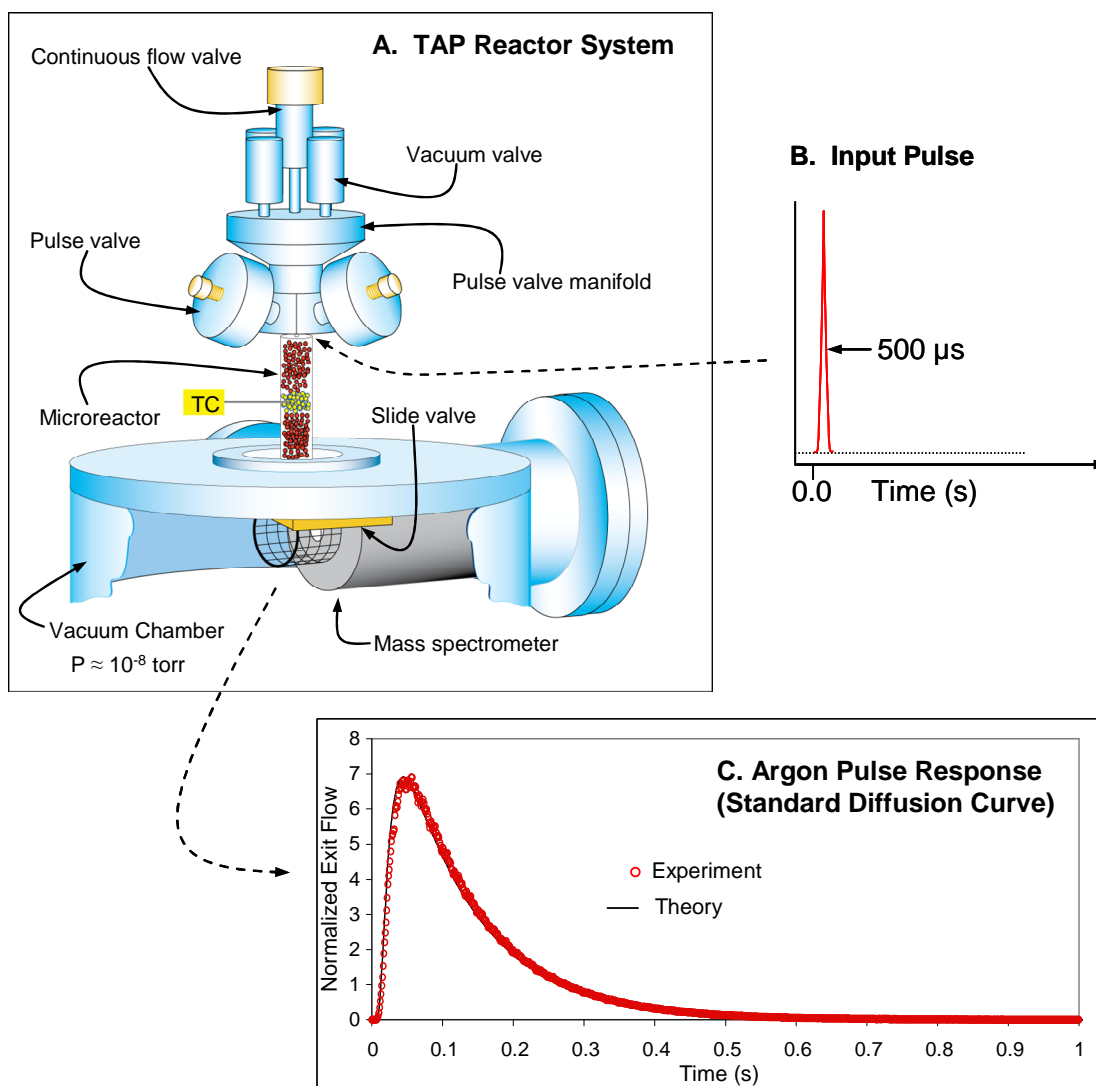


**Figure 3.1** (A) Schematic of TAP-2 reactor system. (B) The inlet pulse in a TAP pulse response experiment is represented by a delta function. (C) As the pulse travels through the microreactor, it broadens. The example curve compares an experimentally measured argon exit flow curve to the standard diffusion curve.



**Figure 3.2** TAP-3 Reactor System.

The TAP-3 system can accommodate microreactors of different lengths (up to 25 cm) and diameters (up to 2 cm), which is useful for handling a variety of catalyst forms. A standard TAP microreactor is constructed of type 316 stainless steel and can be operated at atmospheric pressures or at vacuum conditions. Reactors are heated electrically and the reactor temperature controller provides an array of control options, which include constant temperature operation, programmed heating or cooling at a user defined rate, and the ability to perform multi-step ramp-soak programs. The standard microreactor can be heated to 800 °C. Microreactors have also been fabricated from inconel and quartz, which allow operation to temperatures as high as 1000 °C.

The TAP-3 vacuum system is comprised of two chambers separated by a pneumatically operated gate-valve, which is closed in the standby position. The lower chamber is evacuated by a 40 cm diameter diffusion pump and associated mechanical pump. The chamber contains a cylindrical liquid nitrogen trap and adjustable baffle that closes when data is not being acquired. The upper chamber holds the mass spectrometer and is pumped by a turbo molecular pump. The background pressure in the mass spectrometer chamber is typically  $\approx 10^{-9}$  torr.

The microreactor is positioned directly above the ionizer of the mass spectrometer, and is attached to a movable stainless steel bellows. A unique rotary-valve assembly is located between the ionizer and the microreactor. It permits the microreactor to be operated at vacuum conditions or atmospheric pressures, and allows the reactor to be removed from the system without venting the vacuum chambers. The reactor can be easily and rapidly switch from one kinetic regime to another without exposing the catalyst sample to the atmosphere. When the slide valve is closed, the TAP microreactor can be operated as a continuous plug-flow type reactor at atmospheric or higher pressures. In the “high-pressure” mode, the bulk of the reactor effluent exits through an external vent. A small amount can be leaked into the vacuum chamber through a variable leak valve. The leaked material can be monitored with the mass spectrometer. In high-pressure experiments, the mass signal usually changes relatively slowly, and can be collected in a scan mode. In this mode, a complete mass spectrum can be acquired about once every 0.25 seconds. After performing an experiment at atmospheric pressures, the microreactor

can be quickly switched to vacuum conditions by opening the slide valve. With the slide valve in the open position, all of the reactor effluent vents into the vacuum chamber. The movable bellows allows the reactor outlet to be positioned within 2 millimeters of the ionizer so that most of the effluent passes through the ionizer. As a result, very small inputs of gas can be detected, with a very high the signal to noise (S/N) ratio (Figure 3.3). The high S/N ratio allows accurate calculation of the zeroth, first, and second moments of the response curves, and direct determination of many important kinetic characteristics. For example, reactant conversion for a series of pulses can be determined from the zeroth moment. This change in conversion can be related to a change in the concentration of the active catalytic species. The following quantities can be directly calculated from 0<sup>th</sup>, 1<sup>st</sup>, and 2<sup>nd</sup> moments: Conversion, selectivity, product yield, residence time, apparent rate constants, apparent intermediate gas constants, and apparent time delay.

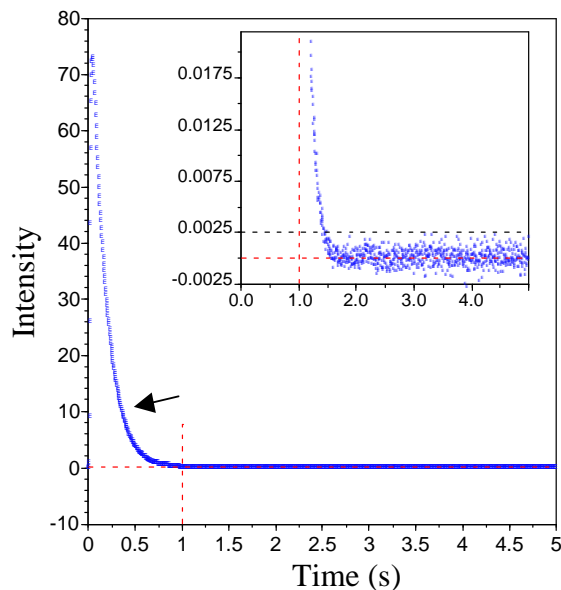


**Figure 3.3** Typical TAP pulse response curve with inset showing the noise magnitude in the tail of the response. Signal to noise ratio is > 30,000 to 1.



### 3.1.2 The TAP Experiment

The TAP experiment was conceived in the late 1970's to study catalytic reaction mechanisms on industrial catalysts [22, 23, 78, 79]. The initial thought was to devise a simplified "molecular beam" experiment for multi-component catalysts (e.g., mixed metal oxides and supported metals) that have high surface areas and complex pore structures. Molecular beam scattering (MBS) experiments [82-87] can provide fundamental information on surface structure, reaction dynamics, the elementary steps of a reaction, and the kinetic parameters of individual steps. When used in conjunction with surface characterization techniques, data from the TAP experiment can establish the link between kinetic properties and surface structure. On the other hand, MBS experiments use planar or decorated planar targets to take advantage of the spatial characteristics of the beam. Industrial catalysts have complex surfaces, are composed of multi-component mixtures of different metal oxides or metals combined with metal oxides, and are generally not suitable for MBS experiments. The goal of early TAP designs was to retain the time-dependent features of a molecular beam experiment, minimize gas phase interactions, and provide a way to extract intrinsic kinetic information from reactions on bulk catalysts. The TAP experiment can be viewed as a bridge between MBS experiments and conventional microreactor experiments.

A variety of MBS setups have been described in the literature, and they generally fall into two different classes: (1) systems designed to study gas-surface dynamics, and (2) systems designed to study the kinetics and mechanism of surface reactions [88]. Figure

3.4 presents a simplified diagram showing key components of a MBS apparatus. In a typical experiment a well-collimated beam of molecules having a known translational energy is directed toward a target surface, and the velocity and angle distributions of the scattered molecules are measured. Molecular beam experiments are performed under single collision conditions so that reactant molecules collide once with the target surface but not with each other. The observed distributions contain dynamic information, which describes the process of energy exchange between gas and surface atoms, as well as kinetic and mechanistic information. Scattered molecules from a collimated beam may also exhibit diffraction effects, which provide information on surface structure and bond lengths [82-87].

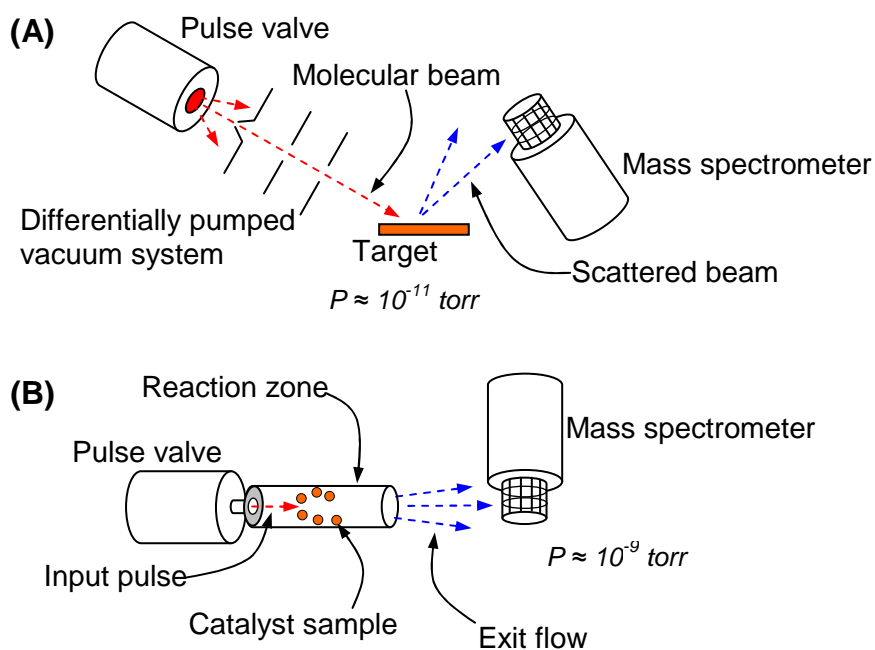


**Figure 3.4** Conceptual comparison of key components of (A) molecular beam scattering experiment and (B) TAP experiment.

MBS experiments obtain essential kinetic and mechanistic information by modulating the reactant flux, and measuring the shift in arrival times at the detector between scattered reactant and product molecules. The difference in arrival times can be used to determine reaction sequences, surface lifetimes of adspecies, and rates of surface reactions. TAP pulse-response experiments [22, 23, 78, 79, 89, 90] extract kinetic information following a similar fashion. Injection of a narrow gas pulse into the reaction zone initiates an experiment. The gas molecules travel through the reaction zone where they encounter the catalyst and can react to form product molecules. Molecules that exit the reaction zone are monitored by the mass spectrometer positioned at the outlet. An experiment ends when the flow of reactant and product molecules is no longer detected by the mass spectrometer. The observed characteristic feature in a TAP-experiment is the time dependent gas flow  $F(t)$  [moles/s] or [molecules/s] that escapes from the exit of the microreactor. The flow dependencies also have integral characteristics that are related to the moments of the "flow-time" dependencies [22, 23, 91]. Kinetic and mechanistic information is obtained by analyzing these dependencies, and gas transport is used as a "measuring stick" to determine the rates of chemical transformations. In addition to kinetic and mechanistic information, TAP experiments have been used to study transport processes in porous materials, such as zeolites, and oxygen diffusion in metal and metal oxide catalysts. The temperature dependence of TAP transient response curves provides intrinsic rate parameters that can be associated with the surface composition of a catalyst. The number of active sites can be determined in TAP titration experiments.

In both TAP and MBS experiments, the sample is maintained under vacuum conditions, which strongly promote desorption of adspecies. Prior to performing a TAP experiment, it is common to heat the catalyst sample and monitor the desorption spectrum. During the heating process, adspecies (e.g., water, CO, CO<sub>2</sub>, etc.), which cover the surface at ambient pressures, vacate the surface leaving the coverage to more closely resemble that of an MBS target. Conversely, by pulsing a molecule into the reaction zone can increase the molecule's coverage so that it resembles the coverage at ambient pressures. Pulsing different molecules into the reaction zone in an alternating sequence can adjust the surface coverage of two or more species. As a result, coverage in a TAP experiment can be manipulated to resemble coverage in an MBS experiment or coverage in a conventional microreactor experiment.

The input pulse in a TAP experiment typically contains  $\approx 10^{14}$  molecules, and the local pressure in an empty reaction zone may reach  $\approx 10^{-3}$  torr during a pulse. If unimpeded, an oxygen molecule can traverse the reaction zone in under 100  $\mu$ s. If the reaction zone is filled with particles the pressure may reach  $\approx 10^{-2}$  torr in the void spaces if no adsorption occurs. The mean free path in an empty reaction zone is about half the length of the reactor. In an empty reactor, molecules move in beam-like fashion and suffer relatively few collisions. In a packed reactor, the mean free path is  $\approx 4000$   $\mu$ m, which is significantly larger than the space between particles. As a result, in a packed bed reactor, molecules collide with particles, but seldom with one another.

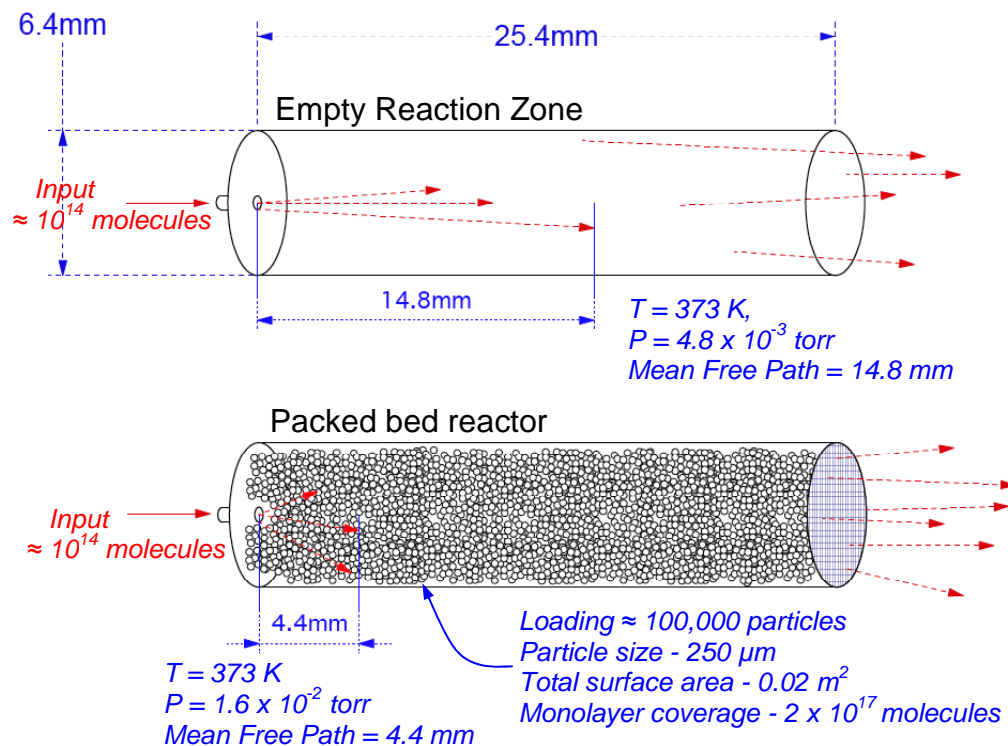


**Figure 3.5** Scale drawing of a TAP "reaction zone" and packed bed microreactor containing a loading of nonporous spherical particles  $\approx 250 \mu\text{m}$  in diameter.

At sufficiently small pulse intensities, a one-pulse TAP experiment can be considered a state-defining experiment. The number of molecules in a reactant pulse is typically much smaller ( $10^2$  to  $10^5$  times smaller) than the number of surface atoms in the catalyst sample being probed [23]. As a result, the reactant pulse does not significantly perturb the catalyst surface.

The TAP menu of experiments includes, but is not limited to, high-speed vacuum pulse response experiments (TAP Knudsen pulse response experiments, TAP pump-probe

experiments, and TAP multipulse experiments), atmospheric pressure steady-state, step-transient and SSITKA experiments, temperature programmed desorption (TPD), and temperature programmed reaction (TPR). In addition, newly developed software allows the user to create programmed experimental sequences, which can be stored in memory, and then performed automatically. Sequences may include complex temperature treatments, switching back and forth between atmospheric pressure and vacuum experiments, switching from continuous flow to transient response experiments, or combinations of step-transient, pulse transient, steady-flow, and temperature programmed experiments.

### **3.1.3 Theory of TAP Microreactor Configurations**

The analysis of TAP pulse response experiments are based on specific microreactor models that describe the catalyst zone. Current models apply to packed bed reactors, starting with a one-zone reactor, and progressing to a reactor containing a single particle, which is part of the new work presented in this dissertation. When the input pulse intensity is  $\approx 10^{14}$  molecules/pulse, transport in the reactor is dominated by Knudsen diffusion, which is mainly driven by a gas concentration gradient. The magnitude of the gradient is dependent on the reactor length and the vacuum boundary condition at the reactor outlet. Under the conditions of catalytic reaction, the gas concentration gradient causes a surface concentration gradient in the catalyst bed. When the length of the catalyst bed is a significant fraction of the reactor length, the reactant can cause non-uniformity in the catalyst composition [9, 75, 76, 90]. TAP microreactor development

has focused on minimizing the effects of temperature and concentration gradients. An axial temperature gradient exists because of the close proximity of the microreactor outlet to the vacuum chamber. Typically the temperature near the center of a microreactor will be higher than the temperature close to the microreactor outlet. The evolution of TAP microreactor configurations and their theoretical description will be presented in the following sections below.

**One-Zone TAP Microreactor** In the one-zone microreactor model, the total reactor volume is uniformly packed with catalyst particles. The one-zone model and its mathematical framework were introduced in the first TAP paper published in 1988 [22].

The mathematical model is based on the following assumptions:

1. The fractional voidage of the catalyst bed is constant.
2. There is no radial concentration gradient in the catalyst zone.
3. There is no radial or axial temperature gradient in the catalyst zone.
4. There is no intra-particle or surface diffusion.
5. The diffusivity of each gas is constant and independent of the composition of the mixture as a whole.

The last assumption results from using an evacuated microreactor and small pulse intensities, which guarantees the validity of the Knudsen diffusion regime. The mass balance equations for a number of important gas transport and transport-kinetics interactions in the one-zone reactor are presented below.

In a packed bed reactor, the mass balance equation for Knudsen diffusion of a non-reacting gas A, (e.g., neon, argon, krypton) is given by

$$\varepsilon_b \frac{\partial C_A}{\partial t} = D_{eA} \frac{\partial^2 C_A}{\partial z^2} \quad (3.1)$$

with initial condition  $0 \leq z \leq L, \quad t = 0, \quad C_A = \delta_z \frac{N_{pA}}{\varepsilon_b A}$  (3.2)

and boundary conditions  $z = 0, \quad \frac{\partial C_A}{\partial z} = 0$  (3.3)

$$z = L, \quad C_A = 0. \quad (3.4)$$

The initial condition (Equation 3.2) specifies that at  $t = 0$ , the gas concentration at the reactor inlet can be represented by the delta function. Boundary condition one (Equation 3.3) specifies that the input flux is zero at the microreactor entrance when the pulse valve is closed. Boundary condition two (Equation 3.4) specifies that the gas concentration at the microreactor outlet is very close to zero. This condition results from the continuous evacuation of the microreactor outlet by the vacuum system. The diffusivity term in the Knudsen diffusion regime is determined by the following equation [89]

$$D_e = \frac{\varepsilon_b}{\tau} \frac{d_i}{3} \sqrt{\frac{8RT}{\pi M}}, \quad d_i = \frac{4\varepsilon_b}{3(1-\varepsilon_b)} r_p \quad (3.5)$$

The flow rate,  $F_A$ , at the microreactor outlet is described by the following equation

$$F_A = -AD_{eA} \left. \frac{\partial C_A}{\partial z} \right|_{z=L} \quad (3.6)$$



and the gas flux by 
$$Flux_A = \frac{F_A}{A}. \quad (3.7)$$

In order to solve for the gas exit flow rate, it is useful to express Equation 3.1 and the initial and boundary conditions, Equations 3.2-3.4, in dimensionless form.

Dimensionless axial coordinate: 
$$\zeta = \frac{z}{L}. \quad (3.8)$$

Dimensionless concentration: 
$$\bar{C}_A = \frac{C_A}{N_{pA}/V_{void}} = \frac{C_A}{N_{pA}/\varepsilon_b AL}. \quad (3.9)$$

Dimensionless time: 
$$\tau = \frac{tD_{eA}}{\varepsilon_b L^2}. \quad (3.10)$$

Written in dimensionless form, Equations 3.1-3.4 are as follows:

$$\frac{\partial \bar{C}_A}{\partial \tau} = \frac{\partial^2 \bar{C}_A}{\partial \zeta^2} \quad (3.11)$$

with initial condition 
$$0 \leq \zeta \leq 1, \quad t = 0, \quad \bar{C}_A = \delta_\zeta \quad (3.12)$$

and boundary conditions 
$$\zeta = 0, \quad \frac{\partial \bar{C}_A}{\partial \zeta} = 0 \quad (3.13)$$

$$\zeta = 1, \quad \bar{C}_A = 0. \quad (3.14)$$

The solution for the dimensionless concentration,  $\bar{C}_A$ , can be found by applying the method of separation of variables, and is expressed as

$$\bar{C}_A(\zeta, \tau) = 2 \sum_{n=0}^{\infty} \cos((n+0.5)\pi\zeta) \exp(-(n+0.5)^2 \pi^2 \tau) \quad (3.15)$$

The dimensionless flow rate can be expressed in terms of the negative gradient of the dimensionless concentration as

$$\bar{F}_A(\zeta, \tau) = -\frac{\partial \bar{C}_A(\zeta, \tau)}{\partial \zeta} = \pi \sum_{n=0}^{\infty} (2n+1) \sin((n+0.5)\pi\zeta) \exp(-(n+0.5)^2 \pi^2 \tau). \quad (3.16)$$

At the microreactor outlet, where  $\zeta = 1$ , the dimensionless flow rate can be written as

$$\bar{F}_A = \pi \sum_{n=0}^{\infty} (-1)^n (2n+1) \exp(-(n+0.5)^2 \pi^2 \tau). \quad (3.17)$$

Equation 3.17 describes the dimensionless exit flow rate as a function of dimensionless time. The resulting curve (Figure 3.6) is known as the standard diffusion curve. For any TAP vacuum pulse response experiment that involves only gas transport, the standard diffusion curve should be the same regardless of the gas, microreactor bed length, catalyst particle size, or reactor temperature. The dimensionless initial condition from Equation 3.12 requires the area under the standard diffusion curve to equal unity. In dimensional form, Equation 3.17 can be rewritten as

$$\frac{F_A}{N_{pA}} = \frac{D_{eA} \pi}{\varepsilon_b L^2} \sum_{n=0}^{\infty} (-1)^n (2n+1) \exp(-(n+0.5)^2 \pi^2 \frac{t D_{eA}}{\varepsilon_b L^2}). \quad (3.18)$$

Equation 3.18 indicates that the pulse shape of the curve generated in a diffusion only experiment should be independent of the pulse intensity if the gas molecules are transported through the microreactor in the Knudsen diffusion regime.

A unique feature of the standard diffusion curve is the time,  $\tau_p$ , at which the curve

maximum occurs is given by 
$$\tau_p = \frac{1}{6} \quad (3.19)$$

and the corresponding height of the peak maximum is given by

$$\bar{F}_{A,p} = 1.85. \quad (3.20)$$

Equations 3.19 and 3.20 can be rewritten in dimensional form in terms of time and height

as 
$$t_p = \frac{1}{6} \frac{\varepsilon_b L^2}{D_{eA}} \quad (3.21)$$

And 
$$H_p = 1.85 \frac{D_{eA}}{\varepsilon_b L^2}. \quad (3.22)$$

By multiplying Equation 3.19 with 3.20 and Equation 3.21 with 3.22 gives a relationship between the time at which the peak maximum occurs on a standard diffusion curve and its corresponding peak height. This calculation can be used to verify that gas transport through the reactor is Knudsen diffusion.

$$\bar{F}_{A,p} \tau_p = t_p H_p \approx 0.31 \quad (3.23)$$

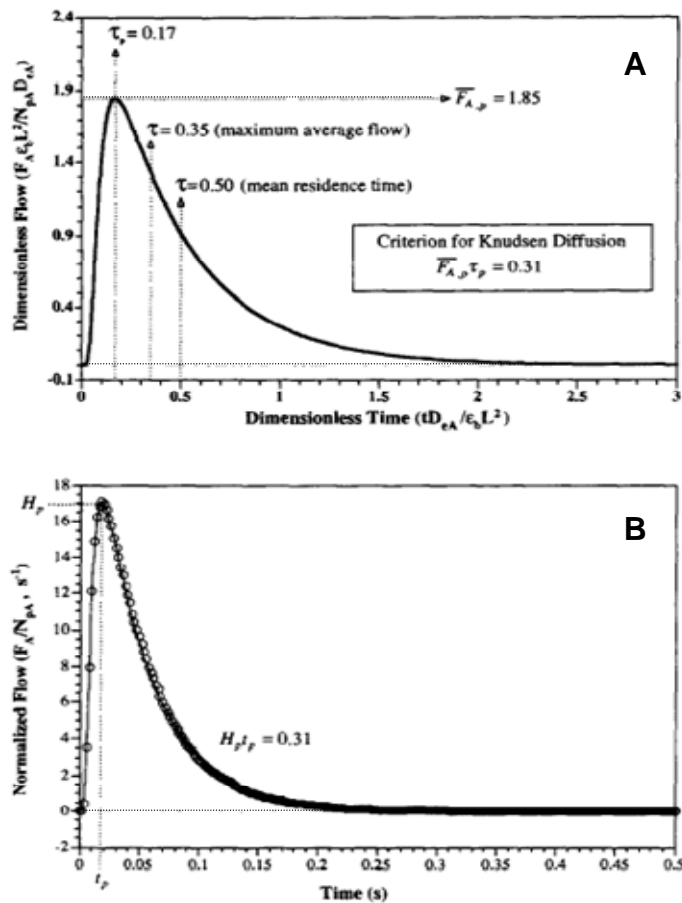


**Figure 3.6** (A) Standard diffusion curve showing key time characteristics and the criterion for Knudsen diffusion. (B) Comparison of standard diffusion curve with experimental inert gas curve over inert packed bed [23].

One of the simplest but most important processes studied in the TAP experiment is irreversible gas adsorption or reaction combined with Knudsen diffusion. If adsorption or reaction is first order in gas concentration, and the catalyst surface coverage is negligible (result of small pulse intensity) compared to the total amount of active catalytic material, then the mass balance for the gas phase component A is given by

$$\varepsilon_b \frac{\partial C_A}{\partial \tau} = D_{eA} \frac{\partial^2 C_A}{\partial z^2} - a_s S_v (1 - \varepsilon_b) k_a C_A. \quad (3.24)$$

Equation 3.24 can also be written in dimensionless form. The initial and boundary conditions for the dimensionless form of Equation 3.24 are the same as those presented previously for the diffusion only case (see Equations 3.12-3.14).

$$\frac{\partial \bar{C}_A}{\partial \tau} = \frac{\partial^2 \bar{C}_A}{\partial \zeta^2} - \bar{k}_a \bar{C}_A, \quad \bar{k}_a = \frac{a_s S_v (1 - \varepsilon_b) k_a L^2}{D_{eA}} \quad (3.25)$$

The dimensionless exit flow rate for irreversible adsorption or reaction combined with Knudsen diffusion process is given by

$$\bar{F}_A = \pi \exp(-\bar{k}_a \tau) \sum_{n=0}^{\infty} (-1)^n (2n+1) \exp(-(n+0.5)^2 \pi^2 \tau). \quad (3.26)$$

Equation 3.26 can also be written in dimensional form as

$$\frac{F_A}{N_{pA}} = \frac{D_{eA} \pi}{\varepsilon_b L^2} \exp(-k'_a t) \sum_{n=0}^{\infty} (-1)^n (2n+1) \exp(-(n+0.5)^2 \pi^2 \frac{D_{eA}}{\varepsilon_b L^2}), \quad (3.27)$$

where

$$k'_a = \frac{a_s S_v (1 - \varepsilon_b) k_a}{\varepsilon_b}. \quad (3.28)$$

A comparison between the dimensional forms of the exit flow for the irreversible adsorption/reaction case, Equation 3.27, and the standard diffusion curve, Equation 3.18, shows that the values of the normalized exit flow for irreversible adsorption/reaction is less than the values obtained in the diffusion only case by a factor of  $\exp(-k'_a t)$ . Therefore, the normalized exit flow curve versus time for irreversible adsorption/reaction is always smaller than the standard diffusion curve (Figure 3.7).

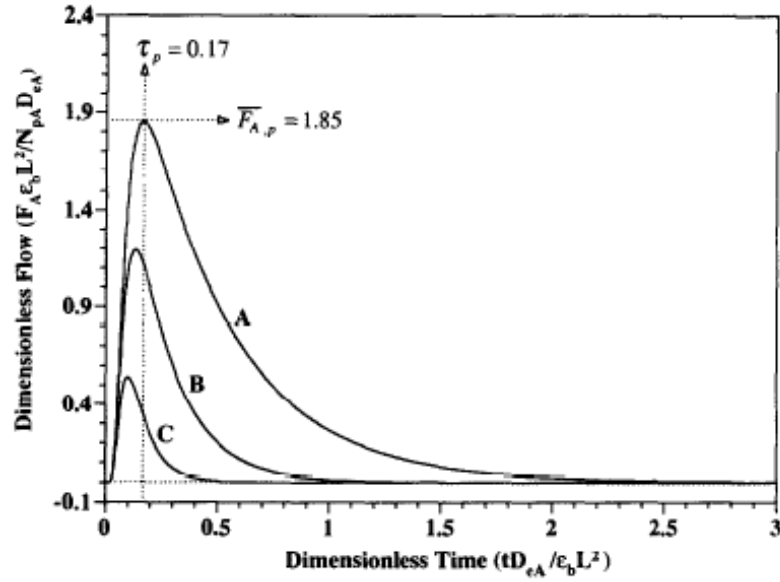


**Figure 3.7** Comparison of diffusion + irreversible adsorption/reaction exit flow curves with the standard diffusion curve. (A) Standard diffusion exit flow curve,  $\bar{k}_a = 0$  (B) Diffusion + irreversible adsorption/reaction curve,  $\bar{k}_a = 3$  (C) Diffusion + irreversible adsorption/reaction curve,  $\bar{k}_a = 10$  [23].

When diffusion + reversible adsorption occurs, and the number of gas molecules is small compared to the total number of catalytically active sites, the mass balances of component A in the gas phase, and on the catalyst surface are described respectively by the following two equations

$$\varepsilon_b \frac{\partial C_A}{\partial t} = D_{eA} \frac{\partial^2 C_A}{\partial z^2} - a_s S_v (1 - \varepsilon_b) (k_a C_A - k_d \theta_A) \quad (3.29)$$

$$\frac{\partial \theta_A}{\partial t} = k_a C_A - k_d \theta_A. \quad (3.30)$$

The dimensionless desorption rate constant is defined as

$$\bar{k}_d = k_d \frac{\varepsilon_b L^2}{D_{eA}}. \quad (3.31)$$

Equation 3.29 and 3.30 can be rewritten in dimensionless form as

$$\frac{\partial \bar{C}_A}{\partial \tau} = \frac{\partial^2 \bar{C}_A}{\partial \zeta^2} - \bar{k}_a \bar{C}_A + \bar{k}_d \bar{\theta}_A \quad (3.32)$$

$$\frac{\partial \bar{\theta}_A}{\partial \tau} = \bar{k}_a \bar{C}_A - \bar{k}_d \bar{\theta}_A, \quad (3.33)$$

where

$$\bar{\theta}_A = \alpha \theta_A \quad (3.34)$$

and

$$\alpha = (1 - \varepsilon_b) AL \frac{a_s S_v}{N_{pA}}. \quad (3.35)$$

Equations 3.32 and 3.33 can be solved using the dimensionless initial and boundary conditions for the diffusion only process (Equations 3.12-3.14) with the additional initial condition for the coverage of adsorbed component A

$$t = 0, \quad \bar{\theta}_A = 0. \quad (3.36)$$

The complete solutions for the dimensionless concentration and exit flow can be found in the literature [23].

In contrast to the normalized exit flow curve in the process of diffusion + irreversible adsorption/reaction, the exit flow curve for the diffusion + reversible adsorption crosses the standard diffusion exit flow curve (Figure 3.8). The point at which the curves intersect depends on the adsorption and desorption rate constants. The diffusion + reversible adsorption exit flow curve is wider and crosses the standard diffusion curve

because of the time delay in molecular transport resulting from the interaction of gas molecules with the catalyst surface. The shape and magnitude of the diffusion + reversible adsorption exit flow curve is also strongly influenced by the adsorption-desorption parameters. For example, when the adsorption rate constant is large and the desorption rate constant is small; the exit flow curve has two peaks. The first peak resembles an irreversible adsorption exit flow curve, and is governed by the interaction between diffusion and adsorption. The second peak is the result of slow desorption, and its shape is dependent on the parameters of adsorption, desorption, and diffusivity. Mathematical modeling of the two peaks shows that the catalyst surface coverage initially increases with time due to fast gas adsorption, and then decreases at which time desorption becomes more significant [23].



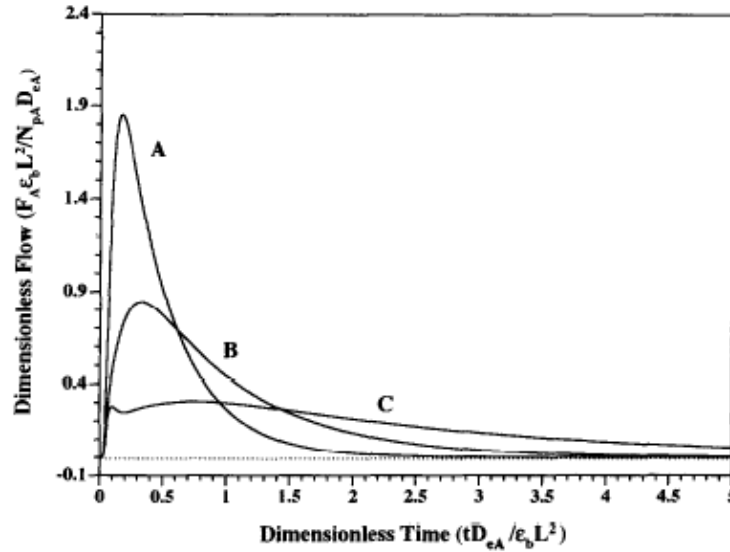


**Figure 3.8** Comparison of standard diffusion and diffusion + reversible adsorption exit flow curves. (A) Standard diffusion exit flow curve,  $\bar{k}_a = 0$  (B) Diffusion + reversible adsorption curve,  $\bar{k}_a = 20, \bar{k}_d = 20$  (C) Diffusion + reversible adsorption curve,  $\bar{k}_a = 20, \bar{k}_d = 5$  [23].

**Three-Zone TAP Microreactor** In the three-zone microreactor, the catalyst zone is sandwiched between two inert zones, and all three zones are of equal length [23]. An important advantage of the three-zone configuration is that the catalyst zone can be more easily maintained under isothermal conditions. However, the gas concentration gradient across the catalyst zone can be significant making it difficult to maintain uniform surface coverages. Also, it is difficult to analyze the transcendental functions that contain the kinetic parameters that are solutions of the three-zone TAP model.

The three-zone mathematical model is the same used in the one-zone model with two additional boundary conditions between the inert and catalyst zones. The additional boundary conditions are given by

$$C_{A,zone1}|z_1 = C_{A,zone2}|z_1, \quad (3.37)$$

$$C_{A,zone2}|z_2 = C_{A,zone3}|z_2, \quad (3.38)$$

$$-D_{eA,zone1} \frac{\partial C_{A,zone1}}{\partial z} |z_1 = -D_{eA,zone2} \frac{\partial C_{A,zone2}}{\partial z} |z_1, \quad (3.39)$$

$$-D_{eA,zone2} \frac{\partial C_{A,zone2}}{\partial z} |z_2 = -D_{eA,zone3} \frac{\partial C_{A,zone3}}{\partial z} |z_2, \quad (3.40)$$

where  $z_1$  is the axial coordinate at the end of zone 1, and  $z_2$  is the axial coordinate at the end of zone 2. Equations 3.37 - 3.40 describe the continuity of the gaseous concentrations and flows inside the microreactor.

**Thin-Zone TAP Microreactor (TZTR)** The thin-zone TAP microreactor (TZTR) model [9, 75, 76, 90, 92] is a three-zone configuration in which the thickness of the catalyst zone is made very small in comparison to the whole length of the microreactor. The advantage of the TZTR configuration is that any change in gas concentrations across the catalyst bed can be neglected when compared to their average values. Diffusional gas transport can be explicitly separated from the chemical reaction rate.

The TZTR mathematical model determines the active zone reaction rate as the difference between two diffusional flow rates at the boundaries of the thin catalyst (active) zone.

$$Rate = Flow^{left}(t) - Flow^{right}(t) \quad (3.41)$$

Equation 3.41 is analogous to a steady-state CSTR where the reaction rate is determined by the difference between two convective flow rates. For the first-order irreversible adsorption/reaction process, conversion in the TZTR can be found from the following

expression

$$X = \frac{k_{ads} \tau_{res,cat}^{dif}}{1 + k_{ads} \tau_{res,cat}^{dif}}, \quad (3.42)$$

where

$$\tau_{res,cat}^{dif} = \varepsilon_b \frac{(\Delta L)L_{II}}{D_{eA}}. \quad (3.43)$$

The apparent adsorption/reaction rate constant,  $k_{ads}$ , can be found from the relationship

$$k_{ads} = K_a \frac{D_{eA}}{L\Delta L\varepsilon_b} \quad (3.44)$$

where the dimensionless parameter  $K_a$  can be found from the zeroth moment

$$\frac{1}{M_0} = 1 + K_a \frac{L_{II}}{L}. \quad (3.45)$$

The zeroth moment can be found by measuring the area under experimentally determined exit flow curves (Figure 3.9). The dimension of the zeroth moment,  $M_0$ , is number of molecules and represents the total number of gas molecules exiting the microreactor. When normalized to the number of molecules injected into the microreactor, the zeroth moment indicates conversion ( $X$ ).

$$X = 1 - M_0 \quad (3.46)$$

From the zeroth moment, the first and second moments can be calculated. The first moment,  $M_1$ , is a time weighted function of  $M_0$ . The dimension of the first moment is number of molecules multiplied by time.  $M_1$  determines the residence time in the

microreactor that is related to the average delay in transport through the microreactor void space caused by a kinetic process. The dimension of the second moment,  $M_2$ , is number of molecules multiplied by time squared. The second moment provides information on the relative duration of time different molecules reside in the microreactor as compared to the average residence time, and can be correlated with the characteristic times of specific kinetic processes. The ratio of moments,  $M_1/M_0$  and  $M_2/M_1$ , has a physical meaning associated with different relaxation times, which are governed by combinations of kinetic coefficients of different reactions. Exit flow data combined with the moments, can be used to formulate a detailed reaction mechanism.

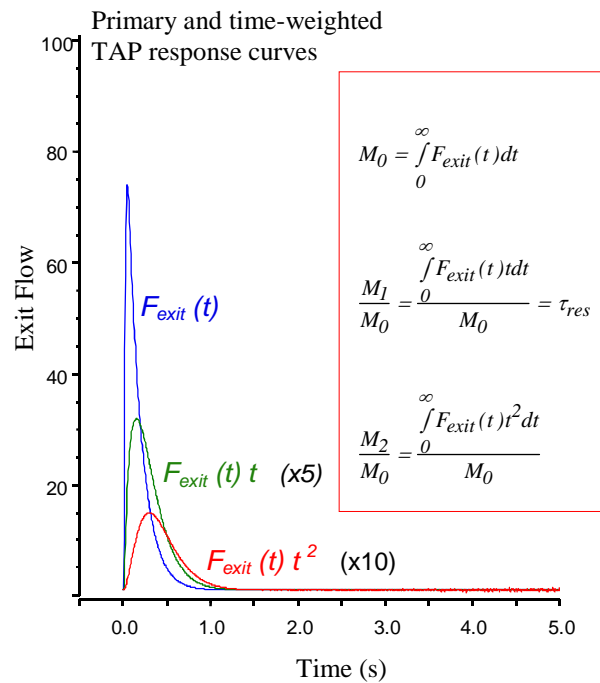


**Figure 3.9** Moment analysis in TAP experiments is the time weighted areas under the exit flow curves.

Although concentration and temperature gradients in the catalyst zone are very small in the TZTR, some non-uniformity will still be present. Non-uniformity can be attributed to two factors: the applied concentration gradient, which drives diffusion and is present even when no reaction occurs, and chemical reaction, which changes the concentration profile in the catalyst zone [9, 75, 76, 90, 92]. These factors are taken into account in the

following equation:

$$\frac{C_{in} - C_{out}}{C_{in}} \approx 2 \frac{L_c}{L_r} + \frac{X}{1 + (1 - X)L_r / L_c} \quad (3.47)$$

The first term on the right hand side of Equation 3.47 relates only to the geometric configuration of the reactor, and the second relates to the influence of chemical reaction and geometry. As with a differential PFR, non-uniformity in a TZTR is proportional to conversion, but the proportionality is not linear. Figure 3.10 shows a comparison of non-uniformity in the TZTR and a PFR as a function of increasing conversion. Over a wide range of conversions (up to 75%), the level of non-uniformity in a TZTR is not higher than 20 percent, and only becomes significant at conversions greater than 80%.

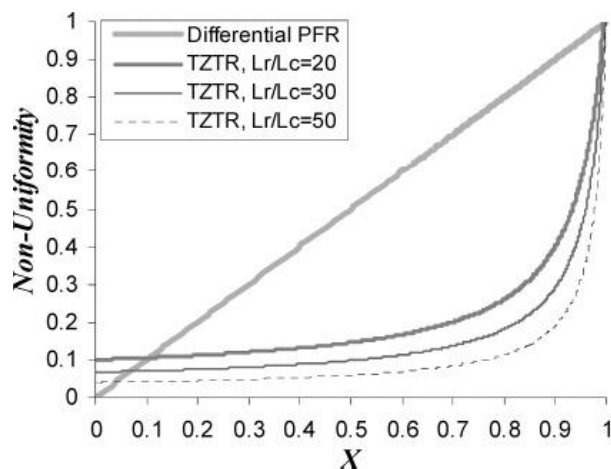


**Figure 3.10** Comparison of non-uniformity versus conversion for the differential PFR and TZTR. Different ratios of microreactor length to length of catalyst zone are given for the TZTR.

Theory for the newly developed single particle TAP microreactor will be discussed in detail in Chapter 4. In this configuration, temperature and concentration gradients are assumed to be negligible in the catalyst zone because there is only one micron-sized catalyst particle in the microreactor bed.

## 3.2 Catalyst Preparation and Surface Analysis

### 3.2.1 Pt Bulk Metal Particle

The Pt bulk metal catalyst used for the single particle experiments is a 400  $\mu\text{m}$  diameter platinum (Pt) powder supplied by the Goodfellow Corporation. The platinum powder was reported with a purity of 99.95%. Platinum was chosen for these experiments

because platinum is known to have high catalytic activity for CO oxidation, reduced “bulk oxygen storage,” and it is fairly easy to purchase. In a typical experiment, the microreactor was packed with approximately 100,000 quartz particles (210 - 250 microns in diameter) and a single catalyst particle (300 - 400 microns in diameter) usually positioned in the center of the bed (Figure 3.11). The quartz particles were made by grinding large quartz fragments and then passing the ground particles through a sieve to extract the appropriate size. The microreactor is heated resistively, and the internal temperature adjacent to the catalyst particle is sampled with a shielded thermocouple. The catalyst particle and the inert quartz particles are nonporous so that gas diffusion or mass transfer within particles does not occur. When packed in the microreactor, the particle occupies less than 0.3% of the cross-sectional area of the microreactor, so that the reaction zone can be considered a point source. An important advantage of this configuration is that for most reactions, concentration and temperature gradients can be assumed to be negligible.

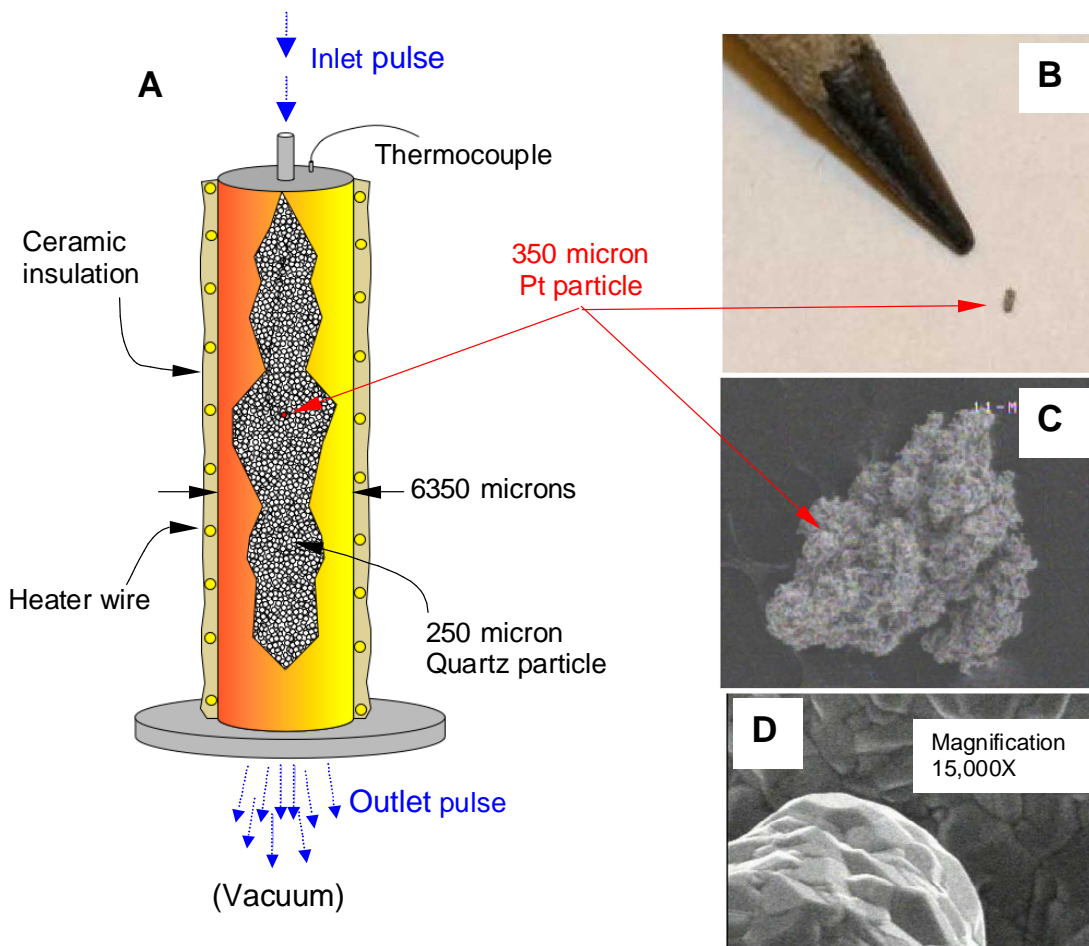


**Figure 3.11** (A) Schematic of TAP microreactor single particle configuration. (B) Digital camera image comparing the Pt particle to a pencil point to demonstrate the actual size of the catalyst particle. (C) SEM image showing the entire polycrystalline Pt particle. The diameter of the particle is estimated to be 350  $\mu\text{m}$ . (D) High magnification (15,000X) SEM image of Pt particle surface, which shows the surface is nonporous.

### 3.2.2 Pt Foil

A Pt foil catalyst particle was used in the single particle experiments to demonstrate the influence of catalyst position in the microreactor on conversion. A Pt foil was used



because it closely resembled the experimental configuration created for the single particle TAP microreactor theoretical model. The Pt foil was cut to be circular with a diameter of 0.125 in. and a thickness of 0.004 in. The Pt foil was packed in the microreactor surrounded by inert quartz particles with diameters between 210-250  $\mu\text{m}$ . The catalyst was placed in three different positions within the microreactor, at the very top located near the microreactor inlet, in the middle, and at the bottom of the microreactor close to the outlet. The Pt foil was packed in the microreactor with the flat circular surfaces facing towards the microreactor inlet and outlet. The length of the Pt foil occupies approximately 0.496 of the radial length of the reactor.

### **3.2.3 Supported Pt Catalysts**

Pt nanoparticles supported on two types of mesoporous silica was studied in the TAP reactor to understand the role of the support during chemical reaction as well as any metal-support interactions. The supported Pt catalysts were supplied by our collaborators at Kasetsart University in Thailand. The two types of mesoporous silica supports used in the experiments are SBA-15 and unimodal porous silica (UPS). The mesoporous silica SBA-15 was prepared from rice husk ash (RHA) with the chemical composition of the materials used in the molar ratio of  $\text{SiO}_2$ : Pluronic P123: HCl:  $\text{H}_2\text{O}$  as 1: 0.0875: 4: 200, respectively. First, Pluronic P123 was dissolved in distilled  $\text{H}_2\text{O}$ . Next, the rice husk ash derived sodium silicate was slowly added to the Pluronic P123 – water solution while it was being rapidly stirred at 40 °C. Then, HCl was rapidly added into the solution in order to initiate the hydrolysis-condensation reaction. The hydrolysis-condensation

reaction was allowed to continue for 24 h after the addition of HCl, and the solution was continuously stirred during this time. After 24 h, the solution turns into a silica gel, which is then transferred to a Teflon-lined autoclave for hydrothermal aging to take place at 100 °C for 24 h. After this time period, the solid products can be collected by filtration, then dried in an oven at 140 °C for 3 h, and finally calcined in air at 500 °C for 6 h [93].

The unimodal porous silica (UPS) was also prepared using sodium silicate ( $\text{Na}_2\text{Si}_3\text{O}_7$ : 27 wt.%  $\text{SiO}_2$ ; 4 wt.% NaOH) that was derived from rice husk ash. In the first step of the procedure, 3.7 g of sodium silicate (based on 1 g of  $\text{SiO}_2$ ) was slowly added to 60 mL of 2% v/v acetic acid in water solution that was being stirred and heated at 40 °C in a water bath. In order to simultaneously initiate the hydrolysis-condensation reaction and control the pH of the mixture in the range of 2 to 6, various amounts of 1 M HCl or 1 M NaOH were rapidly added into the solution. The final pH of the solution was measured to be 5. After the hydrolysis-condensation reaction has continued for 24 h, the resulting gel was transferred to a Teflon-lined autoclave where the hydrothermal aging process was set at 100 °C for 24 h. The final products were filtered, dried in an oven at 120 °C for 3 h, and calcined in air at 550 °C for 5 h [94].

Figure 3.12 compares the SEM and TEM images of the mesoporous silica SBA-15 and unimodal porous silica (UPS) supports. From the SEM images, the morphology of the SBA-15 (Figure 3.12a) contains an agglomeration of uniform, slightly bent (U-shaped),

short rod-like shapes, while the UPS support (Figure 3.12b) shows a much more dense surface morphology caused by the agglomeration of much smaller silica nanoparticles. The TEM image of the SBA-15 support (Figure 3.12c) shows a highly ordered mesoporous silica matrix with a hexagonal pore structure. In contrast, the TEM image of the UPS support (Figure 3.12d) shows inter-particle spaces between the mesoporous silica structure caused by the agglomeration of the silica nanoparticles.

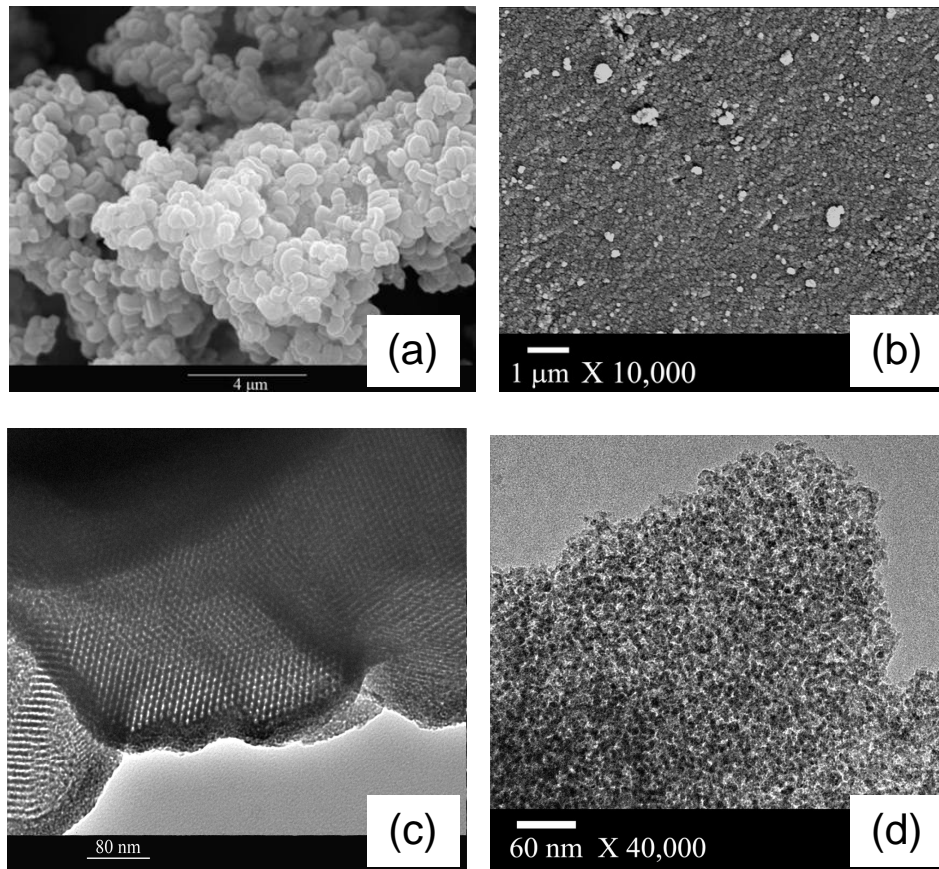


**Figure 3.12** (a)-(b) SEM images of mesoporous silica SBA-15 and unimodal porous silica (UPS), respectively. (c)-(d) TEM images of SBA-15 and UPS, respectively.

There are many methods to deposit metal particles on metal oxide supports. The most common method to prepare metal-supported catalysts is incipient wetness impregnation [95-98]. In this method, a small amount of metal salt solution, just enough to cover the support material surface, is dropped onto the surface of the dry support material. After the metal salt solution comes into contact with the support material, the solution is drawn into the pores of the support by capillary forces inside the pores. Incipient wetness occurs when all pores of the support material are filled with liquid, and there is no excess moisture left over on the support. If the support material is nonporous, a layer of metal coating is left on the outer surface of the support.

The Pt nanoparticles were loaded on the mesoporous silica SBA-15 and unimodal porous silica (UPS) by incipient wetness impregnation using a solution of hydrogen hexachloroplatinum (IV) hexahydrate ( $\text{H}_2\text{PtCl}_6 \cdot 6\text{H}_2\text{O}$ ) and water. The metal salt solution was dropped onto the support so just enough is needed to coat the support surface, and the mixture was stirred for 30 min. After 30 min, the wet catalyst was placed in an oven to be dried at 120 °C for 24 h. Once the catalyst is dry, it was calcined with  $\text{H}_2$  at 550 °C for 4 h with a heating rate of 4 °C/min. The calcination process was performed to remove any volatile matter left on the catalyst surface during the impregnation step such as chlorine. Figure 3.13 shows the SEM images of the SBA-15 and UPS supports after they were compressed to form 400 micron-sized particles and impregnated with Pt.

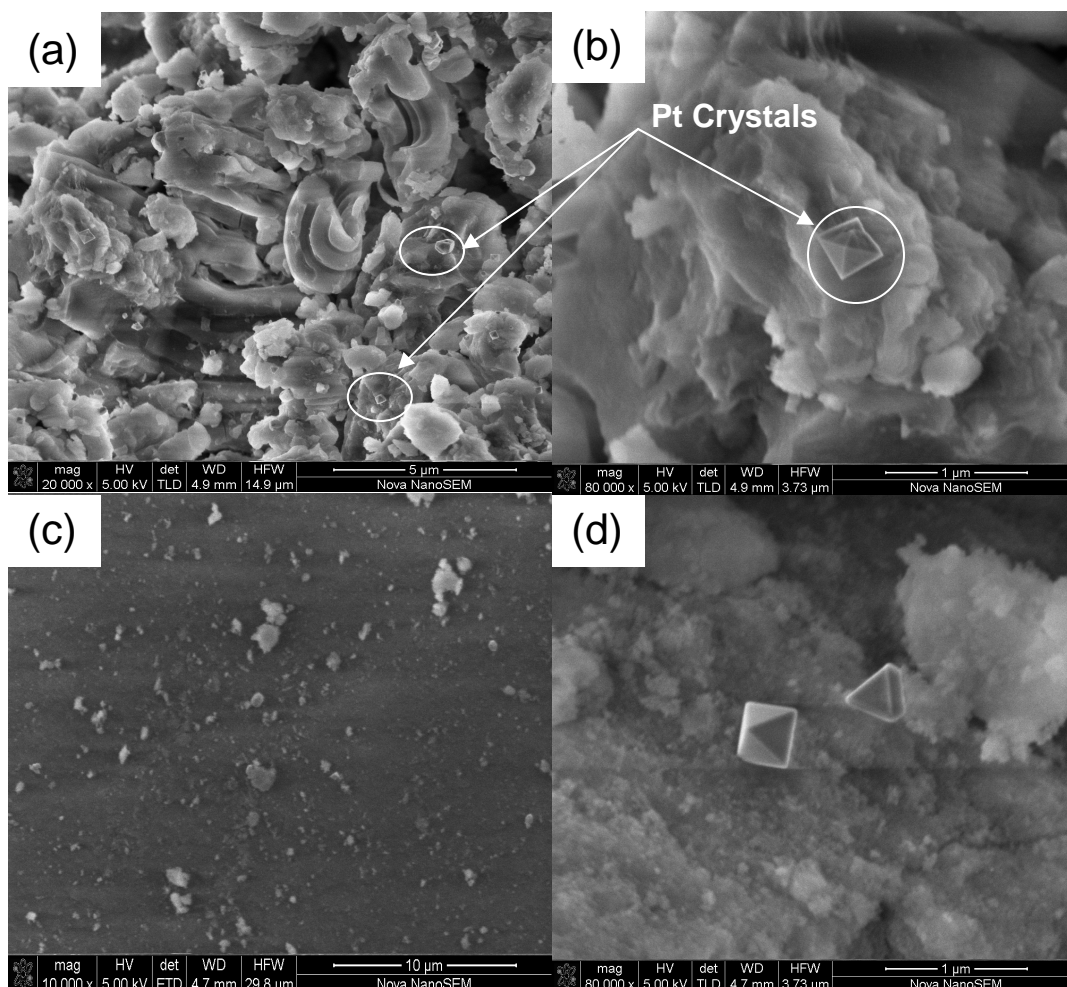


**Figure 3.13** (a)-(b) SEM images of mesoporous silica SBA-15 after compression to form 400  $\mu\text{m}$  sized particles and impregnation with Pt at magnification of 20,000X and 80,000X, respectively. (c)-(d) SEM images of UPS after compression to form 400  $\mu\text{m}$  sized particles and impregnation with Pt at magnification of 10,000X and 80,000X, respectively.

The SBA-15 support after compression still retains some of the physical characteristics of the support prior to compression, such as the preservation of the slightly bent, U-shaped rods. The support is very porous as seen by the appearance of holes in between the

structure of the SBA-15 support. After impregnation of the SBA-15 with the Pt salt solution, Pt and Pt single crystal nanoparticles were deposited on the surface. The Pt single crystals formed as a result of support surface defects from the compression process.

The formation of Pt single crystals was also apparent on the compressed UPS support. The surface and structure of the UPS support after the compression process was very similar to the structure prior to compression. The structure of the UPS support was already very densely packed with silica nanoparticles; therefore, the compression process did not change the structure very much. Compared to the SBA-15 support, the UPS support is not as porous, and the silica particles are much smaller. Because the UPS support is less porous, there is less surface area for the Pt particles to deposit on. Using SEM, an area of equal size on the SBA-15 and UPS surface was selected to determine Pt composition percentage. For the SBA-15, there was 6.55 wt. % Pt on the surface, and 4.88 wt. % Pt on the surface of the UPS support. The rest of the catalyst composition was composed of Si and O. The weight percent determined by SEM is only an estimate because there could be Pt in the pores of the catalyst that cannot be seen with SEM.

### **3.2.4 VPO Catalysts**

Vanadium phosphorus oxide catalysts were prepared by refluxing a mixture of 7340 cm<sup>3</sup> of isobutyl alcohol, 513.5 grams of V<sub>2</sub>O<sub>5</sub> and 663.97 grams of H<sub>3</sub>PO<sub>4</sub> (100%) for 16 hours to give a light blue precipitate. Upon cooling, the precipitate was filtered and dried

at ambient temperature under vacuum. The dried precipitate was washed with isobutyl alcohol, dried for 2.5 hours at 145 °C and calcined in air for 1 hour at 400 °C. The resulting powder was then "reactor equilibrated" by switching the feed to an air-butane mixture (1.5% butane) at 15 psig reactor inlet pressure and 2000 GHSV. After a sufficient break-in period (300 hours), the catalyst gave steady-state selectivities to maleic anhydride of approximately 66% at 78% conversion. XRD analysis of the reactor equilibrated samples showed that they were monophasic  $(VO)_2P_2O_7$  or (VPO). Chemical analysis gave a P/V ratio of 1.01 and vanadium oxidation state of 4.02. The samples had a BET surface area of 16.5 m<sup>2</sup>/gram. Figure 3.14 shows an SEM image of the microstructure of a VPO particle, which has the characteristic layered structure of VPO prepared by a non-aqueous route.

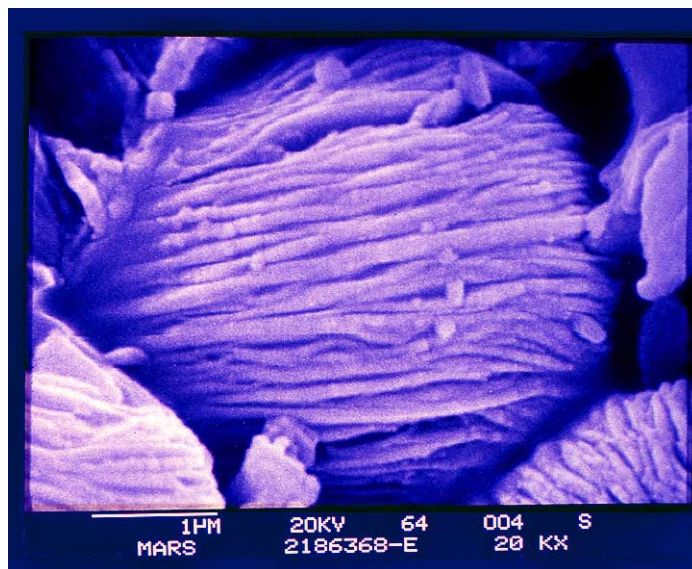


**Figure 3.14** SEM image of VPO particle. The image shows a characteristic layered structure.

# Chapter 4

## CO Oxidation on Pt Catalysts

This chapter presents results from TAP experiments performed on a variety of Pt catalysts including a single Pt bulk particle, Pt foil, and Pt nanoparticles supported on two types of SiO<sub>2</sub> support. The catalysts are probed using the CO oxidation reaction to understand reactor transport properties, metal-support interactions, influence of reaction pressure, and the role of surface oxygen lifetime on catalytic performance.

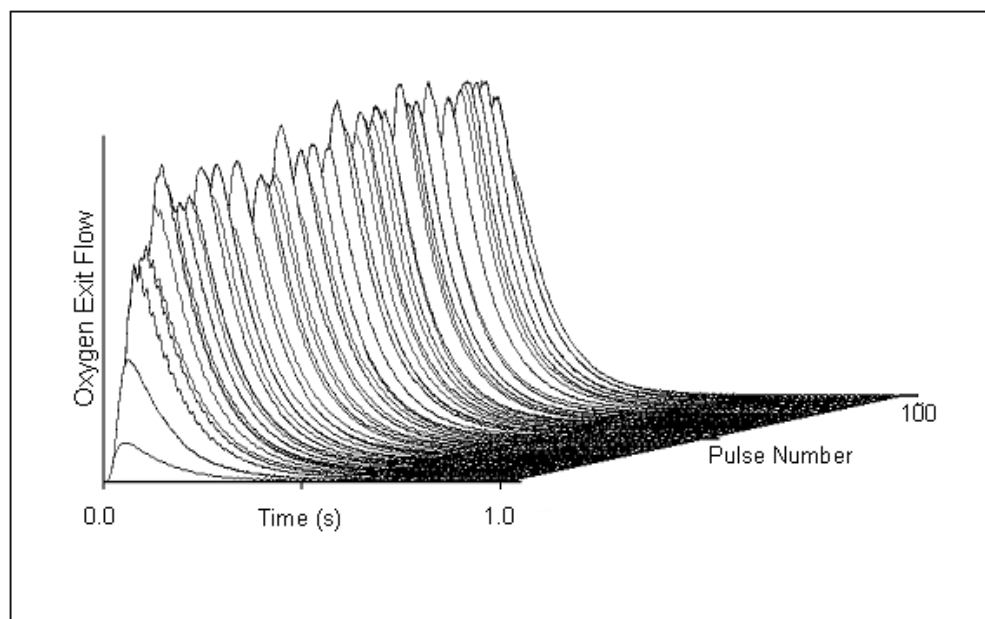
### 4.1 Single Pt Bulk Particle TAP Experiments

#### 4.1.1 Oxygen Uptake

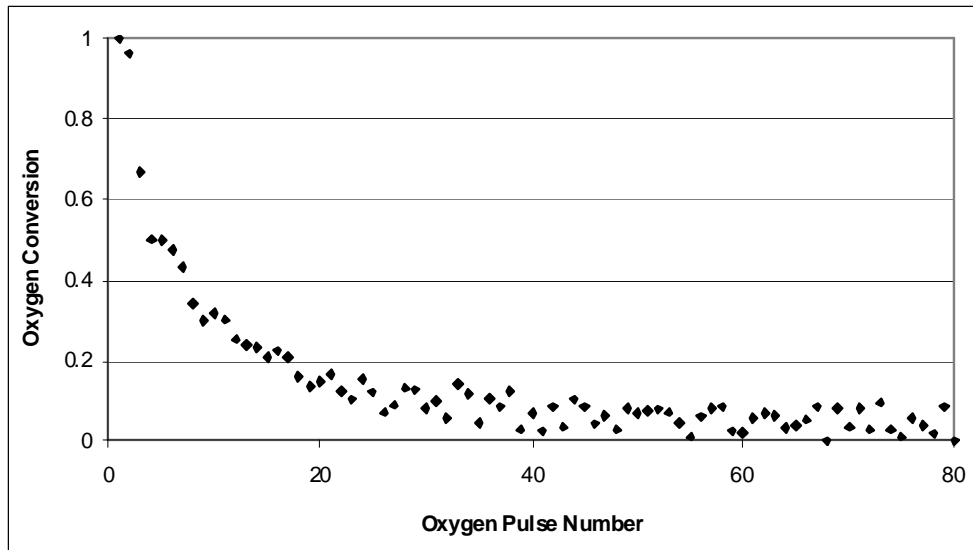
To determine the number of oxygen adsorption sites a mixture of O<sub>2</sub>/Ar (70/30 feed ratio) was pulsed into the microreactor over a reduced catalyst particle. The Pt particle was reduced in a hydrogen flow (H<sub>2</sub>/Ar = 1, Flow rate = 40 cc/min, T = 350 °C, P = 1 atm) for 1 hour and the reduction was assumed complete when water production was no longer observed. After flowing hydrogen for 1 hour, the reactor temperature was reduced to 50 °C and the Pt particle was exposed to a series of oxygen pulses. Low temperature oxidation limits migration of O atoms to the particle subsurface.



Figure 4.1 shows a typical series of oxygen exit flow response curves observed after reduction with a hydrogen flow. The oxygen conversion is calculated from the area under each of the pulse curves shown in Figure 4.1, and the oxygen conversion per pulse is plotted in Figure 4.2. Each pulse contains approximately  $10^{14}$  oxygen molecules. After approximately 40 oxygen pulses conversion is zero and the area under the zero-conversion curve can be used to calculate the conversion in previous curves and the total oxygen conversion. The  $O_2$  responses were also normalized with respect to the standard Ar diffusion curve to take into account changes in pulse shape related to changes in pulse intensities. The first oxygen pulse is completely adsorbed on to the Pt particle. As the number of oxygen pulses increases, the number of available oxygen binding sites decreases until, after approximately 40 pulses, the particle surface is saturated.



**Figure 4.1** Oxygen exit flow response curves obtained from single Pt particle oxygen uptake experiment at 50 °C.



**Figure 4.2** Oxygen conversion per pulse found by taking the area under each of the exit flow pulse curves from Figure 4.1.

#### 4.1.2 Reaction under Vacuum Conditions

CO oxidation Pt particle pulse response experiments were performed using the "pump-probe" format (Figure 4.3). Mixtures of O<sub>2</sub>/Ar (70/30) and CO/Ar (70/30) stored in separate pulse valves were injected into the microreactor forming a train of alternating pulses of O<sub>2</sub> and CO. Similar to oxygen uptake experiments, in CO oxidation experiments argon is mixed with the reactant gases to act as a reference. Because it is inert, its transient response depends only on the transport process. It is used as a measuring stick to calculate diffusivities, conversion, and kinetic parameters. The pump-probe format maintains a relatively steady oxygen concentration on the catalyst by re-supplying any consumed oxygen in alternating O<sub>2</sub> pulses. In single Pt particle experiments, CO conversion was constant during multi-pulse pump-probe experiments at

a steady reactor temperature. Therefore, based on experimental evidence, it can be stated that the oxygen coverage on the Pt particle is restored to the same value prior to each CO pulse.

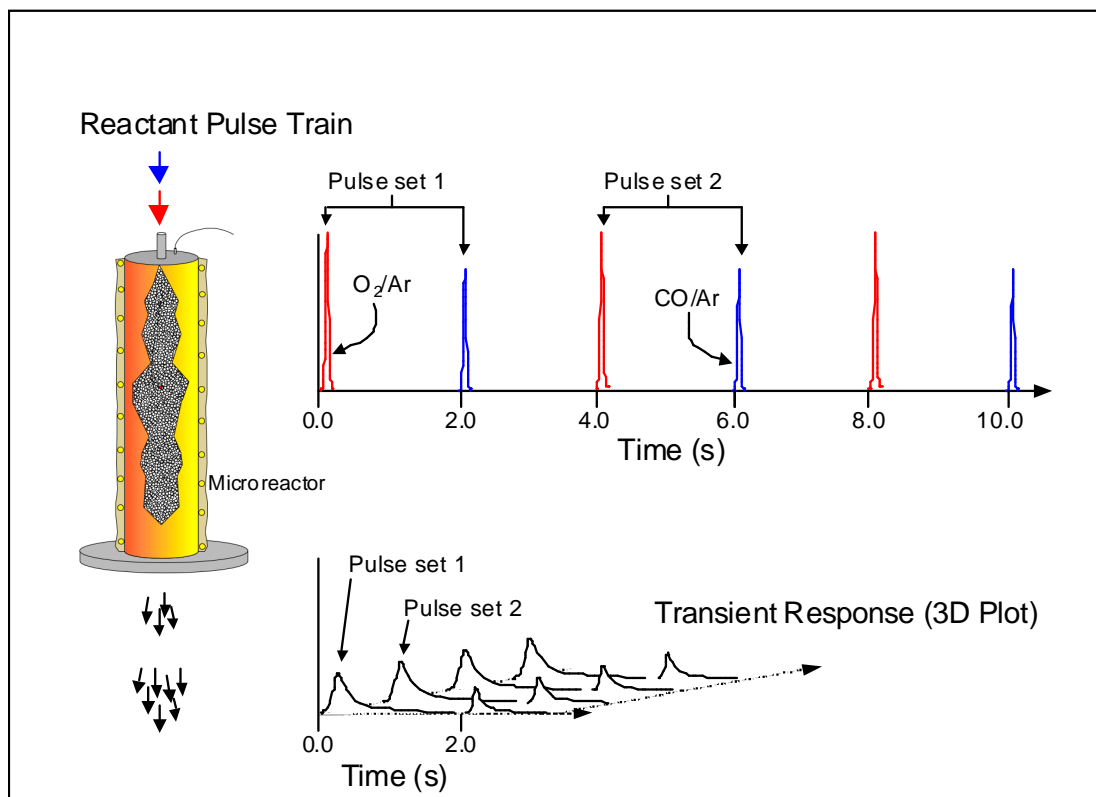


**Figure 4.3** Schematic of TAP single Pt particle pump-probe experiment.

In a pump-probe experiment [22, 23], the separation time between reactant pulses can be varied. Time delay between the reactant pulses can be changed to investigate the effect of changes in the surface lifetime of reactive adspecies on the dynamics of catalyst surface processes. For example, by changing the time between the O<sub>2</sub> and CO pulses, the relative desorption rates can be determined.

In the experiments plotted in Figure 4.4, the O<sub>2</sub> and CO pulses were evenly spaced and separated by 2 seconds. Identical experiments using time delays of 1 second and 3 seconds were also performed, and no difference in the amount of CO<sub>2</sub> produced was observed. This indicates that the surface oxygen storage is approximately constant within the pump-probe time delays. The argon response curve in the Pt particle pump-probe experiments shows that > 99% of the Ar escapes the reactor in less than 2 seconds. Thus, when a CO pulse enters the reactor < 1% of the gas phase oxygen from the previous O<sub>2</sub> pulse remains, and vice-versa when oxygen is pulsed. The amount of CO<sub>2</sub> produced in the pump-probe transient response experiment (Figure 4.4A and 4.4C) can be determined by measuring the area (zeroth moment) under the transient response curve [91]. To determine the CO<sub>2</sub> yield, the zeroth moment is normalized relative to the amount of CO in a single pulse. If the amount of CO<sub>2</sub> produced is equal to the amount of CO injected then the yield is equal to 100%. The absolute amounts of O<sub>2</sub>, CO, and CO<sub>2</sub> are determined by comparing the response obtained in a reaction with one obtained using a standard blend. All responses are compared to the Ar response, which is the internal reference. Remove the platinum particle, leaving only the quartz particles, and the responses disappear demonstrating that no CO<sub>2</sub> is produced.

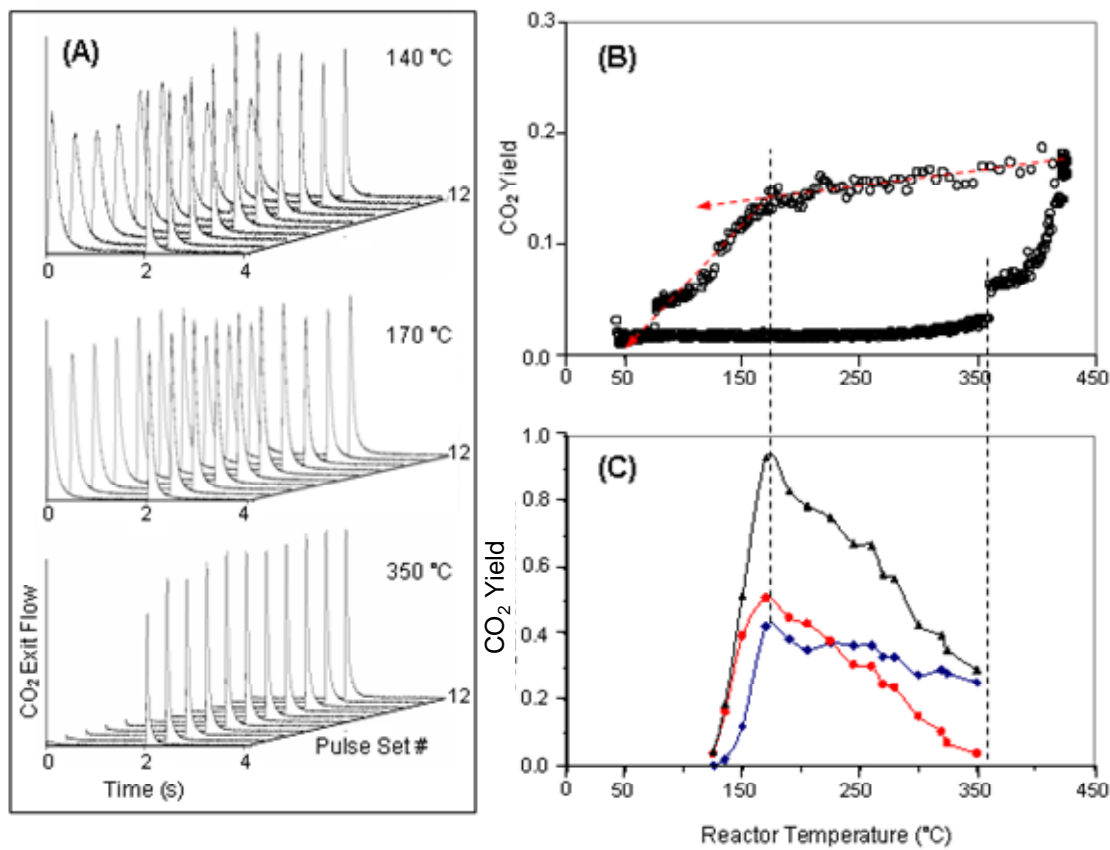


**Figure 4.4** Comparison of CO<sub>2</sub> produced during TAP vacuum pump-probe and atmospheric flow experiments for CO oxidation over single Pt particle with the same composition of reactants. (A) A typical set of pump-probe CO<sub>2</sub> responses ( $m/e = 44$ ) for reaction at 140, 170, and 350 °C. (B) CO<sub>2</sub> production observed from atmospheric flow experiment. (C) CO<sub>2</sub> production observed from vacuum pump-probe experiment. The black line (-▲-) represents the total CO<sub>2</sub> yield. The red (-●-) and blue lines (-◆-) represent the CO<sub>2</sub> yield on the oxygen pulse and CO pulse, respectively.

The black plot (Figure 4.4C) represents the total CO<sub>2</sub> yield during one pump-probe cycle. The red and blue plots (Figure 4.4C) show the CO<sub>2</sub> yield for O<sub>2</sub> pulses and CO pulses respectively. The striking feature of these dependences is the high CO<sub>2</sub> yield that is

achieved despite the catalyst particle occupies less than 0.1% of the total reactor volume. At 170 °C, the yield for the individual O<sub>2</sub> and CO pulses reach a maximum, making the total yield equal to approximately 95% during one pump-probe cycle. This result seems counterintuitive, however it has physico-chemical ground. Under Knudsen diffusion conditions, at least 95% of the CO molecules pulsed into the reactor must strike the particle. The probabilistic mathematical theory of this phenomenon together with additional experimental data will be presented in Chapter 4.2. Above 170 °C the CO<sub>2</sub> yield decreases, more rapidly for the O<sub>2</sub> pulse than the CO pulse. From 170 to 350 °C, the CO<sub>2</sub> yield on the oxygen pulse decreases from a maximum of 52% to < 5%. In the same interval, the yield on the CO pulse decreases from 43% to 25%, so that the overall yield drops from 95% to less than 30%.

The difference between CO<sub>2</sub> dependences obtained in O<sub>2</sub> and CO pulse experiments can be explained within the modified adsorption mechanism (Langmuir-Hinshelwood mechanism). During the O<sub>2</sub> pulse, adsorbed oxygen may react with adsorbed CO molecules which are likely isolated at the reaction temperatures. In contrast, during the CO pulse, the adsorbed CO molecule may interact with different forms of stored oxygen, e.g. via the gradual destruction of the surface oxygen structure (surface phase islands). In this case, the CO<sub>2</sub> yield decreases not so rapidly. However, there is a general feature of both dependences. The yield peak (“turning point”) occurs at the same temperature of 170 °C for both CO and O<sub>2</sub> pulses. Based on the adsorption mechanism, it is reasonable

to assume that it is the point of transition from the CO dominated catalyst surface (below 170 °C) to the O<sub>2</sub> dominated catalyst surface (above 170 °C).

### **4.1.3 Reaction at Atmospheric Pressures**

After completing the set of vacuum pulse response experiments, the slide valve was closed so that the reactor could be operated at atmospheric pressure. Prior to introducing an O<sub>2</sub>/CO mixture, the particle bed was exposed to a hydrogen flow (20 cc/min diluted in Ar, H<sub>2</sub>/Ar = 1) at 350 °C for 1 hour. The hydrogen flow was used to remove any memory of the previous pump-probe experiments. The reactor was then cooled and a total flow of 50 cc/min of O<sub>2</sub>, CO, and Ar (O<sub>2</sub>/CO/Ar = 1) was introduced through the continuous valve, giving a gas residence time in the reactor of 1.8 s. Conversion under atmospheric conditions was quite high despite the short contact residence time inside the reactor (Figure 4.4B).

The temperature dependence of CO<sub>2</sub> production was obtained by heating or cooling the reactor at a constant rate while maintaining an input flow of 50 cc/min. The internal reactor temperature was ramped from 40 °C to 430 °C over a 40 minute interval. Upon reaching 430 °C, the reactor temperature was held constant for 5 minutes and then decreased at the same ramp rate to room temperature.

During atmospheric pressure experiments, a small amount of the reactor effluent was diverted into the mass spectrometer chamber, and its mass spectrum was continuously

monitored. The temperature dependence of the CO<sub>2</sub> yield is characterized by two branches, which form a counter-clockwise hysteresis loop (Figure 4.4B). The lower branch occurs during the up ramp and the upper branch during the down ramp. On the lower branch of the hysteresis loop, at approximately 350 °C, a dramatic rise in CO<sub>2</sub> yield is observed. On the upper branch of the hysteresis loop, a maximum in CO<sub>2</sub> production of 20% is observed at 430 °C. At the temperature of approximately 170 °C (“turning point”), a significant decrease of CO<sub>2</sub> occurs. The phenomenon of yield hysteresis is well known in heterogeneous catalysis, particularly in the heterogeneous CO oxidation reaction over noble metals [99]. Such behavior is also explained based on the adsorption mechanism in which O<sub>2</sub> and CO compete for active catalytic sites on the metal surface. From this point of view, the “turning point” is the temperature at which O<sub>2</sub> domination on the Pt surface is changed by the CO domination of the catalyst.

#### **4.1.4 Comparison of Results from Vacuum and Atmospheric Pressure Regimes**

Both vacuum and atmospheric pressure data exhibit several striking features. Perhaps most surprising is the very high conversion observed in TAP pulse response experiments. Despite the fact that the Pt particle occupies less than 0.1% of total reactor volume and 0.3% of its cross sectional area, it is struck by at least 95 out of 100 CO molecules pulsed into the reactor. Similarly since oxygen conversion is 100% during the first oxygen pulse in oxygen uptake experiments every oxygen molecule must strike the Pt particle. In a TAP vacuum pulse response experiment, gas molecules move independently, primarily



colliding with particles and the reactor walls. On average, a CO molecule experiences between 100,000 to 500,000 collisions before it exits the microreactor [100]. As a result, a molecule that initially bypasses the Pt particle can reverse its direction during its next collision and return to the Pt particle.

Conversion in atmospheric pressure experiments is quite high. The residence time in the microreactor is longer than in a TAP experiment, but the apparent contact residence time in the reaction zone is about 2 orders of magnitude less. Nevertheless, CO conversion reaches 20%. Clearly, the real residence time in the reaction zone is larger, and mixing is also significant in atmospheric flow experiments.

An essential requirement for obtaining precise kinetic data is uniformity within the reaction zone in the reactant concentration profile and catalyst composition. The reactant concentration can be defined as uniform if its spatial difference is small compared to its maximum value. In single particle experiments the reaction zone is the particle surface. In vacuum pulse response experiments the reaction zone samples the entire reactor volume, and our estimates show that non-uniformity is negligible [9]. In atmospheric pressure experiments the reaction zone samples an area at least 67 times larger than the particle. Consequently, in both experiments non-uniformity is negligible, so it can be assumed the reaction zone is perfectly mixed.

Pulse response data obtained in high vacuum experiments can be used for direct determination of the number of active sites or storage of an active component [23, 40]. For a single particle, this number is comparable with the number of molecules in a pulse, and can be determined in a single experiment. Data from TAP pulse-response experiments can also provide details related to the steps in a complex reaction, i.e. kinetic coefficients of different reactions (reactant adsorption, interaction of reactants with other pre-adsorbed reactants), energies of activation and pre-exponential factors, and the dependence of all these parameters on the catalyst pre-treatment [23, 24].

Both TAP vacuum and atmospheric pressure data sets exhibit turning points indicating a transition from reaction controlled by one adsorbed species to one controlled by a different adsorbed species. The upper branch in the CO<sub>2</sub> curve corresponds to an O<sub>2</sub> covered surface, and the lower branch to a CO covered surface (Figure 4.4B). The turning point in both data sets occurs at 170 °C (Figure 4.4B – 4.4C). In the region of the CO<sub>2</sub> maximum, the areas under the CO<sub>2</sub> response curves corresponding to the O<sub>2</sub> and CO pulses (Figure 4.4A) are approximately the same, indicating nearly equal coverages for O<sub>2</sub> and CO. The correspondence in “turning points” indicates that the coverage in vacuum and atmospheric pressure experiments is approximately the same and intrinsic kinetic data obtained in vacuum experiments can be used to describe kinetic behavior in the atmospheric pressure domain.

Taking the conversion of CO or CO<sub>2</sub> yield at the “turning point” from vacuum pulse response and atmospheric flow data, the apparent kinetic rate constant can be calculated. In combination with the gas residence time ( $\tau$ ) in the catalyst zone, the apparent kinetic rate constant is given by the following expression:

$$k_{\text{apparent}} = \frac{X}{(1-X)\tau} \quad (4.1)$$

Using an approximate conversion of 90% in the vacuum pulse response experiment, the apparent kinetic rate constant is calculated to be 9000 s<sup>-1</sup>. In the atmospheric flow experiment, using a conversion of 20% the apparent kinetic rate constant is calculated to be 9280 s<sup>-1</sup>. The two apparent kinetic rate constants differ by approximately 3%. Although there may be some error involved in experimentation, the values of the apparent kinetic rate constants are approximately the same. The ability to relate data both qualitatively and quantitatively in the atmospheric pressure domain to the data obtained in vacuum pulse response experiments using a single Pt particle is a step toward bridging across the pressure gap [51].

#### **4.1.5 Inert Experiments**

Blank experiments were run using a microreactor packed only with inert quartz particles to test the validity of the single Pt particle experiments. The blank experiments were conducted in the same manner with all identical reaction conditions as the Pt particle pump-probe experiments. The only difference was that the blank experiments had no catalyst in the reactor. Figure 4.5 plots the CO<sub>2</sub> production (zeroth moment) as a function of reactor temperature. The graph gives the CO<sub>2</sub> produced on the oxygen pulse, CO

pulse, and the total CO<sub>2</sub> production. The temperature range is from 100 °C to 280 °C, which is the range where maximum CO<sub>2</sub> production was observed for the single Pt particle experiments. According to Figure 4.5, the CO<sub>2</sub> produced on the oxygen and CO pulses reached a maximum production of 1.5 and 0.5% at 280 °C, respectively. Although the reactivity of the microreactor or the inert quartz particles is apparent, it is not significant compared to the amount of CO<sub>2</sub> produced with the Pt particle in the microreactor. Also, there is no trend in the maximum CO<sub>2</sub> peak seen with the Pt particle at 170 °C.

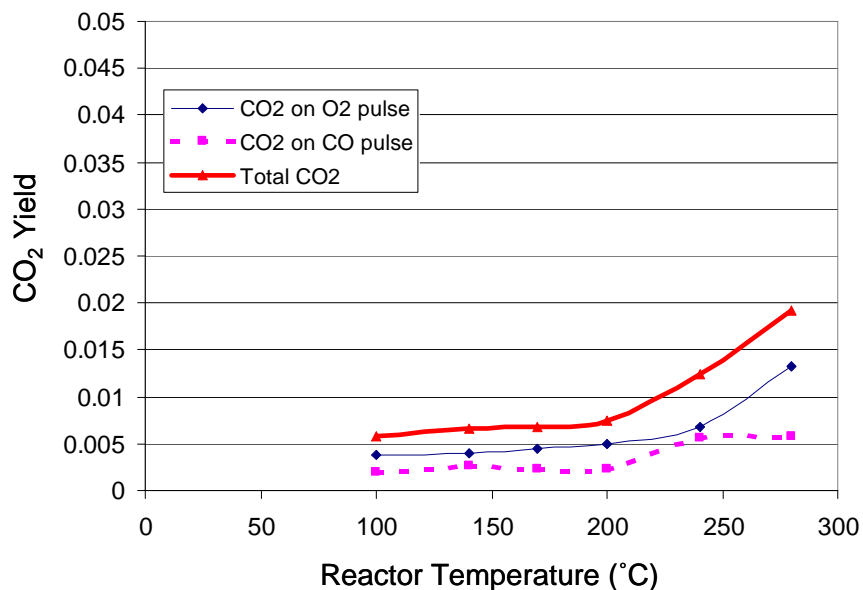


**Figure 4.5** CO<sub>2</sub> production observed in the inert microreactor with quartz packing only.

#### 4.1.6 Surface Lifetimes of Reactive Species

The surface lifetime of an adspecies under reaction conditions is a function of the rate of reaction, the rate of desorption, and the rate at which the adspecies diffuses into the catalyst bulk. The adsorption-desorption characteristics of a species can be determined

in TAP pulse response experiments by comparing the exit flow curve of the species with the standard diffusion curve (STD). If the curve falls inside the STD then the species is irreversibly adsorbed. The surface concentration of an active species can also decrease if the species diffuses into the catalyst bulk or is depleted by reaction with some other surface species. The reactive lifetime of an adspecies can be measured in TAP pump-probe experiments by changing the pump-probe interval.

The reactive lifetime of oxygen on a Pt particle was measured in a series of pump-probe experiments using two separate reactant mixtures of O<sub>2</sub>/Ar (70/30 ratio) and CO/Ar (70/30 ratio), which were injected from two separate pulse valves. The mixtures were pulsed in an alternating sequence into a microreactor containing a single 400 μm Pt particle packed in a bed of inert quartz particles. In the pump-probe experiments, the separation time between the O<sub>2</sub> and CO pulses was varied while keeping the cycle time for one pump-probe cycle at 10 s. For one reactor temperature, O<sub>2</sub> was always pulsed into the microreactor first followed by the CO pulse separated by a delay of 1, 3, 5, 7, and 9 s. For example, when the interval between the oxygen and CO pulse is 5 seconds, the interval between the CO and following oxygen pulse is also 5 seconds. The experiment was repeated for different pump-probe intervals at 150, 250, and 350 °C (Figure 4.6). CO conversion at one reactor temperature from past multi-pulse pump-probe experiments suggests that oxygen coverage on the single point particle is restored to the same value prior to each CO pulse.

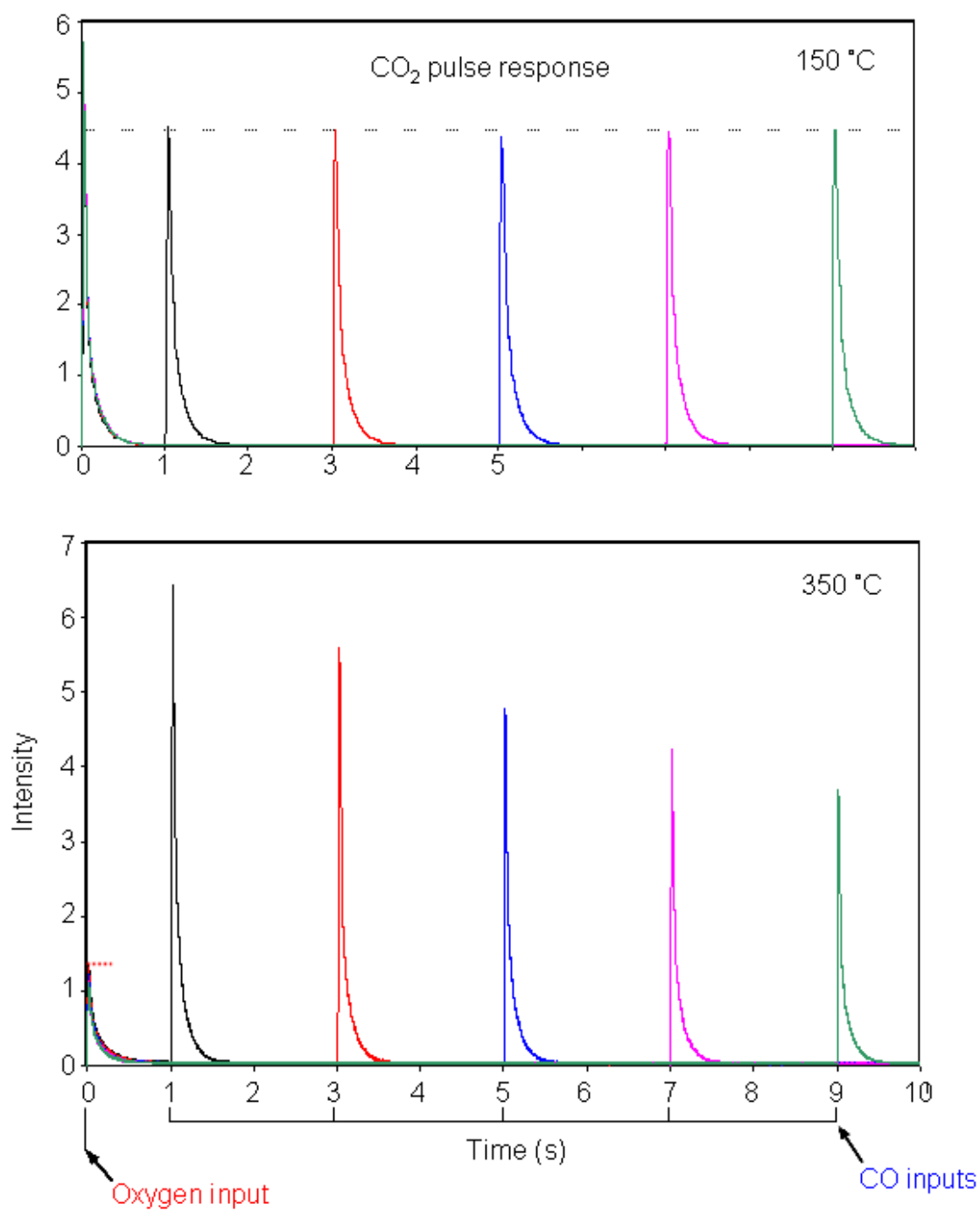


**Figure 4.6** Pump-probe data showing CO<sub>2</sub> production as a function of temperature and pump-probe interval.

CO<sub>2</sub> production on the oxygen pulse at 350 °C is significantly lower than production at 150 °C. It is independent of the pump-probe interval. CO<sub>2</sub> production on the CO pulse at 150 °C is also independent of the pump-probe interval. At 350 °C CO<sub>2</sub> decreases with the pump-probe interval. The drop in CO<sub>2</sub> production can be attributed to a decrease in the amount of active oxygen. The rate of the drop in active oxygen can be calculated from the zeroth moments of the CO<sub>2</sub> and is plotted in Figure 4.7.

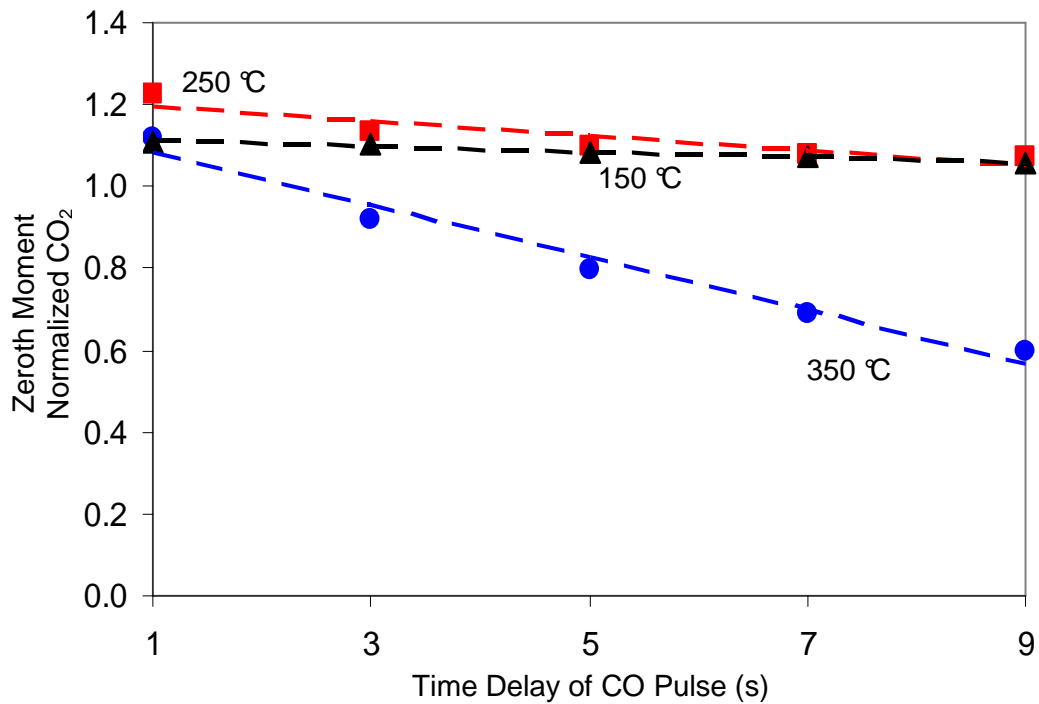


**Figure 4.7** Normalized CO<sub>2</sub> production on the CO pulse calculated from the zeroth moment of the pulse response curve. CO<sub>2</sub> production is constant at 150 °C, and drops to  $\approx 0.5$  times its value in 9 s at 350 °C.

From the CO pulse, the CO<sub>2</sub> is produced as the input of CO reacts with the leftover O<sub>2</sub> from the previous pulse. The data in Figure 4.7 shows that the initial rates of CO<sub>2</sub>

production are approximately the same for all the reaction temperatures. In the literature, it mentions that there are two constituents of the Langmuir-Hinshelwood mechanism for CO oxidation; the reaction between adsorbed oxygen and strongly adsorbed CO, and reaction between weakly adsorbed CO [99]. The mechanism with the latter can be identified as an “impact mechanism” from the collision between adsorbed oxygen and gaseous input of CO. The CO<sub>2</sub> production via the “impact mechanism” does not depend on the temperature. This explains that the initial rates are insensitive to the reaction temperature for a time delay of 1 s. However, for larger delay intervals between the O<sub>2</sub> and CO pulses, there is a dramatic difference in CO<sub>2</sub> production between different temperature dependences. At the highest reaction temperature (350 °C), CO<sub>2</sub> production significantly decreases in time. Between the pulses, no gas should have been in the reactor, and this decrease can be explained only via the presence of the additional “hidden” process, which is acting with no gas presence. This process is oxygen removal from the catalyst surface. Likely, it is a “hidden” process of the oxygen exchange between the surface and the catalyst bulk, and/or between one type of catalyst site and other sites, which are not so active. As for the reaction temperatures of 150 and 250 °C, the CO<sub>2</sub> production decrease is insignificant, especially for 150 °C. Under these temperatures, our catalyst exhibits very stable behavior.

Figure 4.8 plots the CO<sub>2</sub> produced on the O<sub>2</sub> pulse as it reacted with the remaining CO on the surface from the previous pulse. An interesting fact to note from the data displayed in Figure 4.8 is that the increase in reaction temperature does not provoke the reaction rate



to increase as it is usually the case in chemical kinetics. Instead, as the reaction temperature is increased, there is a decrease in the reaction rate. This is less pronounced in the domain between 250 and 350 °C. It is very likely that the temperature dependence of the reaction rate is characterized by a plateau and even by a maximum (see Chapter 4.1.2 and Figure 4.4). In the CO oxidation reaction, which is governed by Langmuir-Hinshelwood mechanism (adsorption mechanism), there is a step in which the two adsorbed substances interact with each other. As the temperature rises, it elevates both the reaction rate between the adsorbed substances (CO and O<sub>2</sub>), and the desorption rate of one of the adsorbed substances (CO). Thus, one can obtain a rate plateau or maximum at some reaction temperature. According to Figure 4.8, there is a slight increase in CO<sub>2</sub> production at every reaction temperature with the increase in spacing interval between the O<sub>2</sub> and CO pulses. This effect is pronounced for 150 °C, but not as significant for 250 and 350 °C.

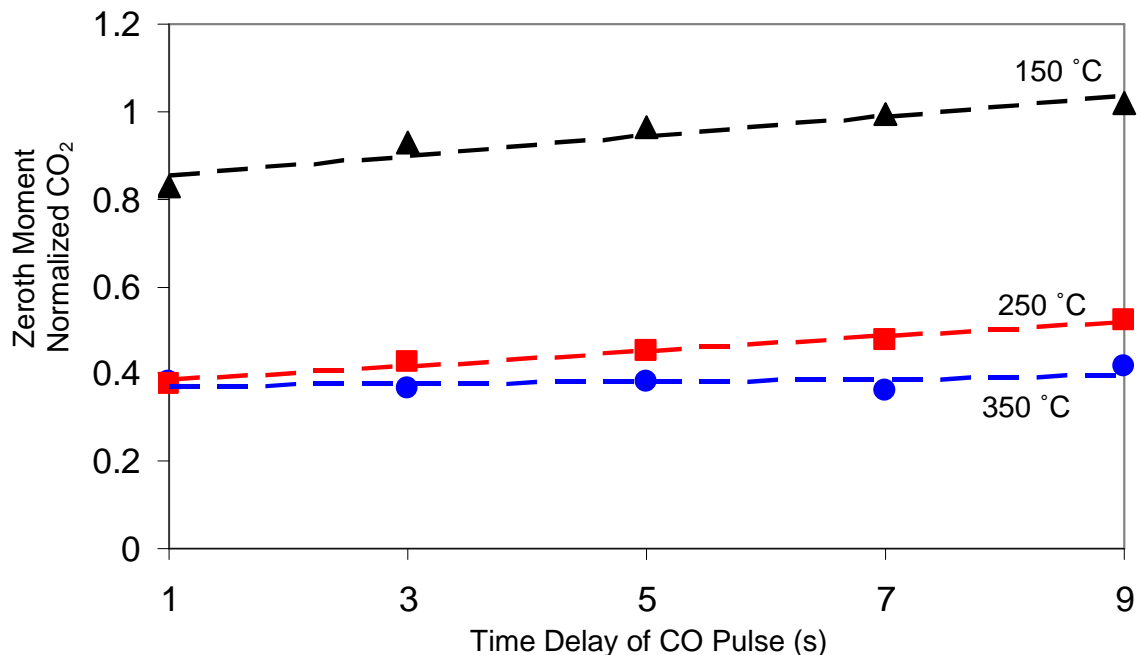


**Figure 4.8** Normalized CO<sub>2</sub> production on the O<sub>2</sub> pulse.

The graph of the total CO<sub>2</sub> production from both the O<sub>2</sub> and CO pulses (Figure 4.9) also demonstrates the advantage of the low temperature regime (in this case, conversion is highest). Two combined factors may contribute to the behavior shown in Figure 4.9:

1. High reaction temperature is not needed because it will promote CO desorption.
2. High reaction temperature is not needed because it will support the process of surface oxygen removal during the interval between pulses.

However, the reaction temperature also cannot be too low. There has to be an optimal temperature, which has to be found experimentally. This will give an indication on the new prototype of the industrial working regime which will be efficient from the point of spending less energy.

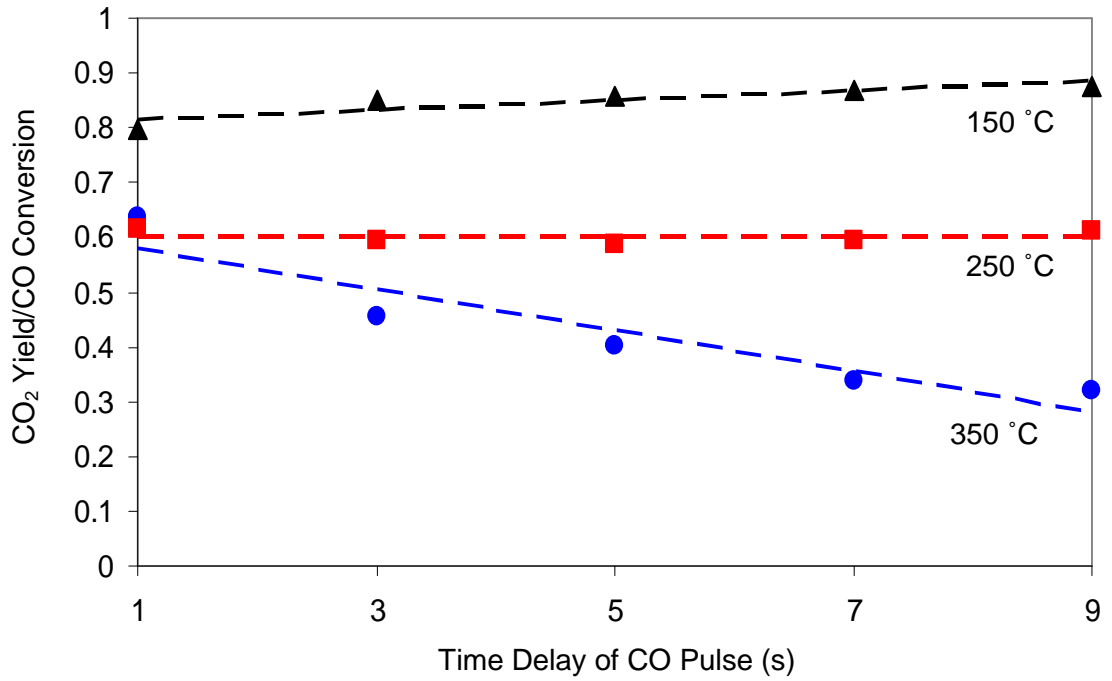


**Figure 4.9** Total CO<sub>2</sub> yield/CO conversion from both O<sub>2</sub> and CO pulses added together.

Apparent kinetic constants can be calculated (Equation 4.1) based on the data shown in Figures 4.7 - 4.9. Figure 4.10 presents the apparent kinetic constant dependence on the time delay of the CO pulse. The apparent kinetic constant is calculated based on the information from the CO pulse because it reveals more information regarding the behavior of surface oxygen. Clearly, the apparent constant at 350 °C demonstrates a significant decay which can be classified as an exponential decay or combination of two exponents. This decay may be interpreted as a process, or a reaction of the pseudo-first order, in which the apparent constant is given by the following equation.

$$K_{app} = K \times (\text{Concentration of surface oxygen}) \quad (4.2)$$

According to the equation above, when surface oxygen is removed, its concentration decreases, therefore, the apparent constant decreases as well. As for dependences at 150 and 250 °C, the temporal decay of apparent constants is insignificant reflecting the similar behavior of conversions.

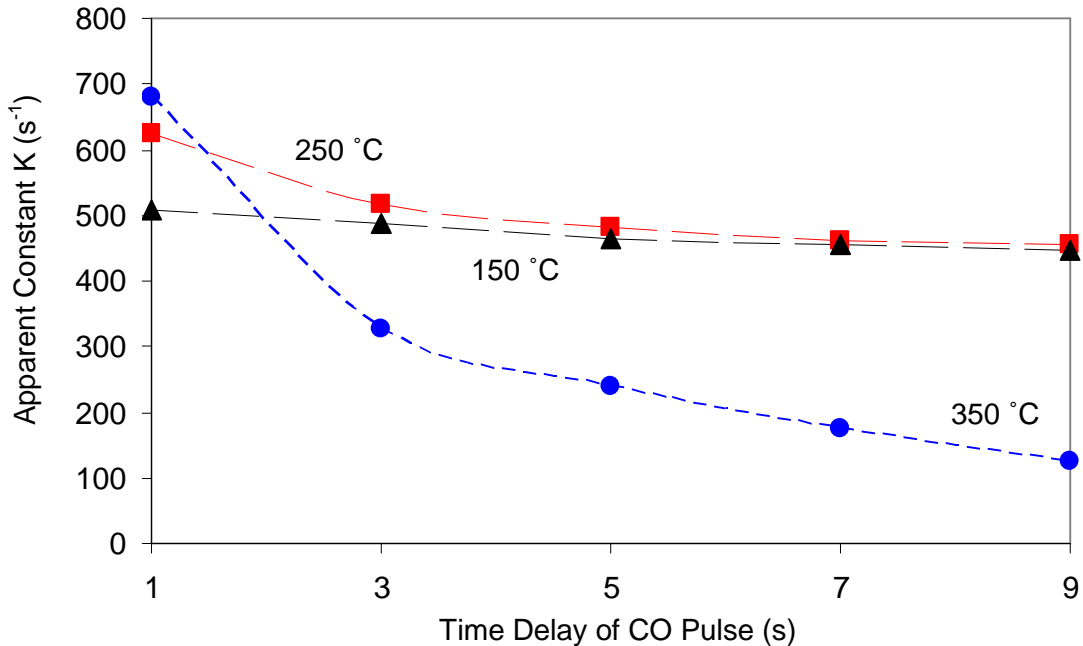


**Figure 4.10** Apparent constant calculated based on the data obtained from the CO pulse (Figure 4.7) as a function of time delay.

Figure 4.11 demonstrates temperature dependences of the apparent constants and its specific features at different time delays. These dependences are not so trivial to understand. There is an interval of temperatures and time delays, between 150 to 250 °C and 3 to 9 s, in which the apparent constant is approximately the same. A “turning point” occurs at 250 °C. Also, the time delay of 1 s is a unique case because the apparent

constant increases with reaction temperature. Based on this behavior, it can be concluded that the process of surface composition is changing between the pulses, and this process is not only due to the simple removal of surface oxygen, but a complex process of oxygen redistribution. Characteristics of oxygen redistribution on the Pt surface should have an optimum as a function of the reaction temperature (it may be between 200 and 250 °C) and the time delay (1 s).

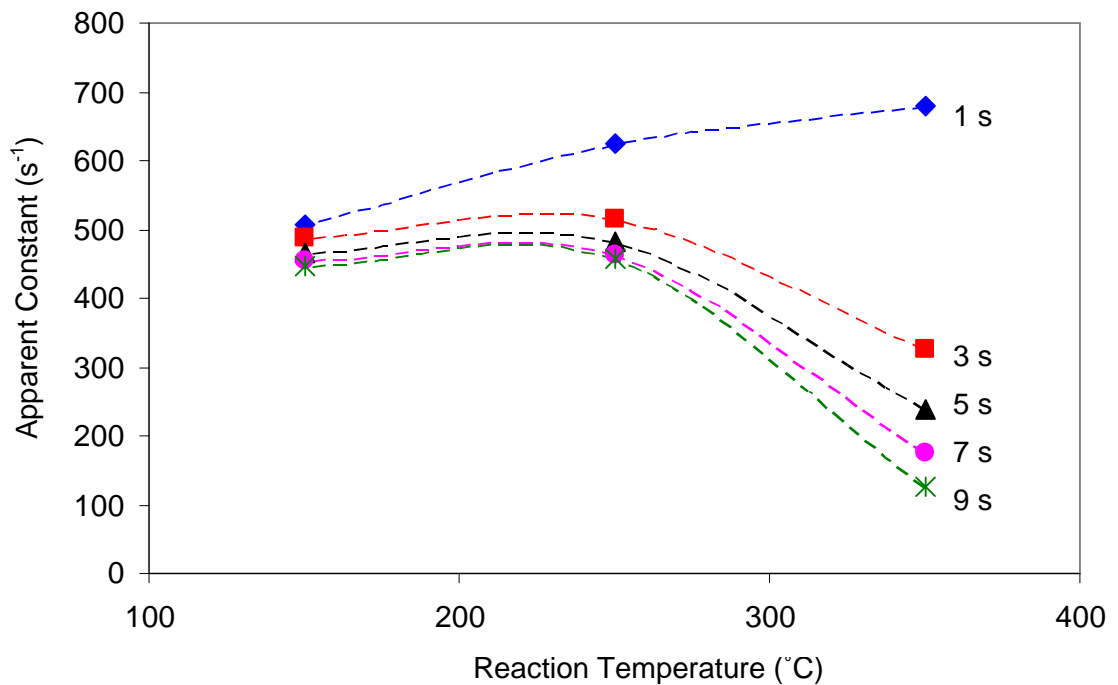


**Figure 4.11** Apparent constant as a function of reaction temperature for different time delays.

The apparent constants can also be used to calculate the activation energy for the CO oxidation reaction, particularly the reaction of pulsed CO with surface oxygen. By plotting the natural log of the apparent constant as a function of the time delay of the CO pulse, one can denote a relationship between the apparent constant to the time delay as

another apparent constant, “B” (Figure 4.12). The relationship can also be shown by the following equation.

$$K_{app} = A \exp(-Bt) \quad (4.3)$$

The constant “B” can then be plotted against (1/RT) to find the activation energy. The activation energy was found to be approximately 26.6 kJ/mol. This is within the order of magnitude for CO oxidation activation energies given in the literature, found to be between 45 - 100 kJ/mol for Pt single crystal surfaces [57, 58, 99] and 25 – 96 kJ/mol for polycrystalline Pt [99]. This value is on the low end which means higher surface oxygen composition on the Pt surface during reaction.

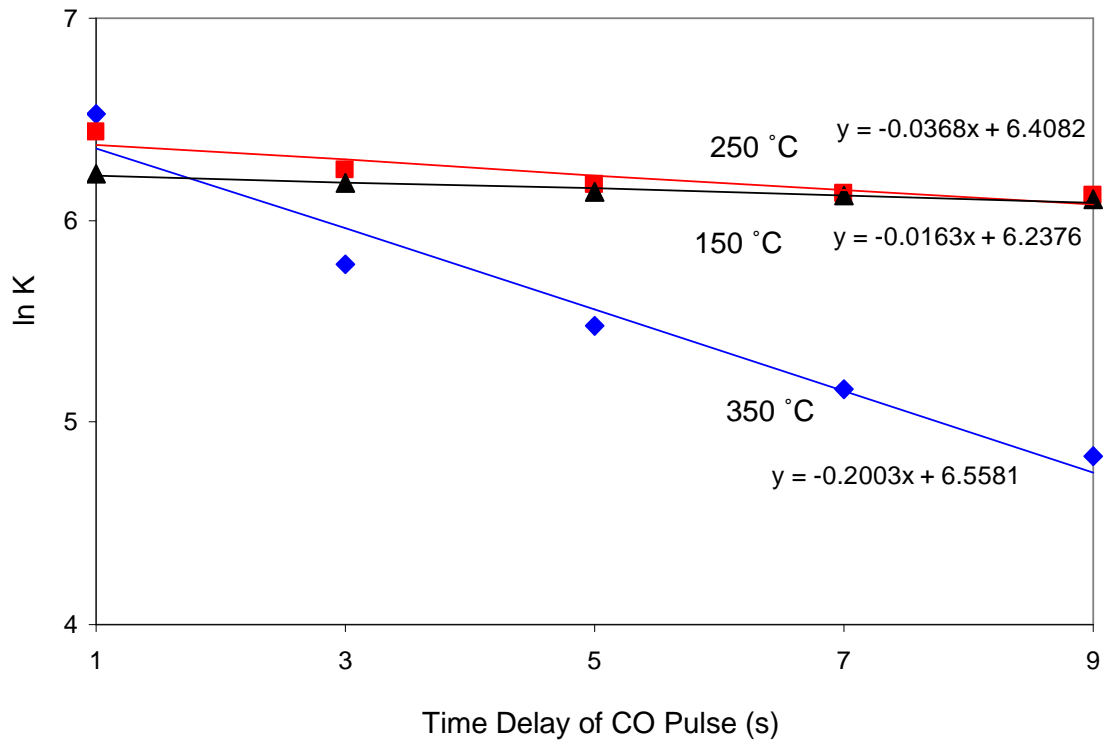


**Figure 4.12** Calculation of apparent constant “B” from the slopes of the linear relationship between the ln (K) and time delay.

## 4.2 Probabilistic Single Particle Theoretical

### Model

The high conversions obtained in TAP single particle experiments can be explained by a probabilistic theory and interpretation of conversion,  $\alpha$ , based on the principle of Brownian motion [101] of reactant molecules inside the microreactor. In this case, Brownian motion denotes that the reactant molecules travel by random motion inside the microreactor. The experiment is modeled in which a pulse of gas of chemical species A is released into the microreactor and the outlet flow is collected at the right-hand open side of Figure 4.13. The model is 2-dimensional. The black disc in the middle represents the catalyst particle. The term “particle” is used as a general term to describe the single piece of catalyst, which is not permeable. The “particle” can be small or big, spherical, cylindrical, or foil shaped, but it is assumed to be nonporous. The smaller, light colored dots represent the inert medium used to pack the microreactor. As the trajectory of A gas molecules nears the active catalyst center, an irreversible reaction  $A \rightarrow B$  may occur. The model is based on the probability of A gas molecules coming into contact or within close proximity to the active catalyst particle, that conversion will occur. The outlet flow gas collected at the microreactor outlet then contains both A and B gas molecules. The probability (conversion) of a reactant gas molecule hitting or coming very close to the active catalyst particle is calculated using the Feynman-Kac formula [102] and solving a time-dependent boundary value problem (BVP).

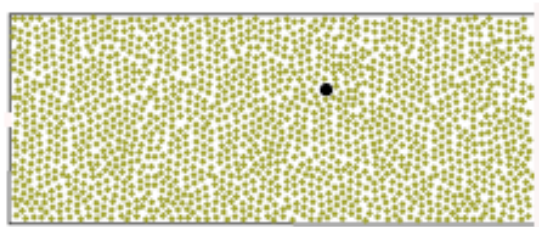


**Figure 4.13** Model of microreactor with catalyst (black dot) and inert quartz particles (light colored dots). The right open side of the figure indicates the microreactor outlet.

The model for molecular motion inside the packed bed of the microreactor is based on the principle of Brownian motion. The interior of the microreactor is regarded as a permeable medium in which reactant gas species A has a diffusion constant  $D$ . Because transport in the TAP reactor is governed by Knudsen diffusion, the transport of gas A in the probabilistic model away from active zones (i.e., ignoring reaction) is also governed by the standard diffusion equation (Fick's Law).

$$\frac{\partial c}{\partial t} = D\nabla^2 c \quad (4.4)$$

In Equation 4.4,  $c$  is the concentration of gas species A. It is known that Fickian diffusion (Equation 4.4) corresponds to a model of stochastic molecular motion known as the Wiener process, which is also referred to as mathematical Brownian motion. The Wiener process is defined by three important properties. The first property states that the trajectories are continuous paths. The second property is the key assumption in the Wiener process model which states that molecular direction changes unpredictably after each collision with the particles in the reactor bed. The third property states that during a short period of time  $h$ , which is nevertheless long enough to contain several collisions,



the trajectory displacement is normally distributed. Figure 4.14 shows a typical molecular trajectory path inside the microreactor based on the above mentioned principle. Brownian motion in the microreactor space  $R$  is defined by essentially the same properties as in open space except that it is subject to reflection on the microreactor walls and on the catalyst surface, and it is “killed” at the exit boundary (or open side) of the microreactor (see Figure 4.13).

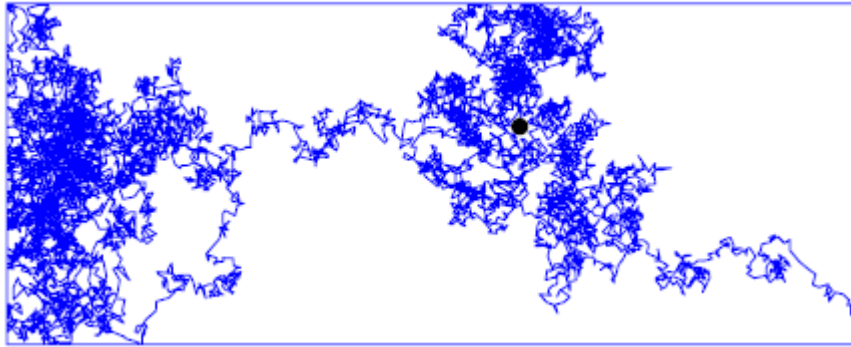


**Figure 4.14** A typical molecular trajectory in the microreactor based on Brownian motion.

### **4.2.1 Conversion Dependence on Catalyst Position**

The following numerical example of conversion is found by specifying the active catalyst center at some position  $(x,y)$  inside the microreactor space  $R$ .  $R$  is defined as a region in  $R^n$ , which is bounded in the sense that it is entirely contained within a finite radius of some point. For simplicity, the microreactor is modeled as a square with a side length of 1. The active catalyst center will be located at the center of sample region  $S$  with lengths of various sizes. A typical example of the microreactor configuration with the active catalyst center is shown in Figure 4.15.

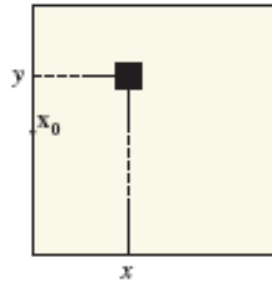


**Figure 4.15** A square catalyst sample of side length 0.1 in  $R$  with active center at  $(x, y)$ . The position  $x_0$  denote the position for reactant gas injection into the space  $R$ .

Figure 4.16 shows how conversion changes as the active catalyst center position  $(x, y)$  is varied inside the microreactor. The square base on the  $xy$ -plane represents the microreactor and the side parallel to the  $y$ -axis where the graph touches the  $xy$ -plane represents the microreactor exit boundary. The initial point where the reactant gas  $A$  enters the microreactor is at  $x_0$  shown in Figure 4.15. Figure 4.16 shows that conversion is highest when the catalyst is right in front of the initial point and declines as it is moved farther away; as a function of  $y$  for any given  $x$ , conversion is at a maximum on the axis of the microreactor (running from the mid-left to mid-right sides of the square reactor) and decreases as the catalyst is moved away from the center axis toward the upper or lower walls.

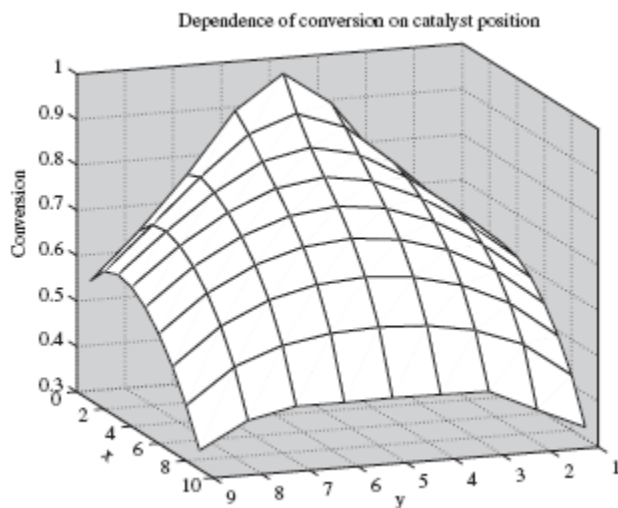


**Figure 4.16** Conversion dependence found as a function of the active catalyst center position ( $x$ ,  $y$ ).

## 4.2.2 Comparison of Experimental Results to Probabilistic Theory

The catalyst used in these experiments is a circular 0.125 in. (0.317 cm) diameter Pt foil packed in the microreactor bed with inert quartz particles with diameters between 210 to 250  $\mu\text{m}$ . The Pt foil was placed in three different positions inside the microreactor: at the very top near the microreactor inlet; in the middle; and at the bottom of the microreactor. The Pt foil was placed in the microreactor with the flat circular surfaces facing the microreactor inlet and outlet. The reaction used is CO oxidation because CO oxidation is a model reaction to demonstrate conversion for the irreversible reaction of reactant A (CO) to produce product B ( $\text{CO}_2$ ). This reaction is ideal for relating the probabilistic theory to experimental data.

In preparation for TAP pulse response experiments, the Pt foil was pre-treated with a continuous O<sub>2</sub>/Ar flow (20 cc/min for each gas, P = 1 atm, O<sub>2</sub>/Ar = 1) for 1 hour at 375 °C to ensure maximum oxygen adsorption on the Pt foil surface. After pre-treatment, the slide valve was opened, evacuating the microreactor and configuring the system for TAP vacuum pulse response experiments. The microreactor temperature was maintained at 375 °C during the course of the experiments to ensure a fast reaction rate. A series of CO/Ar pulses (CO/Ar = 70/30 feed ratio) were injected into the microreactor and CO conversion to CO<sub>2</sub> was measured using the mass spectrometer. The CO<sub>2</sub> yield, or CO conversion (Figure 4.17), was obtained by taking an average of the first 10 CO pulses converted to CO<sub>2</sub> because this is the range of maximum conversion when the catalyst was initially at a completely oxidized state. The x-axis of Figure 4.17 gives the Pt foil position within the microreactor. Position 0 represents the microreactor inlet and position 1 represents the microreactor outlet. The three rectangular boxes represent the experimental data in Figure 4.17. The center of each rectangle gives the measured point estimate of CO<sub>2</sub> yield for the respective position in the microreactor; the height of the rectangle is twice the standard deviation of the measured yield, and the width of the rectangle is a rough estimation of the uncertainty in placing the Pt foil in the microreactor. The vertical line segments represent the theoretical values for CO conversion. The line segment gives a range of values, for a fixed position x along the length of the reactor, for all values of y from the lower to the upper microreactor walls. Figure 4.18 gives a more detailed description for this range when the foil position is at the midpoint of the microreactor, x = 0.5, and y is varied.

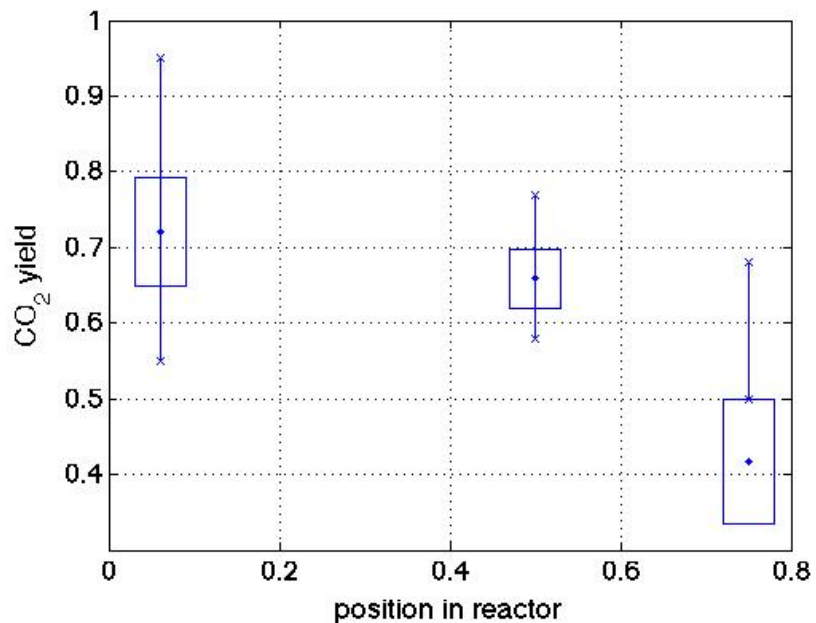


**Figure 4.17** Comparison of experimental and theoretical values for CO<sub>2</sub> yield/CO conversion as a function of Pt foil position in microreactor.

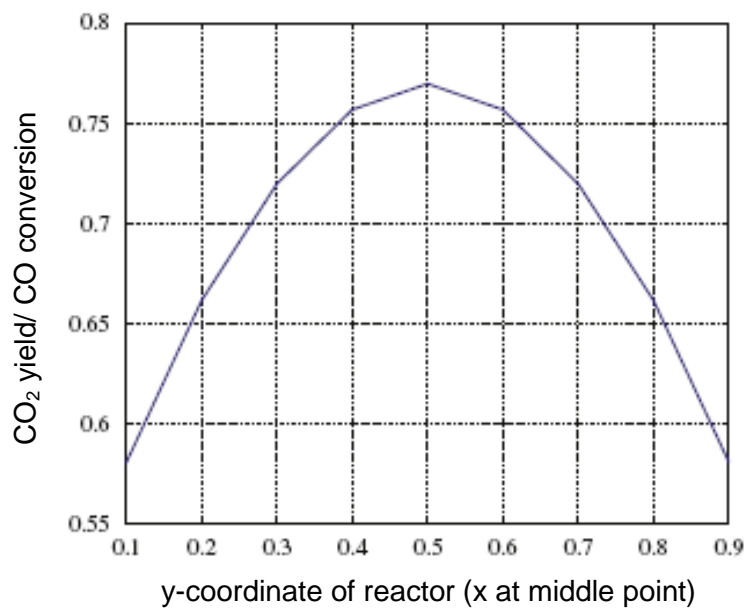


**Figure 4.18** CO<sub>2</sub> yield/CO conversion when  $x = 0.5$  (middle point along axis) and variable  $y$ .

According to Figure 4.17, when the Pt foil is placed in close proximity to the microreactor inlet, CO conversion/CO<sub>2</sub> yield is approximately 72%. In the middle of the microreactor and closer to the microreactor outlet, the CO conversion is approximately 65% and 42%, respectively. CO conversion is highest when the Pt foil is placed near the microreactor entrance due to the transport properties of the CO molecules in the microreactor. In the Knudsen diffusion regime, the diffusivity of each gas in a mixture is independent of the composition of the mixture as a whole [22, 23]. When the Pt foil is placed near the microreactor entrance, there is a greater probability for CO molecules to keep returning near or hit the catalyst particle due to the random (Brownian) motion caused by multiple collisions with the inert particles in the microreactor bed. As the Pt foil is moved closer to the microreactor outlet, the probability of CO coming back to the Pt foil once it has passed the position where the catalyst is located decreases. Notice that the nature of the random motion of the gas molecules is important for explaining both the relatively high yield for a single catalyst particle and the way the yield depends on the catalyst position: random motion creates the opportunity for the molecule to return multiple times to where the catalyst is located, but the number of returns decreases if the distance between the position of the Pt foil and the microreactor outlet decreases. Once a gas molecule reaches the microreactor outlet, it exits the microreactor into the vacuum chamber.

Figure 4.18 shows the numerical values for conversion found at  $x = 0.5$  and  $y$  is between 0 and 1. The range of conversions found numerically for  $x = 0.5$  and  $0 < y < 1$  is between

58 and 77%. This is compared to the experimental conversion result shown in Figure 4.17 of 65%. The qualitative result of decreasing product yield with catalyst position is in agreement with what was obtained numerically. The values for conversion shown in Figure 4.17 seem to be in reasonably good agreement with the numerical values shown in Figure 4.16 for an idealized TAP experiment with a square catalyst particle. Despite the rather idealized nature of the two dimensional numerical model, the experimental values fall within the range of the theoretical values for the first two points, nearer to the microreactor inlet. Greater discrepancy between the numerically and experimentally obtained conversions occurs near the microreactor outlet, indicating that gas molecules near the exit tend to leave somewhat sooner than expected by the theoretical model. It is possible that near outlet, the Brownian motion approximation is not as good as it is deeper inside the microreactor. It is also possible that the simple square reactor model does not serve equally well near the border of transition into the vacuum chamber and a more realistic microreactor shape is needed. It is important to emphasize, however, that a careful quantitative comparison between theory and experiment cannot be done on the basis of two-dimensional numerical experiments, mainly because Brownian motion in dimension 2 is known to differ in important ways from Brownian motion in dimension 3. For example, Brownian motion in 3-space is transient whereas in 2-space it is recurrent [103]. This suggests that conversion in dimension 3 should be less than in dimension 2 for comparable configurations of catalyst size and position.

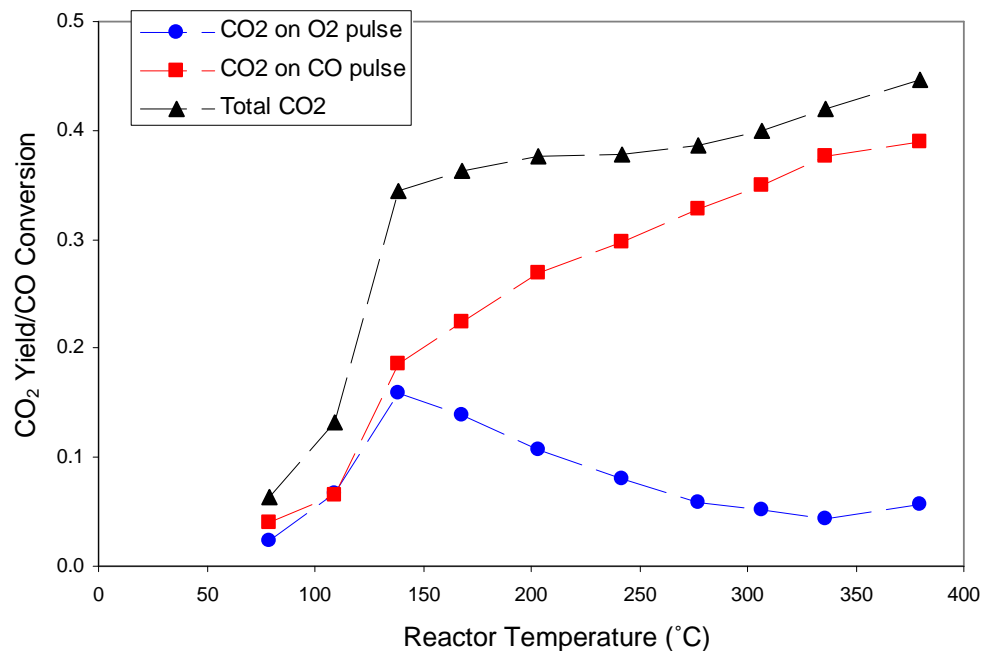
## 4.3 Reaction on Pt Supported Catalysts

### 4.3.1 TAP Vacuum Pulse Response Results

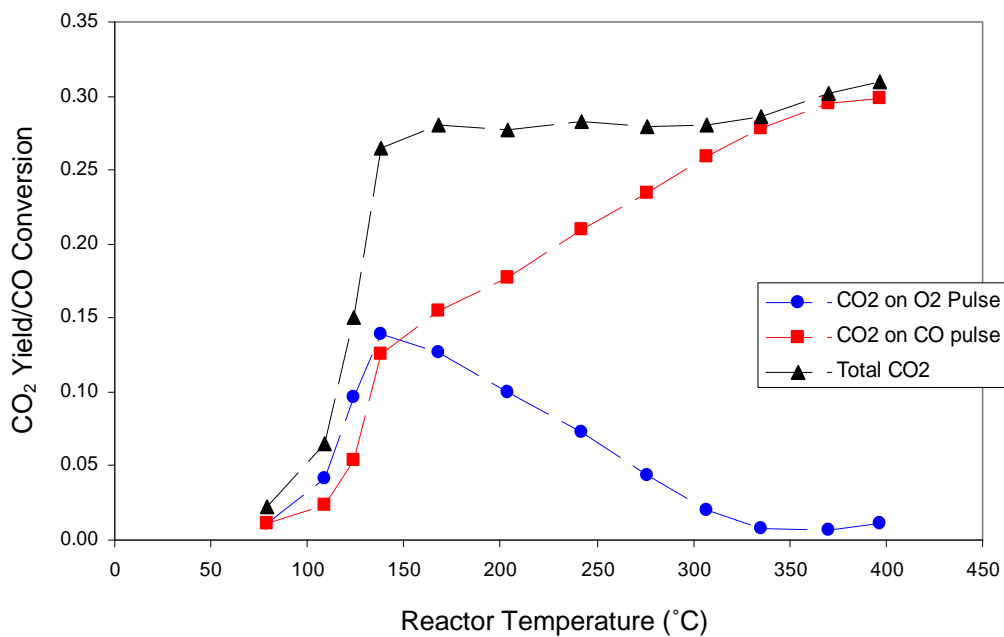
TAP vacuum pulse response experiments were performed on supported catalysts with Pt nanoparticles deposited on two types of SiO<sub>2</sub> supports (see Chapter 3.2.3 for details on catalysts); unimodal porous silica (UPS) support and SBA-15 SiO<sub>2</sub> support. For each experiment, the microreactor was packed with seven 400 μm diameter catalyst particles. Unlike the single Pt particle experiments, more than one catalyst particle is needed because the supported Pt catalysts are not as active as the Pt bulk metal particle. Although 7 catalyst particles are used to pack the microreactor, this is still significantly less than the amount of catalyst needed for a thin-zone configuration. The reaction used is again the CO oxidation reaction. The catalyst particles were pre-treated via an O<sub>2</sub>/Ar atmospheric flow (20 cc/min each gas, T = 400 °C, P = 1 atm) prior to vacuum pulse response experiments. The TAP pulse response experiments were performed using the pump-probe format. First, a mixture of O<sub>2</sub>/Ar (O<sub>2</sub>/Ar = 70/30) was pulsed into the microreactor first followed 2 s later by the CO/Ar (CO/Ar = 70/30) pulse. The total collection time was set for 4 s. The reactant and product exit flow data was collected for a series of reaction temperatures.

Figure 4.19 plots the CO<sub>2</sub> yield/CO conversion found for the Pt nanoparticles supported on the SBA-15 SiO<sub>2</sub> support. Figure 4.20 plots the CO<sub>2</sub> yield/CO conversion found for the Pt nanoparticles supported on the unimodal porous silica (UPS) support.





**Figure 4.19** CO<sub>2</sub> yield/CO conversion found for Pt nanoparticles deposited on SBA-15 SiO<sub>2</sub> support.



**Figure 4.20** CO<sub>2</sub> yield/CO conversion found for Pt nanoparticles deposited on unimodal porous silica (UPS) support.

Figures 4.19 and 4.20 show similar trends in the CO<sub>2</sub> yield found on the O<sub>2</sub> pulse, CO pulse, and the total CO<sub>2</sub> yield found by adding the amount of CO<sub>2</sub> produced on both the O<sub>2</sub> and CO pulses. The only difference lies in the maximum value of the CO<sub>2</sub> yield on the CO pulse. CO<sub>2</sub> yield calculated on the CO pulse reaches a maximum of 40% on Pt/SBA-15 and 30% on Pt/UPS. The difference in yields is a result of the amount of available surface oxygen. The SBA-15 support is bimodal in structure; therefore, there are more pores as well as a greater surface area than the UPS support. In greater surface area allows for more available sites for oxygen adsorption. Also, the dependence of yield on reactor temperature for the CO pulse is approximately linear. As the reactor temperature increases, the CO<sub>2</sub> yield increases as well. This indicates that as the reactor temperature increases, the amount of surface oxygen becomes more available either by an increased rate in O<sub>2</sub> adsorption, storage of O<sub>2</sub> by the catalyst support which results in increased rate of movement to the Pt active sites, or an increase in the rate of reaction. This will be explored in greater detail in the next section as the performance results between the supported Pt catalysts are compared to the Pt bulk metal particle.

The dependence of CO<sub>2</sub> yield on temperature found on the O<sub>2</sub> pulse is almost identical for both types of catalysts. The same maximum CO<sub>2</sub> yield of 15% is achieved at the same reactor temperature, 140 °C. This indicates that the amount CO adsorption on both types of catalysts is approximately the same. CO adsorption most likely occurs on the Pt nanoparticles and it is temperature dependent. At lower reactor temperatures, CO adsorption is favored and as the reactor temperature increases, the rate of CO desorption

also increases. This results in less CO<sub>2</sub> yield because there is essentially less and less CO on the catalyst surface for the O<sub>2</sub> to react with. At approximately 140 °C, there is a turning point in the CO<sub>2</sub> yield which means that at this temperature, this is the optimal conditions for CO adsorption on the Pt supported catalysts.

### **4.3.2 Comparison with Pt Bulk Metal Particle**

In comparison of results with the Pt bulk metal particle (see Figure 4.4C in Chapter 4.1.2), there are 3 distinct differences in the trends for CO<sub>2</sub> production as a function of temperature which will give important insight into the role of the catalyst support during chemical reaction. The first difference and most obvious is the significant decrease in CO<sub>2</sub> yield obtained on the supported Pt catalysts even though there are 7 catalyst particles in the microreactor instead of just one catalyst particle. The single bulk Pt particle is extremely active with 95% total CO<sub>2</sub> yield in comparison with a maximum of 45% CO<sub>2</sub> yield obtained with the Pt/SBA-15 supported catalyst. Although more supported Pt particles were packed in the microreactor, the supported particles were mostly SiO<sub>2</sub> with approximately 4-7 wt% of Pt. This result indicates that reaction between O<sub>2</sub> and CO molecules occurs on the Pt active material.

The second difference between the CO<sub>2</sub> production trends is that for the Pt bulk particle, there is a “turning point” at 170 °C in the CO<sub>2</sub> yield plot on both the O<sub>2</sub> pulse and the CO pulse. There is only a “turning point” on the CO<sub>2</sub> yield plot on the O<sub>2</sub> pulse for the Pt supported catalysts. Although the CO<sub>2</sub> yield plot is decreasing gradually on the CO pulse

for the Pt particle, it is still decreasing. Meanwhile, the CO<sub>2</sub> yield plots on the CO pulse for the supported Pt catalysts are increasing as a function of reactor temperature. For the Pt particle, the slight decrease in CO<sub>2</sub> yield on the CO pulse as a function of increasing reactor temperature suggests that the O<sub>2</sub> content on the catalyst surface is fairly stable. In the case of the supported Pt catalysts, the CO<sub>2</sub> yield on the CO pulse is increasing with the reactor temperature which suggests that the support is playing a role for oxygen storage. As the temperature increases, the rate at which the oxygen stored on the support moves to the Pt nanoparticles increases providing for the extra oxygen for reaction with CO; hence increase in CO<sub>2</sub> yield.

The final difference is the location of the “turning point” of the CO<sub>2</sub> yield plot on the O<sub>2</sub> pulse. For the Pt particle, the “turning point” occurs at 170 °C and for the supported Pt catalysts the “turning point” occurs at approximately 140 °C. With the presence of the SiO<sub>2</sub> support, perhaps the activation energy for O<sub>2</sub> reaction with surface CO decreases, resulting in the shift to a lower temperature for the “turning point.”

# Chapter 5

## Selective Oxidation of Furan over VPO

### Catalysts

This chapter presents results from TAP multi-pulse studies of furan oxidation over oxygen-treated VPO catalysts. Furan is an intermediate formed in the selective oxidation of *n*-butane to produce maleic anhydride (MA). Furan already has a ring structure similar to the molecular structure of MA, except furan has one oxygen atom and the formation of MA requires two additional oxygen atoms (Figure 5.1). Furan is a good probe reactant molecule because furan can be used to probe the oxidation state of the VPO catalyst. Also, furan oxidation is the simplest to do experimentally because this reaction produces the least number of different products to be monitored.

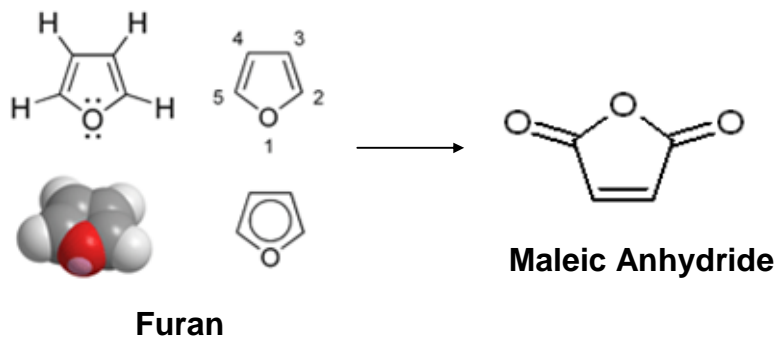


**Figure 5.1** Molecular structures of furan and maleic anhydride.

In all the experiments, the VPO catalyst was initially oxidized in air at 480 °C for approximately 10 minutes with the slide valve closed. After the initial oxidation, the slide valve was opened to configure the reactor for TAP multi-pulse vacuum pulse response experiments. A series of pulses that contained the reactant (furan = 60%) and inert (argon = 40%) gases were sent into the microreactor to reduce the oxidized VPO catalyst for a series of reactor temperatures ranging from 400 to 480 °C. The reduction with furan proceeded until the selective product, maleic anhydride, was no longer being produced. During the reduction experiment with furan, the pulse responses for the reactants and products (furan, maleic anhydride, CO<sub>2</sub>, CO, argon) were monitored separately. The microreactor configuration was a thin-zone configuration with 40 mg of VPO catalyst ranging in diameters from 210-250 μm packed in the center of the microreactor surrounded by inert quartz particles of the same size. The microreactor length is approximately 1 inch and the catalyst zone thickness is approximately 10 percent of the total microreactor length.

## **5.1 Temperature Dependence of Product Yield and Reactant Conversion**

Figures 5.2 – 5.5 presents plots of furan conversion and product yields versus pulse number for four different reactor temperatures (400, 430, 450, and 480 °C). Furan conversion is relatively the same as a function of pulse number for all four temperatures.

However, what is changing is the selectivity of the products as the reaction temperature changes (Figures 5.6 – 5.8). At approximately pulse number 28, there is essentially no more MA being produced and the selectivity is split between the two non-selective products, CO<sub>2</sub> and CO.

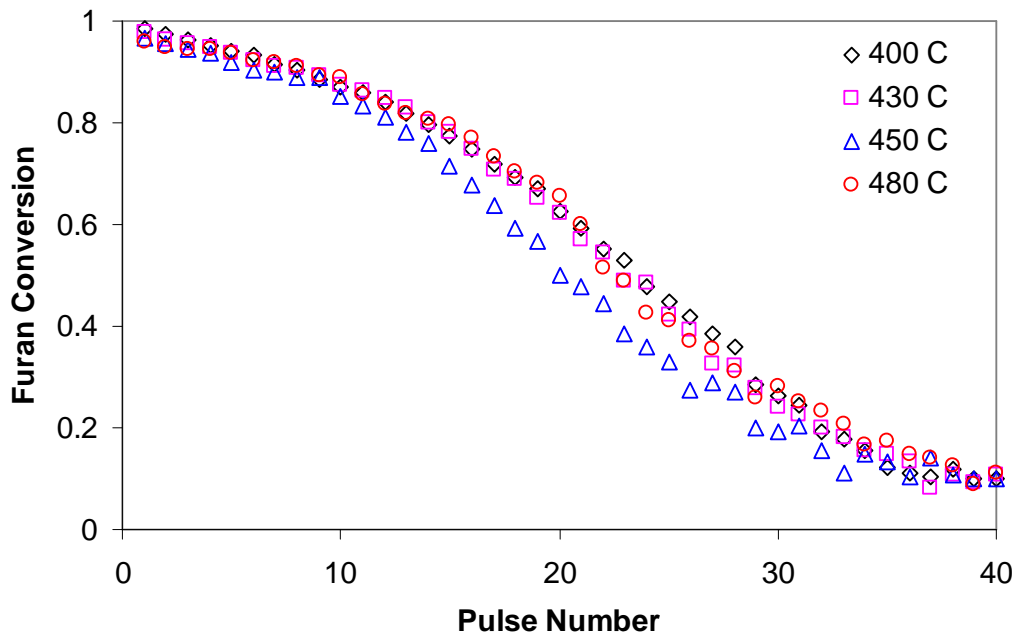


**Figure 5.2** Furan conversion as a function of pulse number for four different reactor temperatures.

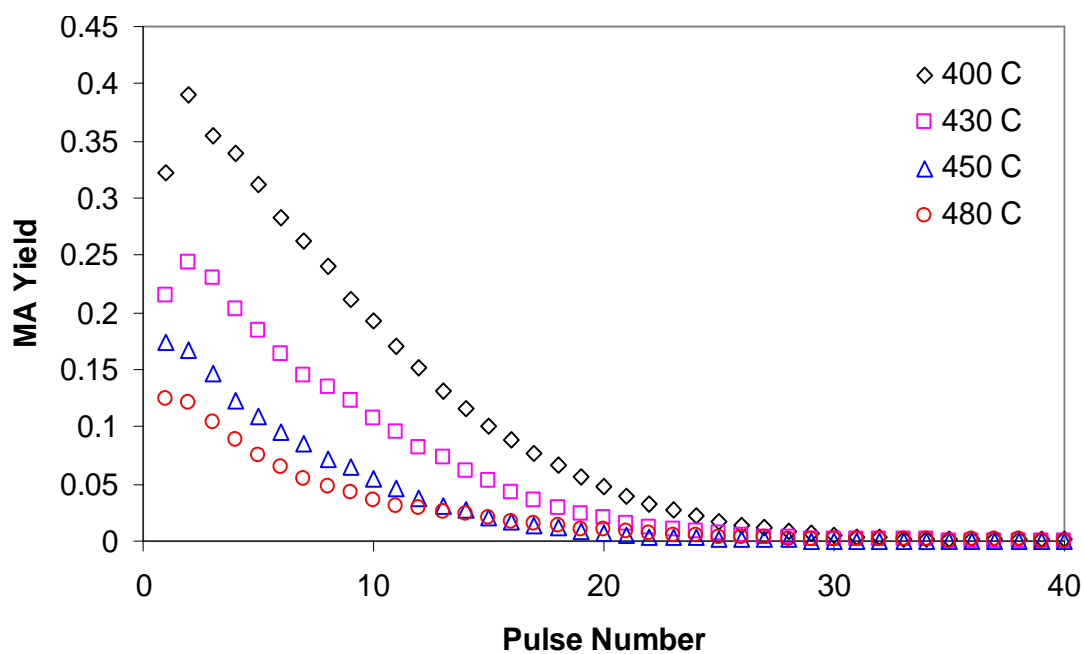


Figure 5.3 MA yield as a function of pulse number for four different reactor temperatures.

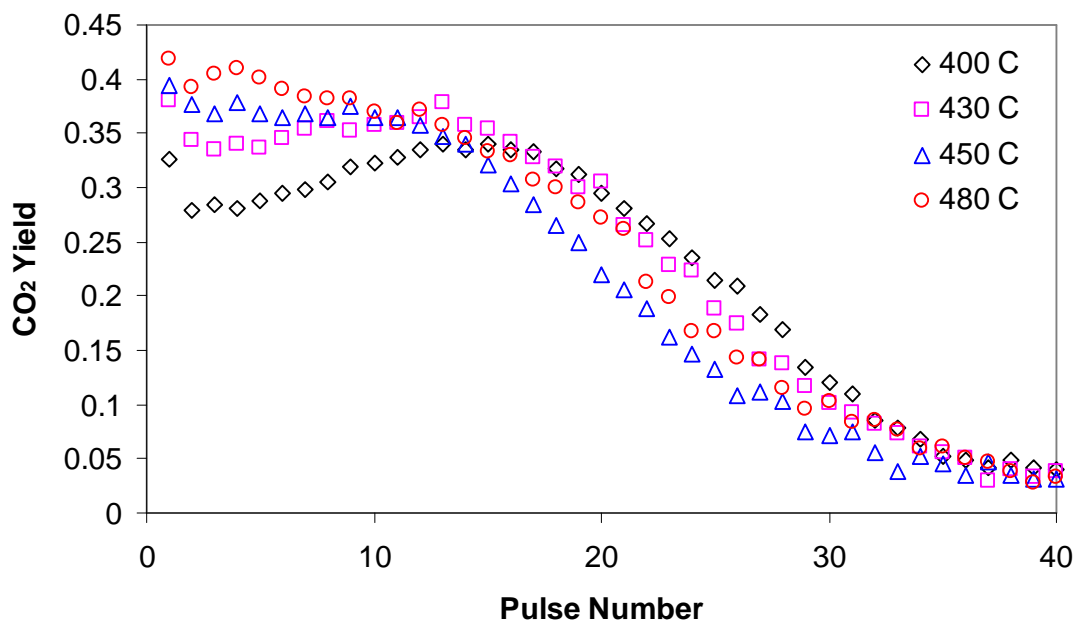
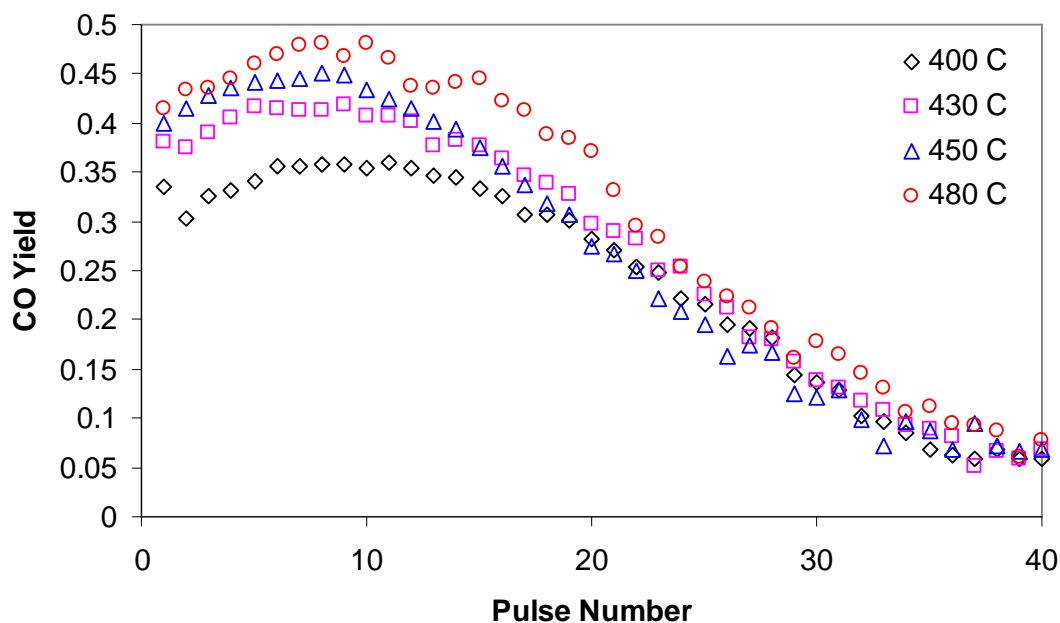
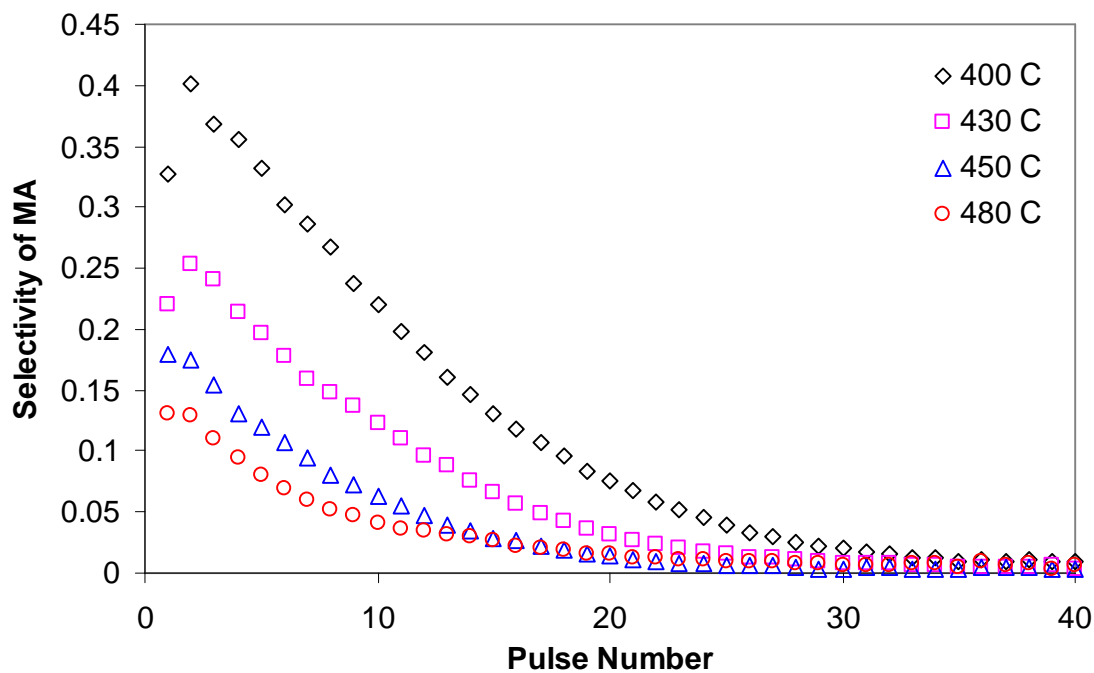


Figure 5.4 CO<sub>2</sub> yield as a function of pulse number for four different reactor temperatures.





**Figure 5.5** CO yield as a function of pulse number for four different reactor temperatures.



**Figure 5.6** Selectivity of MA as a function of pulse number for four different reactor temperatures.

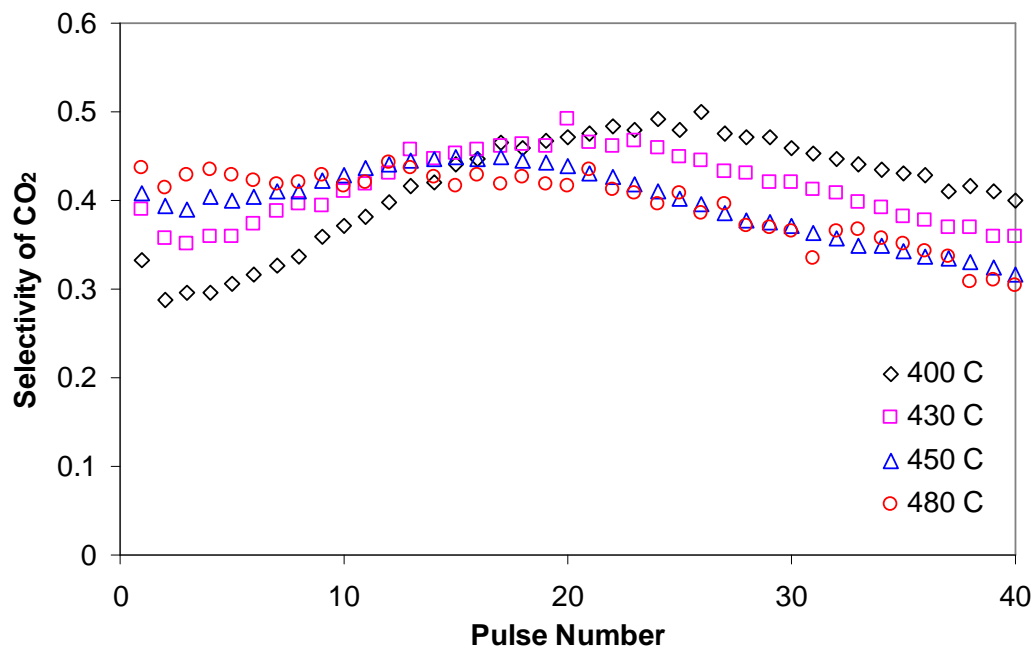


**Figure 5.7** Selectivity of CO<sub>2</sub> as a function of pulse number for four different reactor temperatures.

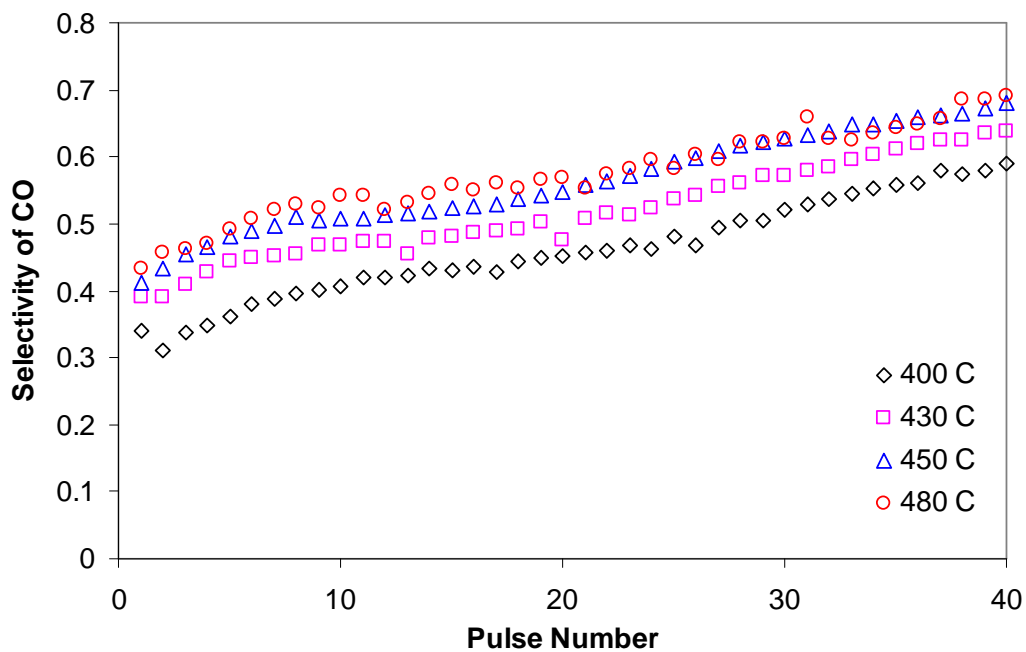


**Figure 5.8** Selectivity of CO as a function of pulse number for four different reactor temperatures.

In Figure 5.2, furan conversion during the first pulse is nearly 100 percent. The products that are being produced are maleic anhydride, CO<sub>2</sub>, and CO. The furan conversion decreases as more and more furan pulses are sent into the microreactor because each furan pulse is reducing the VPO catalyst of oxygen to produce the products. For example, in order to produce MA, each furan molecule has to acquire two additional oxygen atoms. In order to produce CO<sub>2</sub>, each furan molecule dissociates into four carbon compounds which must acquire two oxygen atoms each, making the total oxygen needed to be eight. The selective product, MA, yield is highest at the lowest reaction temperature of 400 °C (Figure 5.3). As the temperature increases, the MA yield decreases, however, the CO<sub>2</sub> and CO yields increase. One of the theories for the production of carbon oxides at high temperatures is related to the number of easily removable oxygens around an adsorbed surface species. If the number of easily removable oxygens around an adsorbed surface species is too high, then over oxidation with the formation of carbon oxides is highly possible [104]. At higher reaction temperatures, the selectivity decreases for the favorable product, MA, and this can also contribute to the higher formation of less favorable products, the carbon oxides. Also, at higher temperatures, the rate of diffusion of oxygen in the catalyst lattice is much faster. If the residence time of adsorbed surface species is long enough, the high mobility of oxygen ions at high temperatures would lead to products with a greater number of oxygens, and eventually to the formation of carbon oxides. According to Grasselli and Callahan [105], they proposed the “site isolation” principle which requires that clusters of sites containing active oxygen should be isolated to prevent the easy diffusion of oxygen

to the adsorbed surface species. In the case of the vanadyl pyrophosphate  $(VO)_2P_2O_7$  catalyst, the  $VO_x$  units are isolated in clusters of four by the pyrophosphate groups.

One of the surprising results found from these experiments is that there is a maximum observed in the MA yield (Figure 5.3). The maximum occurred during the second MA pulse response collected. The second MA pulse response actually corresponds to the sixth furan pulse sent into the microreactor. The mass spectrometer and the TAP data collection can only observe one atomic mass at a time. The experiment was set up to collect the pulse responses in the following order: MA,  $CO_2$ , CO, furan, and then argon. As the reaction temperature is increased, the maximum in the MA yield is not as pronounced. The maximum observed in the MA yield seems to indicate that there may be two types of oxygen species present on the VPO catalyst. The initial, more readily available oxygen on the VPO surface from the oxidation in air may not be as selective as the surface lattice oxygen. Previous TAP multi-pulse experiments on VPO catalyst for *n*-butane oxidation suggest that there are two types of oxygen species present [22, 65]. The first type is suggested to be the activated species of oxygen formed by the strong chemisorption of electrophilic dioxygen molecule. This type of oxygen species is said to be responsible for furan oxidation and butane activation. It is present in low concentrations on the catalyst surface. The second type of oxygen species is suggested to be surface lattice oxygen. In the selective oxidation of *n*-butane, the surface lattice oxygen is responsible for the allylic oxydehydrogenation of olefins and for oxygen insertion with ring closure to form furan. The origin of oxygen incorporated into the *n*-

butane selective oxidation reaction is still a matter of debate. Some authors suggest that both chemisorbed and lattice oxygen participate in the production of maleic anhydride from *n*-butane oxidation [104]. Using isotopic labeling with oxygen-18 and following the production of maleic anhydride, others have proposed that only lattice oxygen is active for MA formation [66]. Based on the furan oxidation results from this dissertation, it suggests that both the chemisorbed dioxygen from the initial oxidation with air and surface lattice oxygen is responsible for the production of MA. However, the chemisorbed dioxygen is not as selective for the formation of MA as the surface lattice oxygen.

This result is confirmed by a similar experiment in which instead of initially oxidizing the VPO catalyst in air, it is oxidized by an O<sub>2</sub>/Ar (O<sub>2</sub>/Ar = 7) atmospheric flow at 480 °C for 15 minutes. Also, more VPO catalyst was packed in the microreactor, approximately 110 mg. The catalyst was then probed with a furan/Ar gas mixture under TAP vacuum pulse-response conditions for a series of temperatures ranging from 400 to 480 °C. The MA yield calculated from the oxidation with an atmospheric flow of oxygen exhibited similar trends to the MA yield obtained from oxidation in air (Figure 5.9). A maximum in MA yield was also observed as a function of pulse number. Also, the highest MA yield was found at the lowest reaction temperature of 400 °C. The differences lie in the number of furan pulses needed to reduce the oxidized VPO catalyst because there was more catalyst packed in the microreactor which means more active sites for oxygen storage.

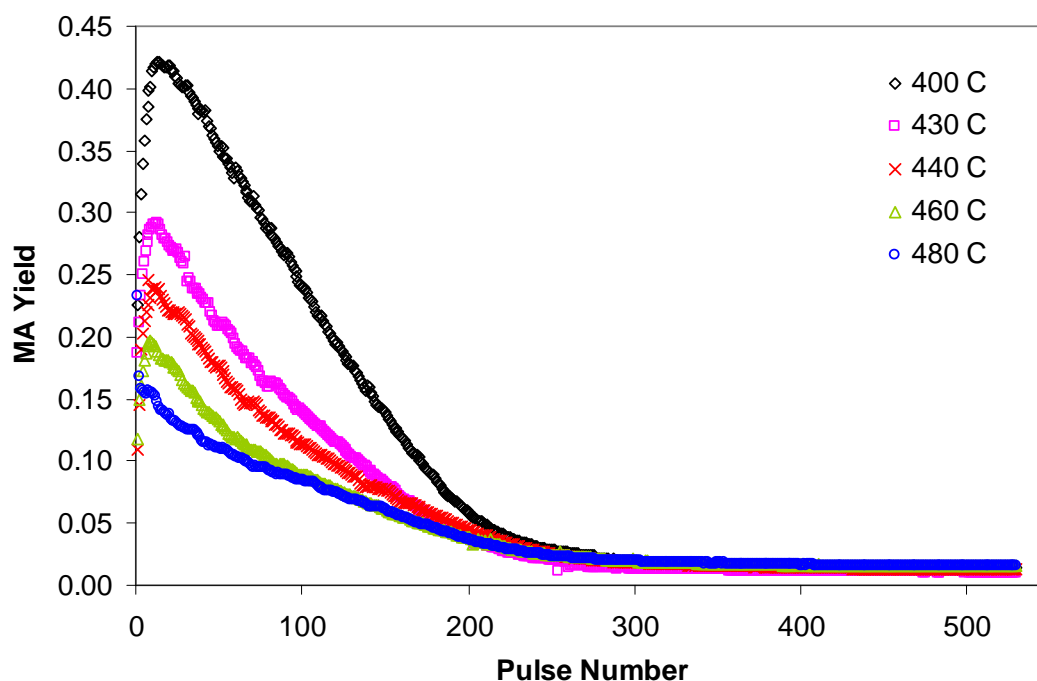


**Figure 5.9** MA yield obtained with VPO catalyst oxidized in an atmospheric flow of O<sub>2</sub>/Ar at 480 °C.

## 5.2 Characterization of VPO Catalyst State from Apparent Kinetic Constants

One of the main ideas of the TAP multi-pulse experiment is to kinetically characterize the changing catalyst states pulse by pulse. Each reactant pulse perturbs the catalyst state in a controlled manner. In the VPO experiments, the initial catalyst state is the oxidized state, which is the starting point of the experiments (oxidation in air at 480 °C), and the final catalyst state is the reduced state in which no reactant conversion is detected. Each

catalyst state can be characterized by directly measuring the integral or cumulative amount of reactant (e.g. furan) converted to reach the final reduced state. Instead of looking at the catalyst state in terms of the amount of reactant converted, the catalyst state can also be defined in terms of how much oxygen is removed from the catalyst. The amount of oxygen removed from the catalyst can be denoted by a catalyst state scale as the “catalyst oxidation degree.” A catalyst oxidation degree of 1 indicates that the catalyst is completely oxidized, and a catalyst oxidation degree of 0 indicates that the oxygen is almost completely removed from the catalyst.

Figures 5.10 – 5.13 plots the apparent kinetic constants for furan, MA, CO<sub>2</sub>, and CO as a function of the catalyst oxidation degree. As can be seen from Figures 5.11 – 5.13, the apparent kinetic constant for the product MA is different than the apparent kinetic constants for CO<sub>2</sub> and CO. This indicates that there are two separate reaction routes: one reaction route for MA production and another route for CO<sub>2</sub> and CO production. This is consistent for the theory that there may be two different types of active sites on the VPO catalyst.

The apparent kinetic constants for all the gases are decreasing as the catalyst is further reduced. The apparent kinetic constant for MA is decreasing almost linearly with the catalyst oxidation degree for all the reaction temperatures. This may reflect that there is a specific site on the VPO catalyst particularly for MA production. The MA apparent kinetic constant decreases linearly because there is less and less available MA-specific

oxygen on the catalyst surface. Meanwhile, the apparent kinetic constants for CO<sub>2</sub> and CO are decreasing nonlinearly with respect to the catalyst oxidation degree. According to the Shekhtman dissertation [106], a nonlinear decrease in the apparent kinetic constant with the catalyst oxidation degree may reflect the influence of oxygen exchange between the surface and bulk oxygen. Initially, the apparent kinetic constants for CO<sub>2</sub> and CO are almost constant and in some parts even increasing as a function of the catalyst oxidation degree. This can be caused by either an abundant amount of surface oxygen specific for CO<sub>2</sub> and CO production or a fast supply of sub-surface oxygen to the VPO surface. The sharp decrease in the apparent kinetic constant for CO<sub>2</sub> and CO at a low catalyst oxidation degree may be caused by a slow supply of bulk oxygen to the VPO surface. The nonlinear dependence of the apparent kinetic constants as a function of the catalyst oxidation degree is usually an indication that the reaction is a multi-step reaction, with a minimum of at least two steps in the reaction scheme, with participation of catalyst oxygen (i.e. sub-surface oxygen, different types of active oxygen specific for the production of particular products). The analysis using apparent kinetic constants is only preliminary and represents the complexity of the VPO catalyst system. Using furan as the reactant probe is the simplest route for understanding the VPO catalyst for the production of maleic anhydride. However, if *n*-butane were used as the reactant probe, it would be an even more complicated process with more independent reaction routes and specific intermediates to keep track of. The exact mechanism for furan oxidation over VPO catalysts is still under debate. In the next section, we will examine real TAP pulse



response data to give more insight into the mechanism for furan oxidation over VPO catalysts.

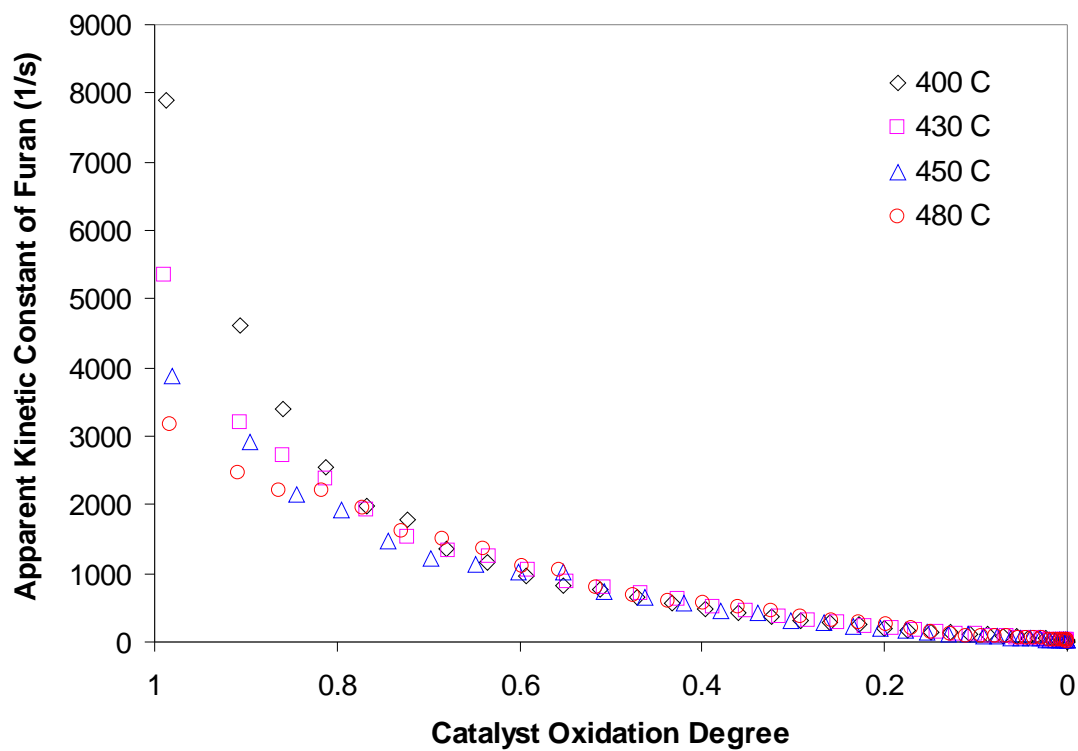


**Figure 5.10** Apparent kinetic constant for furan versus catalyst oxidation degree.

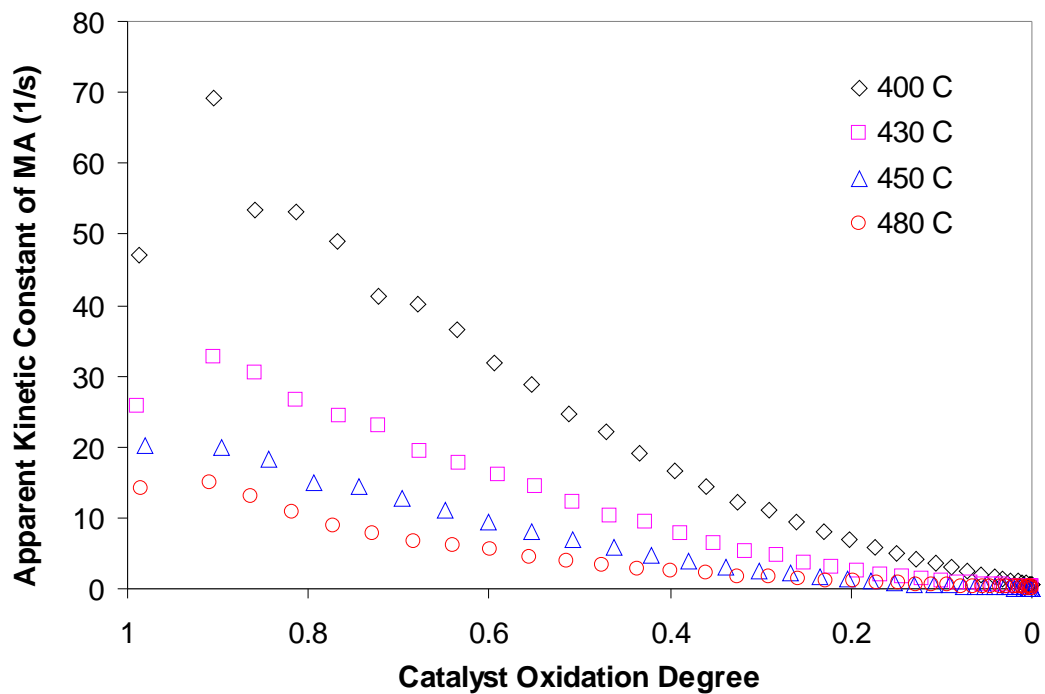


Figure 5.11 Apparent kinetic constant for maleic anhydride versus catalyst oxidation degree.

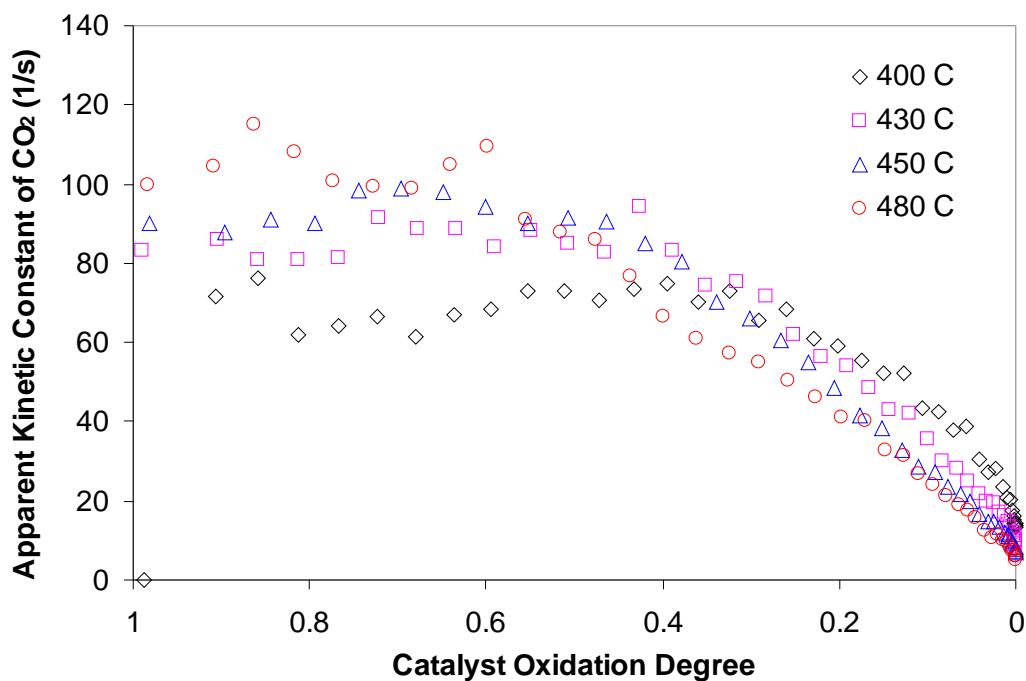
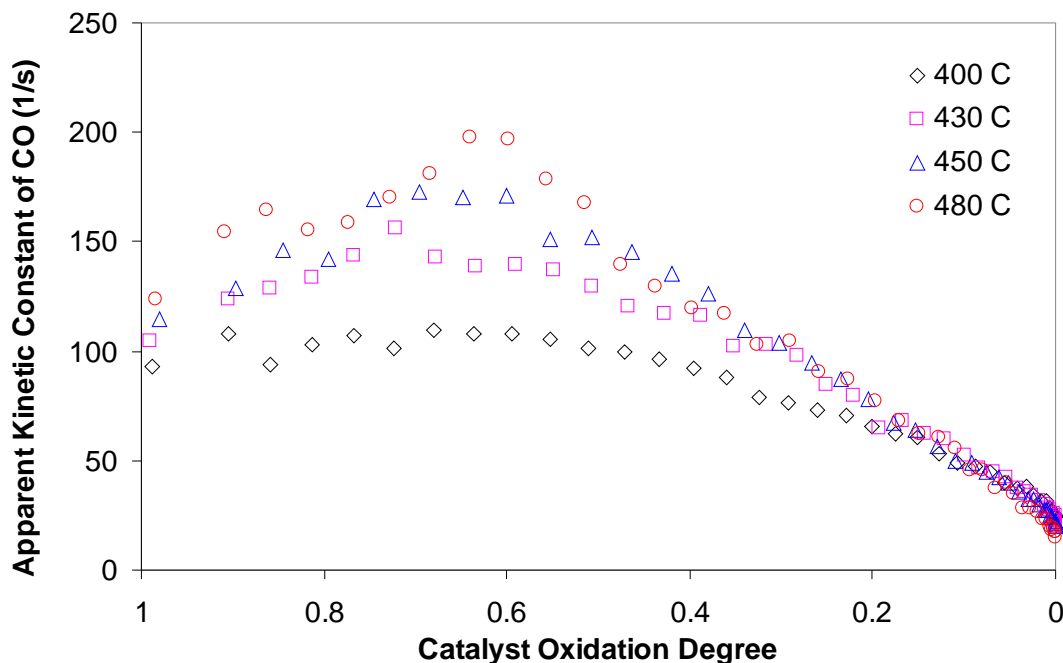


Figure 5.12 Apparent kinetic constant for CO<sub>2</sub> versus catalyst oxidation degree.



**Figure 5.13** Apparent kinetic constant for CO versus catalyst oxidation degree.

## 5.3 Deducing Mechanistic Detail from Real

### TAP Data

TAP pulse response exit flow curves can give abundant information regarding mechanistic details of a reaction just by looking at its shape. The shape of the exit flow curves can provide information as to whether the gas is a product, reactant, or inert, and gas adsorption behavior such as whether it is irreversibly or reversibly adsorbed to the catalyst surface. Figures 5.14 – 5.17 shows examples of the 3-dimensional plots of TAP exit flow pulse curves for the reactant and products in the VPO experiments at 400 °C. Figures 5.18 – 5.21 plots individual pulse curves from the 3-D plots in Figures 5.14 –

5.17 to give a clearer picture of the progression of change in the exit flow pulse curves. The insets in Figures 5.18 – 5.21 show height normalized pulse response curves from an initial curve in the 3-D plot compared to a latter curve in the 3-D plot when the catalyst is further reduced to show any changes in the pulse curve characteristics. Figure 5.22 plots the argon zeroth moment ( $M_0$ ) as a function of the pulse number to show that the pulses sent into the microreactor are consistent, and that the reactant and product pulse responses are real.

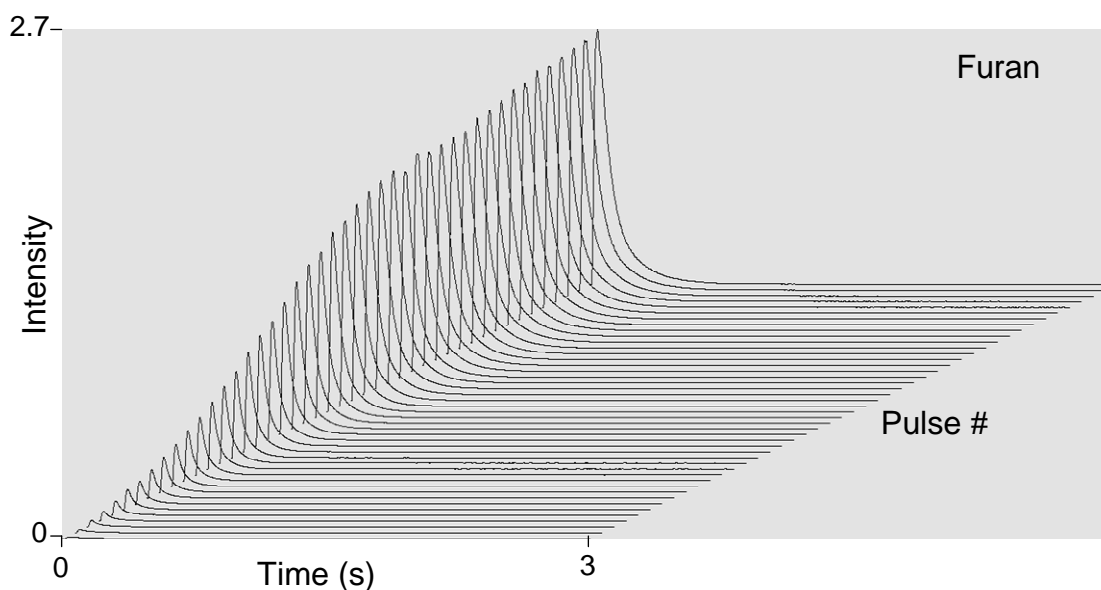


**Figure 5.14** TAP pulse response 3-dimensional exit flow curves for the reactant furan obtained over thin bed of VPO catalysts at 400 °C.

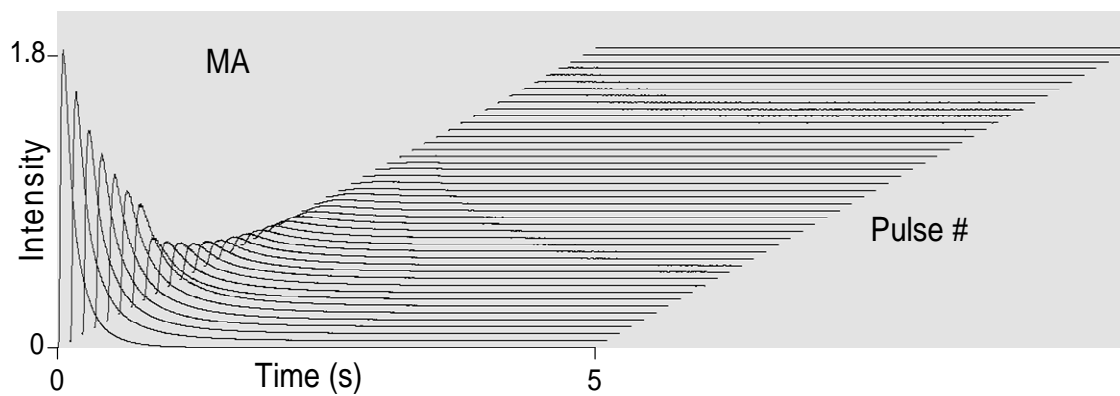


**Figure 5.15** TAP pulse response 3-dimensional exit flow curves for MA obtained over thin bed of VPO catalysts at 400 °C.

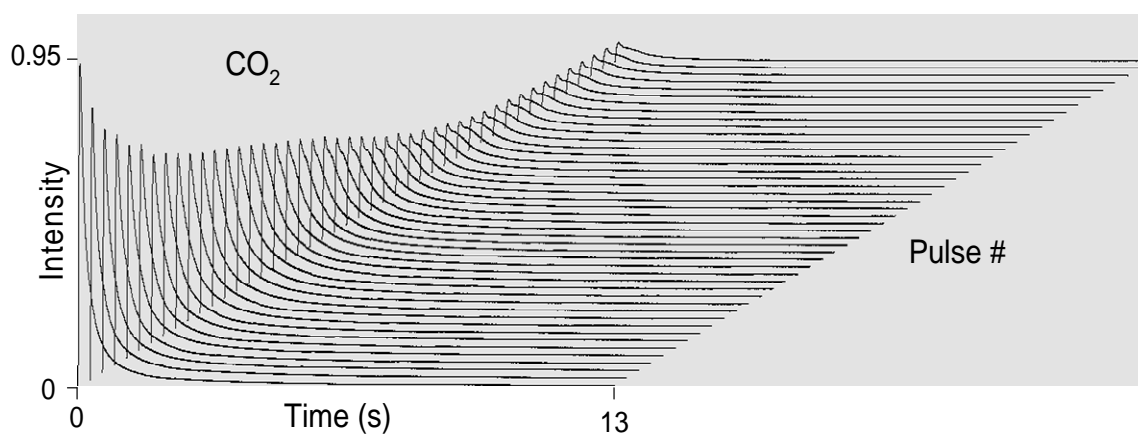


**Figure 5.16** TAP pulse response 3-dimensional exit flow curves for CO<sub>2</sub> obtained over thin bed of VPO catalysts at 400 °C.

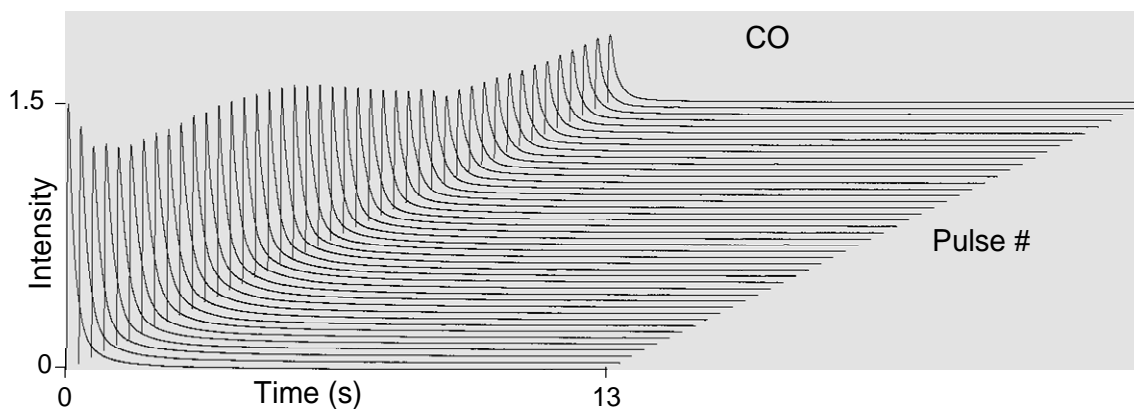


**Figure 5.17** TAP pulse response 3-dimensional exit flow curves for CO obtained over thin bed of VPO catalysts at 400 °C.

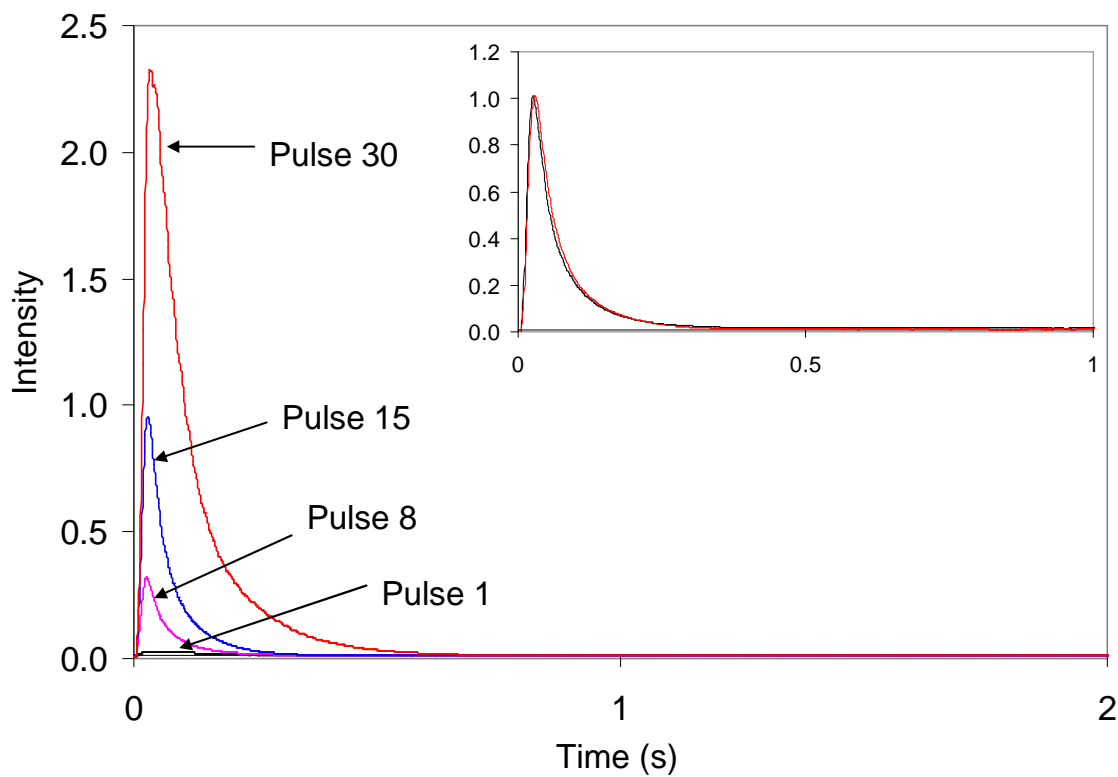


**Figure 5.18** Individual pulse response curves for furan plotted from the 3-D graph in Figure 5.14 obtained over thin bed of VPO catalysts at 400 °C. The inset shows the height normalized pulse curves for pulse 8 and 30.

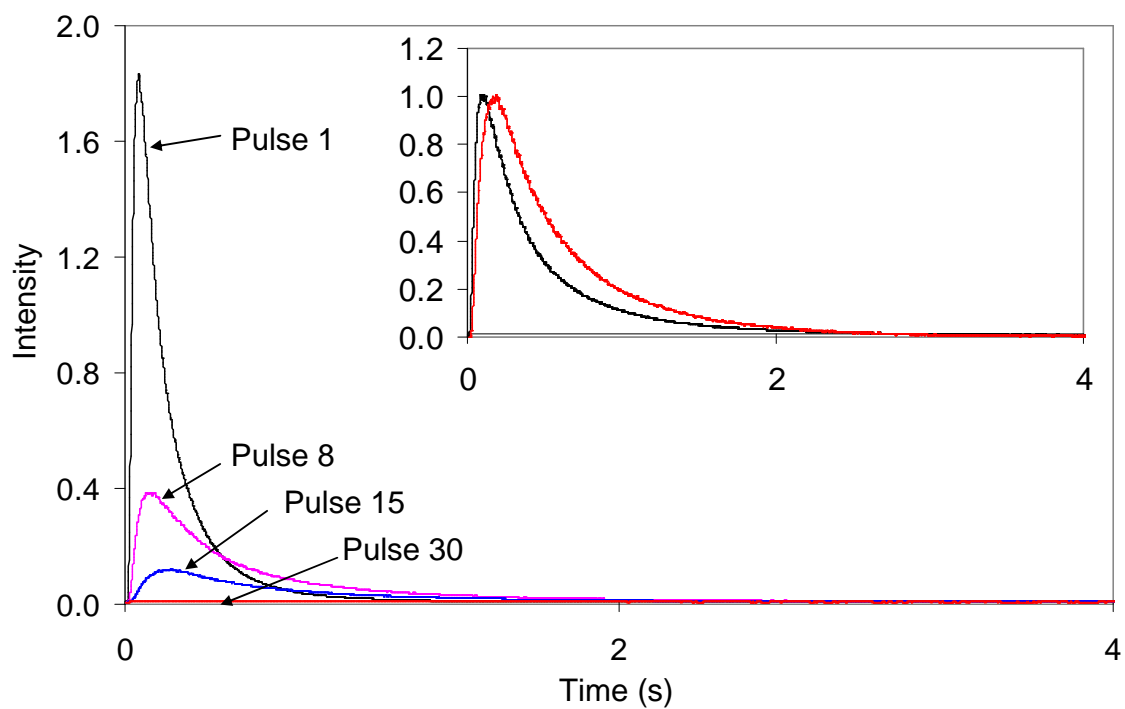


**Figure 5.19** Individual pulse response curves for MA plotted from the 3-D graph in Figure 5.15 obtained over thin bed of VPO catalysts at 400 °C. The inset shows the height normalized pulse curves for pulse 8 and 15.

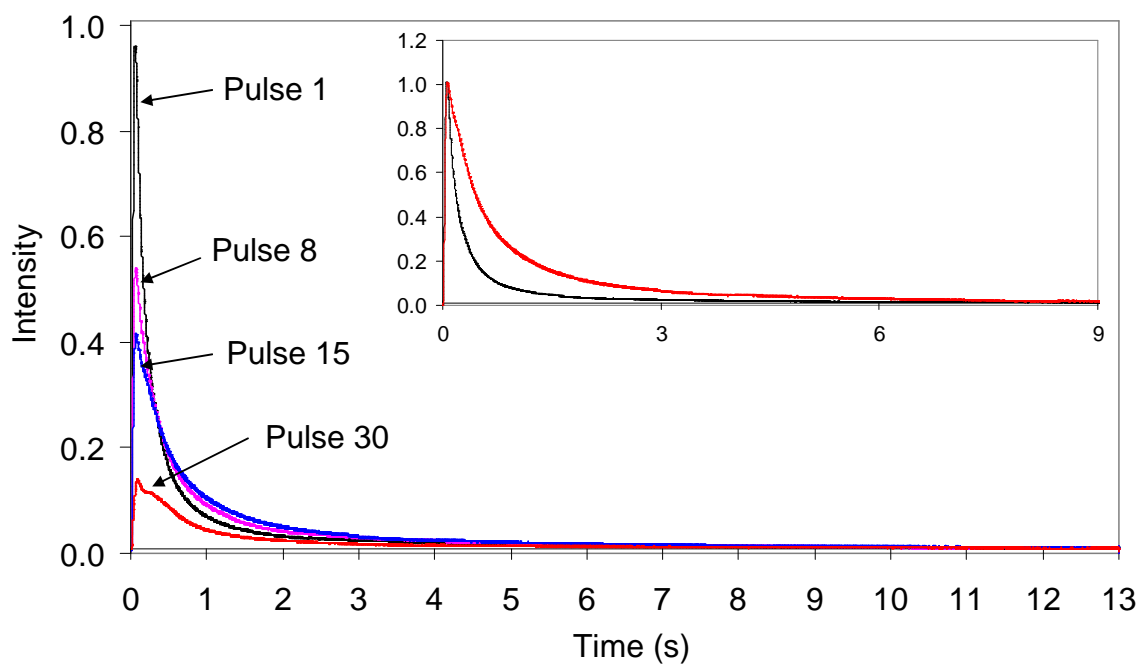


**Figure 5.20** Individual pulse response curves for CO<sub>2</sub> plotted from the 3-D graph in Figure 5.16 obtained over thin bed of VPO catalysts at 400 °C. The inset shows the height normalized pulse curves for pulse 1 and 15.



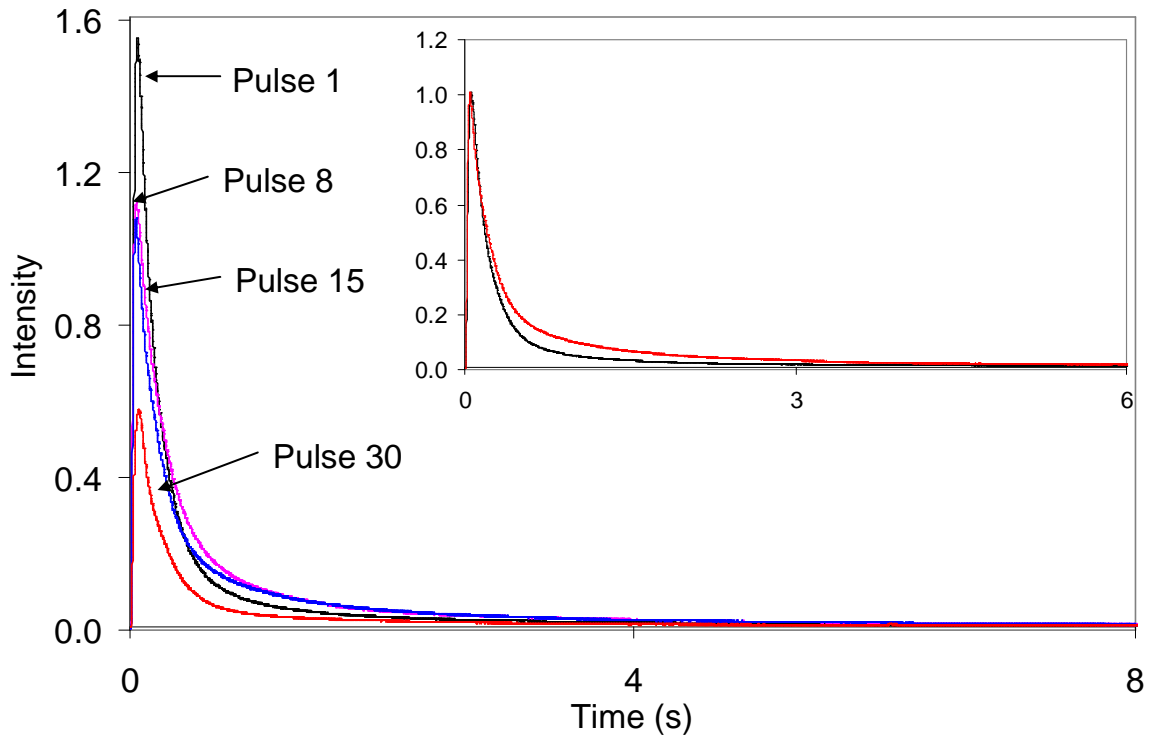


**Figure 5.21** Individual pulse response curves for CO plotted from the 3-D graph in Figure 5.17 obtained over thin bed of VPO catalysts at 400 °C. The inset shows the height normalized pulse curves for pulse 1 and 15.

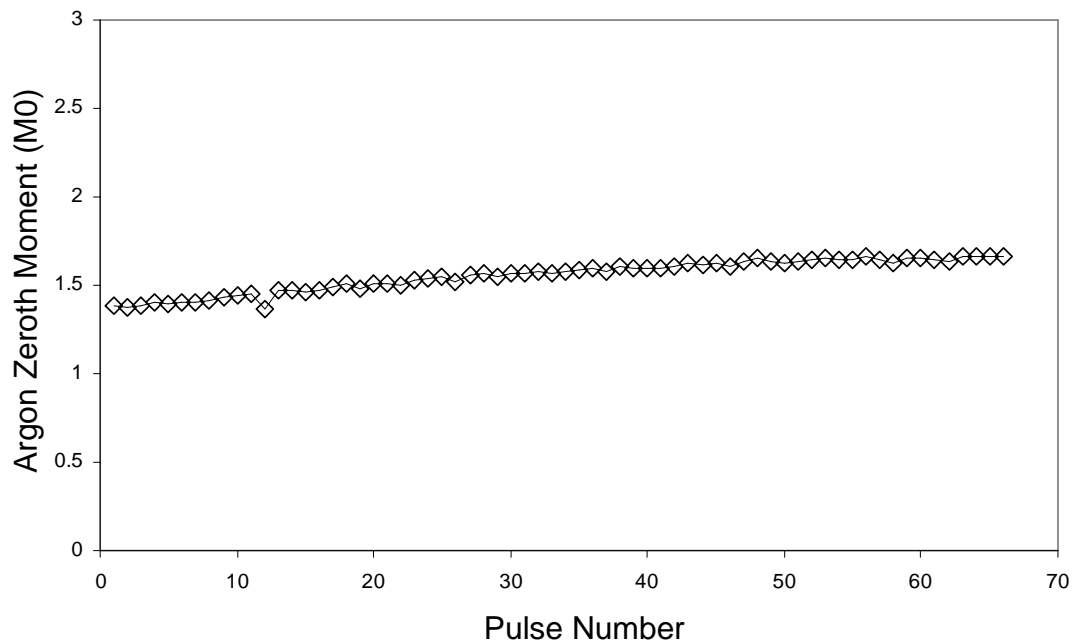


**Figure 5.22** Graph of argon zeroth moment ( $M_0$ ) plotted against the corresponding pulse number at 400 °C. This shows that the pulse valve is very consistent and each pulse contains approximately the same number of gas molecules sent into the microreactor.

Looking at Figure 5.18, the pulse shape for furan is not changing much as more and more furan pulses are introduced into the microreactor. What is changing is the amount of furan coming out of the microreactor exit because the catalyst is changing from an oxidized state to a reduced state. As oxygen on the VPO catalyst is being used up, there is less available oxygen for the furan to react with; therefore, as more furan pulses are sent into the microreactor, an increasing portion of the pulses leave unreacted.

The MA exit flow pulse response curves in Figure 5.19 show that the largest amount of MA produced is during the first pulse because at the beginning, the VPO catalyst is at its

most oxidized state. There is more oxygen on the VPO catalyst for the furan pulse to react with. Notice in the inset in Figure 5.19 that the MA pulse response curve widens with increasing pulses of furan. This widening of the MA pulse curve indicates that as the VPO catalyst reaches a more reduced state, it takes longer for a furan gas molecule to find available oxygen to react with to produce MA.

The most drastic change observed in the exit flow pulse response curves is the one for CO<sub>2</sub> (Figures 5.16 and 5.20). As the VPO catalyst is reduced with furan pulses, the CO<sub>2</sub> production decreases and the pulse shape changes from a single peak to a double peak. Compared to the pulse response curves for CO (Figure 5.21), it can be clearly seen that CO<sub>2</sub> and CO are two separate products that may be formed from two separate reaction pathways. The CO pulse response curves do not exhibit a double peak. An explanation for the double peak seen on the CO<sub>2</sub> pulse curves can be related to how the CO<sub>2</sub> is formed. As the VPO catalyst is reduced, there is less available oxygen, therefore, the CO<sub>2</sub> production decreases. The initial CO<sub>2</sub> production is produced mostly from surface oxygen that is readily available from the initial oxidation in air. This type of oxygen may be specific for the production of CO<sub>2</sub> and CO. Recall from the previous section that we proposed there may be two forms of active oxygen on the VPO catalyst: one type for the production of MA and another type for the production of CO<sub>2</sub> and CO. As time passes and the catalyst is reduced further (see inset in Figure 5.20), the CO<sub>2</sub> exit flow pulse curve widens considerably and the appearance of the double peak is observed. The initial first peak in the CO<sub>2</sub> double peak curve may suggest a portion of the CO<sub>2</sub> produced is

still coming from the reaction of furan with oxygen on the VPO surface, although now it is probably sub-surface oxygen. The second, latter peak in the CO<sub>2</sub> double peak can be explained by two ways. The first explanation is that the second peak in the CO<sub>2</sub> curve is a result of a time delay for a furan molecule to find oxygen to react with. Because the VPO catalyst is in an almost completely reduced state, there is no more readily available surface and sub-surface oxygen, therefore, the furan molecule has to find lattice oxygen to react with. The problem with this explanation is why we do not see this same double peak behavior for CO production. The reason is that CO production is not as an oxygen-rich process as that for the production of CO<sub>2</sub>. Another explanation for the CO<sub>2</sub> double peak is that the second peak is the result of CO<sub>2</sub> production from another pathway, for example the dissociation of MA to CO<sub>2</sub> [11]. Another detail found in the exit flow pulse response curves of CO<sub>2</sub> and CO to support the previous theory is the time it takes for the entire product to come out of the microreactor during a single furan pulse. For example, it takes approximately 4 seconds for the CO pulse in its entirety to come out of the microreactor (Figure 5.21). In comparison, it takes almost 8 seconds for the CO<sub>2</sub> pulse to completely come out of the microreactor (Figure 5.20). This time difference may be used to explain that a portion of the CO<sub>2</sub> produced is from a slower, secondary mechanistic step.

One of the experimental lessons learned and observed from the furan oxidation experiments over VPO catalysts is to set a long data collection time so that enough time is allocated for the entire CO<sub>2</sub> pulse response curve to come out of the microreactor. If

the collection time is set too short, then during a furan pulse, not all of the CO<sub>2</sub> is collected coming out of the microreactor. Therefore, when the next furan pulse is sent into the microreactor, there is still leftover CO<sub>2</sub> on the VPO surface from the previous pulse. This results in a build-up of CO<sub>2</sub> on the catalyst surface which interferes with accurate data measurements. The original collection times were set for 4 seconds and 7 seconds. However, as you can see from the CO<sub>2</sub> data (Figure 5.20) that even 7 seconds is not enough time for all of the CO<sub>2</sub> to exit the microreactor. Finally, a collection time of 13 seconds was set to ensure enough time for all of the CO<sub>2</sub> pulse to exit the microreactor.

The main idea from this section is to show that a tremendous amount of information can be gathered simply by looking at the raw TAP pulse response curves, without any mathematical analysis. Just by looking at the pulse data, we were able to come to the conclusion that furan oxidation over VPO catalysts may involve two separate reaction pathways. The first pathway is the reaction of furan with oxygen to produce MA, CO<sub>2</sub>, and CO. The second pathway is the dissociation and oxidation of MA to produce CO<sub>2</sub>.

## **5.4 Observation of VPO Structure Sensitivity**

The ability to visually detect catalyst structural changes is typically reserved for surface science techniques. Although the TAP reactor system cannot perform catalyst surface analysis in situ right now, it can relate a change in the kinetics to a change in the catalyst

structure and composition. The small amount of gas molecules sent into the microreactor during a single pulse does not alter the catalyst surface composition significantly; therefore, minute changes in the activity can be monitored.

The furan oxidation experiments over VPO catalysts were performed by collecting five different atomic masses during the same experiment (MA, CO<sub>2</sub>, CO, furan, and argon). Recall as previously stated, the TAP data acquisition system and mass spectrometer can only collect one atomic mass per furan pulse at a time. Therefore, for every atomic mass collected, it corresponds to every fifth furan pulse. For example, the first MA pulse response curve observed corresponds to the first furan pulse sent into the microreactor because MA was set to be the first atomic mass to be collected. The second MA pulse response curve collected does not correspond to the second furan pulse sent into the microreactor; instead it corresponds to the sixth furan pulse sent into the microreactor. In order to capture the MA production during the lapsed period between furan pulses, an experiment was conducted in which only MA and argon was collected. Instead of collecting the MA response for every fifth furan pulse, now the MA is obtained for every other furan pulse. Also, the number of furan molecules sent into the microreactor per pulse was lowered significantly to probe the VPO catalyst even further. Typically, one reactant pulse contains on the order of  $10^{14}$  gas molecules. During these experiments, the pulse valve voltage was lowered so that during one reactant pulse approximately  $10^{12}$  furan molecules were sent into the microreactor. The goal of these experiments was to understand what is occurring on the VPO catalyst during the beginning of the furan

oxidation when there was a maximum observed during the production of MA (see Figure 5.3 in Section 5.1). A surprising phenomenon was found as a result of these experiments which demonstrated the sensitivity of the TAP technique.

Figure 5.23 shows the 3-D plot of MA collected for every other furan pulse sent into the microreactor at 400 °C (TAP vacuum pulse response experiments). The VPO catalyst was oxidized the same way as previous experiments by exposing it to atmospheric air at 480 °C for 10 minutes. Figure 5.23 shows that there is a step increase in the amount of MA produced during the very beginning of furan oxidation. Figure 5.24 plots the areas under the MA pulse response curves shown in Figure 5.23 (zeroth moment) normalized to the argon pulse response as a function of the furan pulse number. The MA produced during the first furan pulse starts off low indicating that the initial surface oxygen is not as selective. Then, the MA production rises and reaches the first plateau. At approximately pulse 10, the MA production increases again and reaches a second plateau. At approximately pulse 25, the MA production drops and decreases gradually as oxygen is being depleted from the VPO catalyst. The sudden increases in the amount of MA produced could suggest that as the initial, outermost layer of oxygen atoms is removed from the VPO surface, the oxygen underneath is actually more active. Also, if too much oxygen is present on the VPO surface, there are less available active sites for furan adsorption. As more oxygen is removed, the furan molecule has more available sites to adsorb on the VPO surface and then react with oxygen atoms in its vicinity. The second plateau observed from Figure 5.23 could indicate that the first or second monolayers of

surface oxygen are the most active and selective for MA production. After the surface and sub-surface oxygen is removed, the MA production decreases steadily because the oxygen supply is diminishing and is mostly supplied by VPO lattice oxygen. The two plateaus observed on the MA production plot could also suggest a rearrangement of the VPO surface atoms to allow for a more selective and active orientation. With an improvement in the TAP reactor system design, kinetic experiments could be performed in situ with catalyst surface analysis to confirm this conclusion.

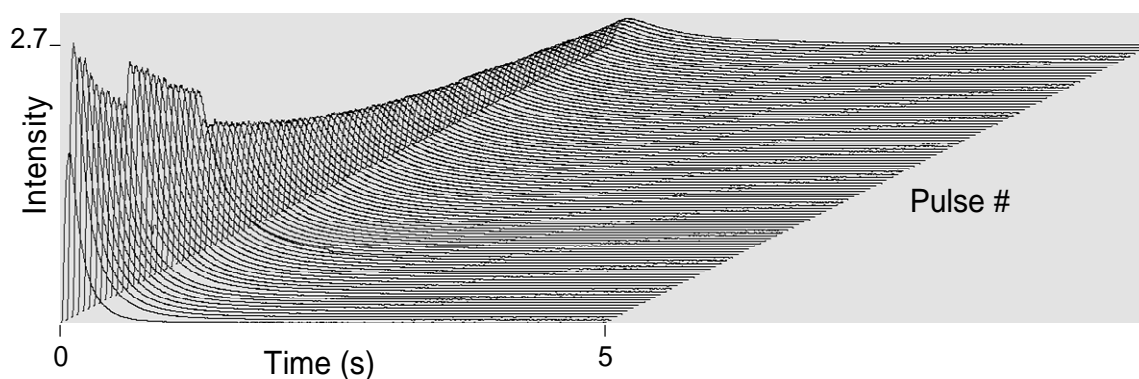


**Figure 5.23** 3-D plot of MA production obtained with smaller furan pulses at 400 °C. Each MA pulse response curve was collected during every other furan pulse sent into the TAP microreactor.



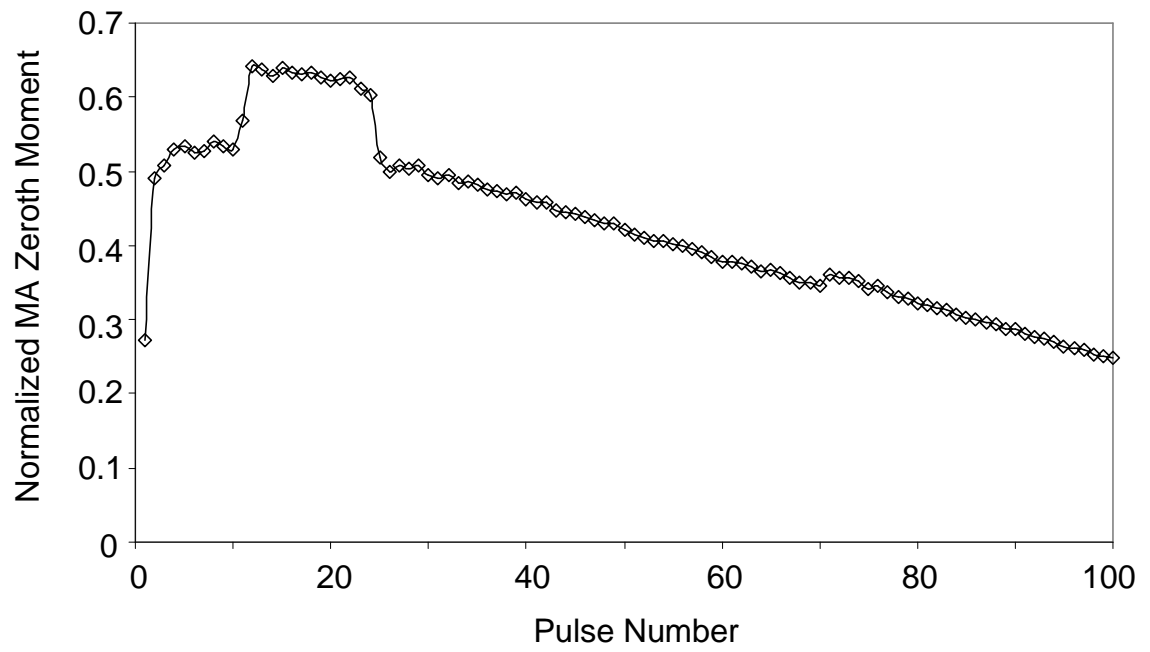


**Figure 5.24** MA normalized zeroth moment found from the areas under the MA pulse response curves shown in Figure 5.23.

# Chapter 6

## Conclusions

The work presented in this dissertation is dedicated to a greater understanding of catalyst development and characterization. The time it takes for a catalyst to be commercialized may take many years of research. The goal of the experimental work in this dissertation is to introduce new approaches for catalyst characterization using the TAP reactor system to simplify and shorten the time for the catalyst development process. At the same time, a tremendous amount of information related to the catalyst structure and composition can be gathered using TAP experiments to understand the catalytic performance. TAP vacuum pulse response, temperature-programmed, pump-probe, and steady-state experiments can be performed on different catalyst samples to obtain kinetic parameters and understand the role of reactive species on the catalyst surface. In particular, two types of catalytic systems were studied in this dissertation. The first system is CO oxidation on Pt catalysts (Pt powder particle, Pt foil, Pt supported on SiO<sub>2</sub>). One of the most significant results found from these experiments was the high conversion of CO on a single 400 micron Pt particle packed in a bed among approximately 100,000 inert quartz particles. The main results for CO oxidation on Pt catalysts are listed below.

1) With a single 400 micron diameter Pt particle packed in the center of the microreactor bed surrounded by inert quartz particles with diameters between 210-250 microns, 95 percent conversion of CO was obtained at 170 °C.

2) The new TAP reactor configuration, the single particle configuration, has demonstrated the high sensitivity of the TAP reactor and the ability to compare kinetic characteristics of the same catalyst under both high vacuum and atmospheric pressures. Experiments performed under vacuum and atmospheric pressures exhibit a “turning point” at 170 °C, which indicates a transition from the O<sub>2</sub> dominating regime to the CO dominating regime (or vice versa) on the Pt single particle. In both cases, the “turning point” temperature is about the same at 170 °C. Therefore, the “turning point” temperature is the pressure independent characteristic which is governed by the steps of the complex catalytic processes with no participation of gas reactants or products (e.g. CO desorption, interaction between adsorbed oxygen and CO). The fact of observation of such pressure independent characteristic creates a new possibility for bridging across the pressure gap.

3) Experimental data obtained with a Pt foil catalyst support a theoretical, probabilistic mathematical model based on the principle of Brownian motion. The Pt foil is placed in three different locations axially in the center of the microreactor. A conversion profile created from the probabilistic model show good agreement with the experimental data. Conversion near the microreactor inlet is the highest and

conversion at the microreactor outlet is the lowest. The conversion profile can be explained by the Knudsen diffusion of gas molecules inside the TAP microreactor. When the catalyst is placed near the microreactor inlet, gas molecules have a greater probability to return to the active catalyst particle by random motion from hitting the catalyst particle, inert quartz particles, or the microreactor walls. When the catalyst particle is placed near the microreactor outlet, the probability for the gas molecules to return to the catalyst is less because it is near the vacuum chamber which draws the gas molecules out of the microreactor.

4) Similar CO oxidation experiments performed on Pt nanoparticles supported on SiO<sub>2</sub> demonstrate the role of the support material in the chemical reaction. At high reaction temperatures, some oxygen is sitting on the surface of the SiO<sub>2</sub> and the rate at which oxygen is supplied to the active Pt nanoparticles increases, allowing for an increase in the amount of CO<sub>2</sub> produced.

5) TAP pump-probe experiments performed on the single 400 micron Pt particle demonstrated the surface lifetime of reactive adspecies on the catalyst surface by varying the time between the oxygen and CO pulses. As the time delay between the oxygen and CO pulse is increased at high reaction temperatures, the oxygen lifetime on the Pt surface decreases dramatically compared to the same experiment performed at a lower reaction temperature. At high reaction temperatures, there may be some exchange of surface oxygen with the bulk.

The second catalytic system studied is furan oxidation over VPO catalysts. In this system, a thin zone containing 40 mg of VPO catalyst particles (210-250 microns) was packed in the center of the microreactor surrounded by inert quartz particles (210-250 microns). The experiment was carried out by first oxidizing the VPO catalyst in air at 480 °C and then reducing the catalyst with a series of furan pulses under TAP vacuum pulse response conditions. The main results for the furan oxidation studies over VPO catalysts are highlighted below.

- 1) The selective product, maleic anhydride (MA), exhibited a maximum in the yield close to the beginning of the experiment. This indicates that the initial surface oxygen from the oxidation in air is not as selective as the oxygen underneath the first layer.
- 2) As the VPO catalyst is further reduced with furan pulses, the selectivity for MA decreases and increases for the non-selective products, CO<sub>2</sub> and CO.
- 3) The maximum yield observed for MA occurred at the lowest reaction temperature taken at 400 °C. At higher reaction temperatures, up to 480 °C, furan tends to oxidize and dissociate to CO<sub>2</sub> and CO.
- 4) The time for CO<sub>2</sub> to come out of the microreactor was considerably longer than the rest of the products formed. This indicates that CO<sub>2</sub> may be formed from a

secondary mechanistic step. For example, part of the CO<sub>2</sub> could be formed from the oxidation of furan and another portion could be formed from the oxidation of MA.

5) By lowering the pulse intensity of the furan pulses, more detailed information regarding surface processes on the VPO catalyst can be observed. By only collecting the MA and argon pulse responses, step increases (two plateaus) in the amount of MA produced was observed during the beginning of the experiment. This could be the result of a rearrangement of surface atoms of the VPO catalyst to achieve a more selective orientation or we are observing the removal of the immediate surface layer of oxygen atoms. This supports our previous conclusion that the initial layer of oxygen on the VPO is not as selective.

The TAP reactor system is a powerful tool to unravel kinetic characteristics of simple and complex catalytic materials. The work presented in this dissertation provides a small part to a much larger, complex problem of relating the surface composition of a catalyst to its activity and selectivity. However, with a combination of new experimental techniques and equipment development, the gap between surface science and industrial research can be bridged.

## Chapter 7

### Recommendations for Future Work

This project was focused on the introduction of a new TAP microreactor configuration known as the single particle TAP microreactor. In this configuration, a single Pt catalyst particle is placed in the reactor bed surrounded by 100,000 inert quartz particles. The oxidation of CO was selected as a simple test reaction. The single particle experiments open the realm for new experiments to provide a fundamental understanding of catalysts and their performance. For example, the single particle can be defined by a variety of materials ranging from structural complexity from single crystals to mixed metal oxides. The materials can then be tested with the appropriate catalytic system. Coupled with reactor development, these experiments can provide valuable information and insight in the field of catalysis and reaction engineering to understand catalysts and their behavior for certain reaction systems, provide understanding of gas transport processes inside the reactor, and with careful experimentation can simplify the catalyst development process. Before these goals can be realized, a continuation of the single particle experimental work needs to be accomplished to support the development of the single particle TAP microreactor mathematical and theoretical model. The following is a list of possible experiments that still needs to be performed:

1) A more comprehensive study of the placement of the single catalyst particle in the microreactor needs to be performed to support the probabilistic theoretical model. The catalyst particle needs to be placed in various locations in the microreactor in both the axial and radial directions. This helps one to understand the transport behavior of gases in different locations of the microreactor. If the transport properties of gases in the microreactor were uniform, then conversion should be the same regardless of the position of the catalyst particle in the microreactor bed at one reaction temperature.

2) In terms of understanding catalyst structure activity relationships, it would be interesting to place a single crystal in the TAP microreactor. This would create a bridging step between surface science and conventional reactor systems. Experiments have already been performed on a single bulk catalyst particle and supported catalysts but experiments have never been performed on single crystals in the TAP microreactor. Different single crystal orientations can be studied to understand how surface structure changes activity. In continuation with the CO oxidation experiments on Pt, it would be interesting to test out the Pt(111) orientation because of its dense atomic packing and its surface structure stability during the course of the CO oxidation reaction. There are companies who can make the single crystals to specified dimensions. For example, the Pt(111) crystal could be made to be a cylindrical disk, so when placed in the TAP microreactor, the top and bottom faces of the crystal will be facing towards the inlet and outlet of the microreactor to



ensure maximum surface contact with any input gases. One of the benefits of using surface science techniques is the ability to monitor changes in the single crystal structure during the course of an experiment. By studying the single crystal in the TAP reactor, any changes in structure can be monitored by a change in the kinetics. For example, through a series and repetition of experiments by increasing and decreasing the reactor temperature, the CO<sub>2</sub> production can be monitored to see if it changes through the course of the experiments. If changes in the CO<sub>2</sub> production is observed, then it can be noted that there may be changes in the orientation of surface atoms on the Pt(111) single crystal and certain surface atom arrangements may be more active than others. Another method to test whether the Pt(111) single crystal undergoes any atomic surface arrangements is to let the single crystal move in and out of the microreactor over a period of time. Kinetic characterization can be performed before and after set periods of time, and any changes in product yields can be related to changes in the single crystal atomic surface orientations, if any change is observed at all. As a check, a scanning electron microscope (SEM) can be used to record images of the Pt(111) surface before and after experiments to see if there is any changes in the arrangement of surface atoms.

3) Coupled with catalyst fabrication, experiments can be performed using a single catalyst particle by depositing different amounts of active substance on each catalyst support. Then TAP experiments can be performed on the different catalyst samples to determine if there are any changes in the kinetics. A change in the kinetics for the

different catalyst samples can be related to a change in the amount of active material on each catalyst particle.

4) One of the unique features of the TAP experiment is the transport of gases in the microreactor known as Knudsen diffusion. The amount of gas sent into the microreactor per pulse is very small in relation to the volume of the microreactor. The trajectory of the gas molecules in each pulse can be modeled by a random motion or walk inside the microreactor because the gas molecules are hitting the inert particles, reactor walls, thermocouple, or the catalyst particle before exiting the microreactor into the vacuum chamber. A possible experiment that can be performed to prove the high conversion achieved with a single catalyst particle in a packed bed TAP microreactor is to simulate the same experiment except there is no packed bed of inert particles inside the microreactor. The active single Pt particle will have to be suspended on a thermocouple tip. In this experiment, a fast response time, stainless steel thermocouple will be used as a substrate to deposit Pt metal on its tip. Fast response time thermocouples typically have very thin probes and in order to deposit Pt metal on the tip, we must be sure that the TAP reactor is sensitive enough to catch activity from a very minute amount of catalyst. Deposition of metals on thermocouple tips enables us to find close to exact temperature profiles of the catalyst in the microreactor. We may also be able to detect the amount of exothermic heat given off during reaction, or the amount of heat rise associated with adsorption of reactant gases. This experiment requires the construction of a new microreactor

where there is a side fitting that allows for the removal and replacement of the thermocouple. The current microreactor has a removable screen at the outlet where inert and catalyst particles can be packed with a stationary thermocouple on the inside of the microreactor. However, if we wanted to deposit different amounts of Pt metal on the thermocouple tip, we would need to transfer the thermocouple in and out of the microreactor constantly. Therefore, the new microreactor with a vacuum tight side fitting to accommodate the thermocouple will be convenient and necessary for these experiments. The hypothesis is that without a packed bed of inert quartz particles, conversion will be extremely low with only a single catalyst particle in the microreactor.

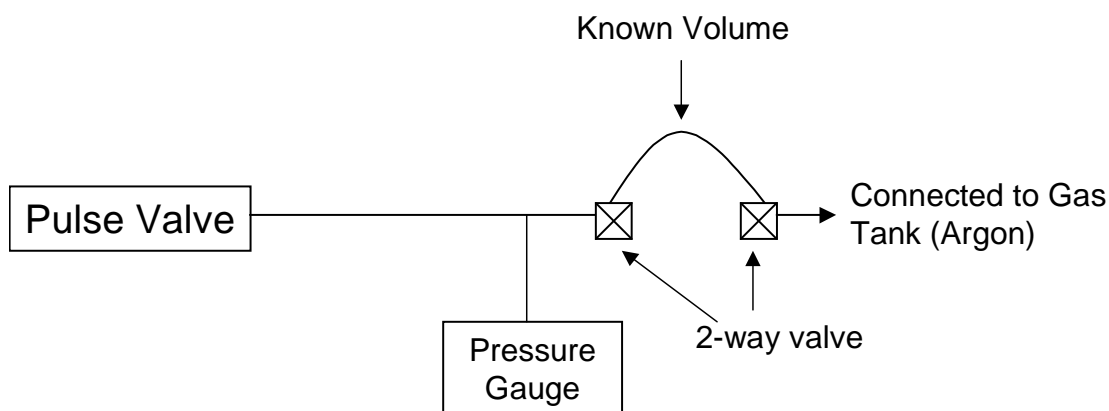
In regards to the VPO experiments, further tests should be performed using other reactant gases besides furan to probe the oxidative state of the VPO catalyst for the production of maleic anhydride. For example, experiments can be performed using the other intermediate products formed from the *n*-butane to maleic anhydride process as the reactant gas such as butenes and butadiene. For the *n*-butane oxidation reaction to produce maleic anhydride, the first step of *n*-butane activation is the rate determining step of the reaction, therefore, information on the reactivity and kinetics of the consecutive steps in the reaction can only be obtained by studying the kinetics of the intermediate olefin products. By studying different reactant gases such as butenes, butadiene, and *n*-butane, one can try to understand the oxygen source on the VPO catalyst. For example, when 1-butene is used as the reactant, the amount of lattice oxygen incorporated in the

products of reaction is much higher than when *n*-butane is used as the reactant [65]. This indicates the substantial difference in the reactivity and the type of interaction of 1-butene and *n*-butane to the oxygen on the VPO. Another experiment that is useful in understanding the active phase of VPO catalysts for maleic anhydride formation is to deposit controlled amounts of vanadium atoms to the surface of the VPO catalyst.

# Appendix A

## Calibration of Pulse Valves

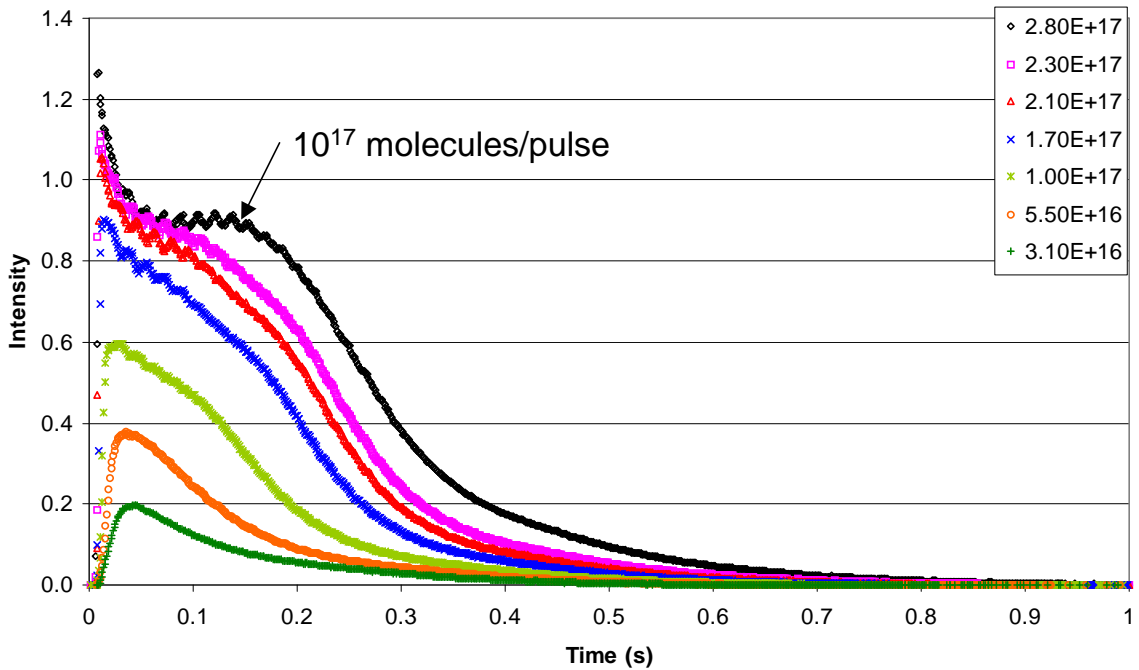
TAP vacuum pulse response experiments measure the amount of gas leaving the microreactor outlet. However, the amount of gas sent into the microreactor needs to be calibrated in order to ensure that the pulse valves are operating in the Knudsen diffusion regime. Also, the number of gas molecules sent into the microreactor can be used to calculate conversion data if one knows the ratio of reactant/inert in the gas blend. Figure A.1 shows a schematic of the assembly used to calibrate the pulse valves. The assembly contains a known volume, two 2-way valves, a manometer that can measure the pressure, and 1/16-inch diameter stainless steel tubing. The known volume used was a U-shaped ¼-inch diameter stainless steel tubing that was weighed before and after being filled with water. The difference in mass and the density of water can be used to calculate the volume. A 2-way valve was connected to either end of the U-shaped tubing. One of the 2-way valves was connected directly to the inert gas tank (argon) and the other valve was connected to the pulse valve. In between the 2-way valve and the pulse valve, a 3-way connector is used to set-up a manometer to measure the pressure.



**Figure A.1** Schematic of assembly used to calibrate pulse valves.

The experimental procedure to calibrate the pulse valves is as follows. Let some gas from the argon gas tank to fill the entire calibration assembly and record the pressure ( $P_1$ ). Close the 2-way valve in the middle (leading up to the pulse valve) and evacuate the 1/16-inch diameter stainless steel tubing all the way from the middle 2-way valve to the pulse valve. Once that line is evacuated, make sure the 2-way valve connected to the argon gas tank is closed. Open the middle 2-way valve and record the pressure ( $P_2$ ).  $P_1$  is the pressure in the known volume and  $P_2$  is the pressure in the entire calibration assembly. The known volume is already calculated, therefore simply use the equation  $P_1V_1 = P_2V_2$  to find the volume of the entire calibration assembly ( $V_2$ ). Start pulsing from the pulse valves and measure the pressure drop. Also make sure to keep track of the number of pulses used. The number of gas molecules per pulse can be calculated using the ideal gas law,  $PV = nRT$ .

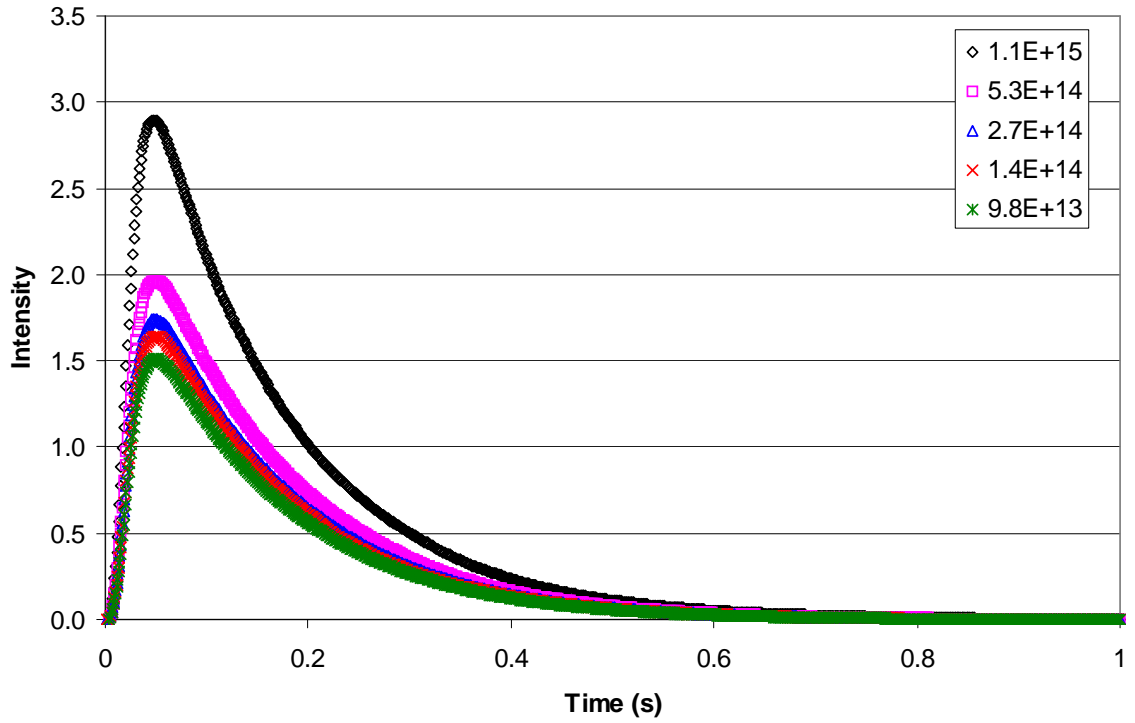
The pulse valves are highly dependent on both the pressure in the gas blend tanks and the pulse valve voltage, which controls its intensity. If too much gas is sent into the microreactor in a single pulse, the gas transport properties are no longer in the TAP Knudsen diffusion regime. Figure A.2 shows how pressure in the gas blend tank can affect the pulse shape. At high pressures, typically around 35 psia, transport in the microreactor is in a transition zone between convective flow and diffusion. At this pressure, it is equal to approximately  $10^{17}$  gas molecules sent into the microreactor per pulse. A typical TAP Knudsen pulse is on the order of  $10^{13}$  to  $10^{14}$  gas molecules per pulse. When too much pressure is in the pulse valves, the appearance of a double peak occurs in the pulse response. The first peak is related to a pressure driven force from the pulse valves and the second peak (plateau) is attributed to diffusion of the remaining gas molecules in the pulse. Once gas transport inside the microreactor reaches the Knudsen diffusion regime, the shape of the pulse curve should be independent of the pulse intensity.



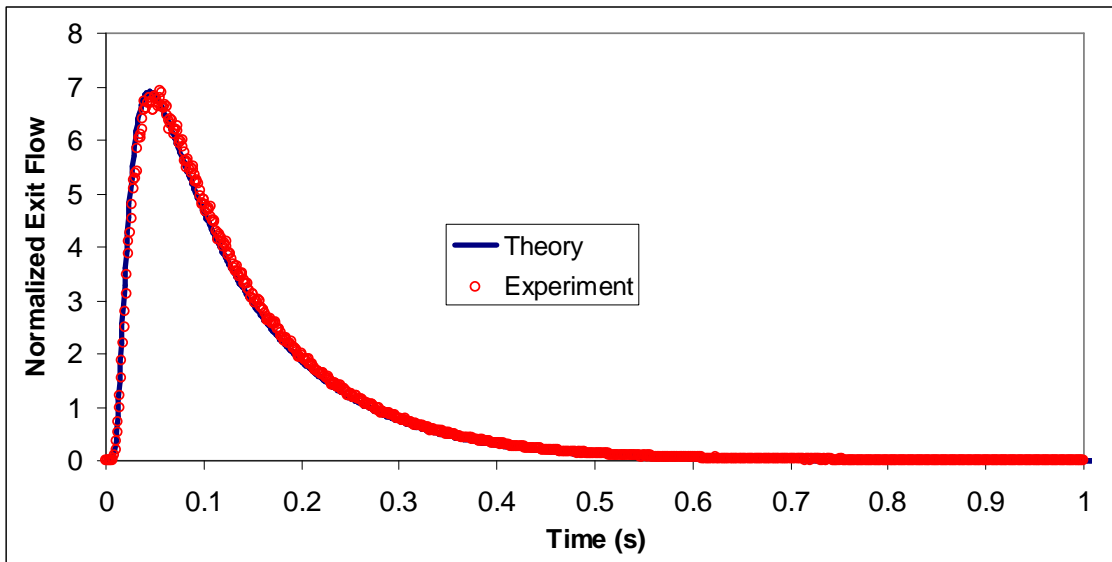
**Figure A.2** Argon pulse response curves showing the pressure dependence on pulse valve operation.

Figure A.3 plots the argon pulse response curves at lower pulse intensities in the Knudsen diffusion regime ( $10^{13} - 10^{14}$  gas molecules/pulse). In Figure A.3, although the size of the pulse curves is changing because the amount of gas in each pulse is decreasing, the shape of the curves is the same. The shape of each Knudsen pulse curve can be fitted to the standard diffusion curve (Figure A.4).





**Figure A.3** Argon pulse response curves at low pulse intensities in the Knudsen diffusion regime.



**Figure A.4** Comparison of experimentally obtained argon pulse response curve and the standard diffusion curve.

# References

- [1] M.W. Roberts, "Birth of the Catalytic Concept (1800-1900)," *Catalysis Letters* 67(1) (2000) 1-4.
- [2] J. Hagen, "Industrial Catalysis: A Practical Approach," Wiley-VCH, Weinheim, Germany (2006) 507 pages.
- [3] M.I. Temkin, *Adv. Catal.* 28 (1979) 173-291.
- [4] F.M. Dautzenberg, "Ten Guidelines for Catalysis Testing," in *Characterization and Catalyst Development*, S.A. Bradley, M.J. Galhuso, R.J. Bertolacini (Eds.), ACS Symposium Series 411, American Chemical Society, Washington D.C. (1989).
- [5] C.O. Bennett, "Experiments and Processes in the Transient Regime for Heterogeneous Catalysis," *Adv. Catal.* 44 (2000) 329-415.
- [6] C.O. Bennett, "A Dynamic Method for the Study of Heterogeneous Catalytic Kinetics," *AIChE Journal* 13 (1967) 890-895.
- [7] M. Eigen, "Technique of Organic Chemistry," A. Weissberger (Ed.), Vol. 8, Part II, Interscience, New York (1963).
- [8] H. Kobayashi, M. Kobayashi, *Catal. Rev.-Sci. Eng.* 10(2) (1974) 139-176.
- [9] S.O. Shekhtman, G.S. Yablonsky, "Thin-Zone TAP Reactor versus Differential PFR: Analysis of Concentration Nonuniformity for Gas-Solid Systems," *Ind. Eng. Chem. Res.* 44 (2005) 6518-6522.
- [10] J.A. Moulijn, M. Makkee, A.E. van Diepen, "Chemical Process Technology," Wiley, West Sussex (2001).
- [11] G.S. Patience, M.J. Lorences, "VPO Transient Oxidation Kinetics," *International Journal of Chemical Reactor Engineering*, Vol. 4, Article A22 (2006).
- [12] Y. Schuurman, J.T. Gleaves, "A Comparison of Steady-State and Unsteady-State Reaction Kinetics of n-Butane Oxidation over VPO Catalysts using a TAP-2 Reactor System," *Catal. Today* 33 (1997) 25-37.

- [13] J. Pérez-Ramírez, A. Gallardo-Llamas, C. Daniel, C. Mirodatos, "N<sub>2</sub>O-Mediated Propane Oxidative Dehydrogenation over Fe-Zeolites. TEOM Studies for Continuous Propylene Production in a Cyclically-Operated Reactor," *Chem. Eng. Sci.* 59 (2004) 5535-5543.
- [14] C.M.L. Scholz, V.R. Gangwal, M.H.J.M. de Croon, J.C. Schouten, "Model for NO<sub>x</sub> Storage/Reduction in the Presence of CO<sub>2</sub> on a Pt-Ba/γ-Al<sub>2</sub>O<sub>3</sub> Catalyst," *J. Catal.* 245 (2007) 215-227.
- [15] G.B. Marin, J.H.B.J. Hoebink, "Kinetic Modeling of Automotive Exhaust Catalysis," *CATTECH 1* (1997) 137-148.
- [16] A.B.K. Lie, J. Hoebink, G.B. Marin, "The Effects of Oscillatory Feeding of CO and O<sub>2</sub> on the Performance of a Monolithic Catalytic Converter of Automobile Exhaust Gas: A Modeling Study: Chemical Engineering Research in the Netherlands," *Chemical Engineering Journal and the Biochemical Engineering Journal* 53 (1993) 47-54.
- [17] M.P. Harold, P.L. Mills, J.F. Nicole, *Stud. Surf. Sci. Catal.* 133 (2001) 87-99.
- [18] R.J. Berger, F. Kapteijn, J.A. Moulijn, G.B. Marin, J. De Wilde, M. Olea, D. Chen, A. Holmen, L. Lietti, E. Tronconi, Y. Schuurman, "Dynamic Methods for Catalytic Kinetics," *Appl. Catal. A: General* 342 (2008) 3-28.
- [19] R.J. Berger, E.H. Stitt, G.B. Marin, F. Kapteijn, J.A. Moulijn, "Eurokin: Chemical Reaction Kinetics in Practice," *CATTECH 5* (2001) 30-60.
- [20] J. Happel, "Isotopic Assessment of Heterogeneous Catalysis," Academic Press, Orlando (1986).
- [21] S.L. Shannon, J.G. Goodwin, "Characterization of Catalytic Surfaces by Isotopic-Transient Kinetics during Steady-State Reaction," *Chem. Rev.* 95 (1995) 677-695.
- [22] J.T. Gleaves, J.R. Ebner, T.C. Kuechler, "Temporal Analysis of Products (TAP)-A Unique Catalyst Evaluation System with Submillisecond Time Resolution," *Catal. Rev.-Sci. Eng.* 30(1) (1988) 49-116.
- [23] J.T. Gleaves, G.S. Yablonskii, P. Phanawadee, Y. Schuurman, "TAP-2: An Interrogative Kinetics Approach," *Appl. Catal. A: General* 160 (1997) 55-88.
- [24] "The TAP Reactor in Catalysis: Recent Advances in Theory and Practice," J. Pérez-Ramírez, E.V. Kondratenko (Eds.), *Catal. Today* 121 (2007) 1-124.

- [25] Y. Schuurman, A. Pantazidis, C. Mirodatos, "The TAP-2 Reactor as an Alternative Tool for Investigating FCC Catalysts," *Chem. Eng. Sci.* 54(15-16) (1999) 3619-3625.
- [26] M. Bron, E. Kondratenko, A. Trunschke, P. Claus, "Towards the Pressure and Materials Gap: Hydrogenation of Acrolein using Silver Catalysts," *Z. Phys. Chem.* 218 (2004) 405-424.
- [27] O.V. Buyevskaya, M. Baerns, "Catalytic Selective Oxidation of Propane," *Catal. Today* 42(3) (1998) 315-323.
- [28] E.V. Kondratenko, M. Cherian, M. Baerns, "Mechanistic Aspects of the Oxidative Dehydrogenation of Propane over an Alumina-Supported VCrMnWO<sub>x</sub> Mixed Oxide Catalyst," *Catal. Today* 99(1-2) (2005) 59-67.
- [29] O.V. Buyevskaya, M. Rothaemel, H.W. Zanthoff, M. Baerns, "Transient Studies on Reaction Steps in the Oxidative Coupling of Methane over Catalytic Surfaces of MgO and Sm<sub>2</sub>O<sub>3</sub>," *J. Catal.* 146(2) (1994) 346-357.
- [30] M. Fathi, F. Monnet, Y. Schuurman, A. Holmen, C. Mirodatos, "Reactive Oxygen Species on Platinum Gauzes during Partial Oxidation of Methane into Synthesis Gas," *J. Catal.* 190(2) (2000) 439-445.
- [31] M. Olea, M. Florea, I. Sack, R. Prada Silvy, E.M. Gaigneaux, G.B. Marin, P. Grange, "Evidence for the Participation of Lattice Nitrogen from Vanadium Aluminum Oxynitrides in Propane Ammoxidation," *J. Catal.* 232(1) (2005) 152-160.
- [32] F. Konietzki, H.W. Zanthoff, W.F. Maier, "The Role of Active Oxygen in the AMM-V<sub>x</sub>Si-Catalysed Selective Oxidation of Toluene," *J. Catal.* 188(1) (1999) 154-164.
- [33] U. Rodemerck, B. Kubias, H.W. Zanthoff, G.U. Wolf, M. Baerns, "The Reaction Mechanism of the Selective Oxidation of Butane on (VO)<sub>2</sub>P<sub>2</sub>O<sub>7</sub> Catalysts: The Influence of the Valence State of Vanadium," *Appl. Catal. A: General* 153 (1997) 217-231.
- [34] J. Pérez-Ramírez, E.V. Kondratenko, V.A. Kondratenko, M. Baerns, "Selectivity-Directing Factors of Ammonia Oxidation over PGM Gauzes in the Temporal Analysis of Products Reactor: Secondary Interactions of NH<sub>3</sub> and NO," *J. Catal.* 229(2) (2005) 303-313.

- [35] A. Setiabudi, J. Chen, G. Mul, M. Makkee, J.A. Moulijn, "CeO<sub>2</sub> Catalysed Soot Oxidation: The Role of Active Oxygen to Accelerate the Oxidation Conversion," *Appl. Catal. B: Environmental* 51 (2004) 9-19.
- [36] T. Gerlach, M. Baerns, "Application of the TAP-2 Reactor and FTIR in Elucidating the Mechanism of NO<sub>2</sub> Reduction by Propene over an Acidic Mordenite," *Chem. Eng. Sci.* 54 (1999) 4379-4384.
- [37] K.S. Kabin, P. Khanna, R. Muncrief, V. Medhekar, M. Harold, "Monolith and TAP Reactor Studies of NO<sub>x</sub> Storage on Pt/BaO/Al<sub>2</sub>O<sub>3</sub>: Elucidating the Mechanistic Pathways and Roles of Pt," *Catal. Today* 114 (2006) 72-85.
- [38] E.V. Kondratenko, J. Pérez-Ramírez, *Appl. Catal. B* 64 (2006) 35-41.
- [39] C.S. Heneghan, G.J. Hutchings, S.R. O'Leary, S.H. Taylor, V.J. Boyd, I.D. Hudson, *Catal. Today* 54(1) (1999) 3-12.
- [40] R. Fushimi, J.T. Gleaves, G.S. Yablonsky, A. Gaffney, M. Clark, S. Han, "Combining TAP-2 Experiments with Atomic Beam Deposition of Pd on Quartz Particles," *Catal. Today* 121(3-4) (2007) 170-186.
- [41] R.H. Nibbelke, M.A.J. Campman, J.H.B.J. Hoebink, G.B.M.M. Marin, "Kinetic Study of the CO Oxidation over Pt/ $\gamma$ -Al<sub>2</sub>O<sub>3</sub> and Pt/Rh/CeO<sub>2</sub>/ $\gamma$ -Al<sub>2</sub>O<sub>3</sub> in the Presence of H<sub>2</sub>O and CO<sub>2</sub>," *J. Catal.* 171 (1997) 358-373.
- [42] Y.J. Merger, J. Hoebink, B.E. Nieuwenhuys, "CO Oxidation over a Pt/CoO<sub>x</sub>/SiO<sub>2</sub> Catalyst: A Study using Temporal Analysis of Products," *J. Catal.* 167(2) (1997) 305-313.
- [43] X. Zheng, J.T. Gleaves, G.S. Yablonsky, T. Brownscombe, A. Gaffney, M. Clark, S. Han, "Needle in a Haystack Catalysis," *Appl. Catal. A: General* 341(1-2) (2008) 86-92.
- [44] D. Briggs, J. Grant, "Perspectives on XPS and AES, Surface Analysis by Auger and X-Ray Photoelectron Spectroscopy," D. Briggs, J. Grant (Eds.), *IM Publications and Surface Spectra*, United Kingdom (2003).
- [45] M. Eiswirth, P. Möller, K. Wetzl, R. Imbihl, G. Ertl, "Mechanisms of Spatial Self-Organization in Isothermal Kinetic Oscillations during the Catalytic CO Oxidation on Pt Single Crystal Surfaces," *J. Chem. Phys.* 90(1) (1989) 510-521.
- [46] R.C. Yeates, J.E. Turner, A.J. Gellman, G.A. Somorjai, "The Oscillatory Behavior of the CO Oxidation Reaction at Atmospheric Pressure over Platinum

- Single Crystals: Surface Analysis and Pressure Dependent Mechanisms,” *Surf. Sci.* 149 (1985) 175-190.
- [47] H.P. Bonzel, H.J. Krebs, “On the Chemical Nature of the Carbonaceous Deposits on Iron after CO Hydrogenation,” *Surf. Sci.* 91 (1980) 499-513.
- [48] J.A. Rodriguez, D.W. Goodman, “High-Pressure Catalytic Reactions over Single-Crystal Metal Surfaces,” *Surf. Sci. Rep.* 14 (1991) 1-107.
- [49] D.W. Goodman, “Model Studies in Catalysis using Surface Science Probes,” *Chem. Rev.* 95 (1995) 523-536.
- [50] P. Stoltze, J.K. Nørskov, *Phys. Rev. Letters* 55 (1985) 2502-2505.
- [51] H.P. Bonzel, “The Role of Surface Science Experiments in Understanding Heterogeneous Catalysis,” *Surf. Sci.* 68 (1977) 236-258.
- [52] T. Engel, G. Ertl, “The Chemical Physics of Solid Surfaces and Heterogeneous Catalysis,” D.A. King, D.P. Woodruff (Eds.), Elsevier, Amsterdam (1982) 73 pages.
- [53] T. Engel, G. Ertl, “Elementary Steps in the Catalytic Oxidation of Carbon Monoxide on Platinum Metals,” D.D. Eley, H. Pines, P.B. Weisz (Eds.), *Advances in Catalysis* 28, Academic Press, New York (1979) 1-78.
- [54] M. Wilf, P.T. Dawson, *Surf. Sci.* 65 (1975) 399-418.
- [55] H.P. Bonzel, R. Ku, “Mechanisms of the Catalytic Carbon Monoxide Oxidation on Pt(110),” *Surf. Sci.* 33 (1972) 91-106.
- [56] T.A. Nijhuis, M. Makkee, A.D. van Langeveld, J.A. Moulijn, “New Insight in the Platinum-Catalyzed CO Oxidation Kinetic Mechanism by using an Advanced TAP Reactor System,” *Appl. Catal. A: General* 164 (1997) 237-249.
- [57] C.T. Campbell, G. Ertl, H. Kuipers, J. Segner, “A Molecular Beam Study of the Catalytic Oxidation of CO on a Pt(111) Surface,” *J. Chem. Phys.* 73 (1980) 5862-5873.
- [58] J.L. Gland, E.B. Kollin, “Carbon Monoxide Oxidation on the Pt(111) Surface: Temperature Programmed Reaction of Coadsorbed Atomic Oxygen and Carbon Monoxide,” *J. Chem. Phys.* 78(2) (1983) 963-974.

- [59] U. Heiz, A. Sanchez, S. Abbet, W.-D. Schneider, "Catalytic Oxidation of Carbon Monoxide on Monodispersed Platinum Clusters: Each Atom Counts," *J. Am. Chem. Soc.* 121 (1999) 3214-3217.
- [60] A.N. Subbotin, B.S. Gudkov, Zh.L. Dykh, V.I. Yakerson, "Temperature Hysteresis in CO Oxidation on Catalysts of Various Nature," *React. Kinet. Catal. Lett.* 66(1) (1999) 97-104.
- [61] J.H.B.J. Hoebink, J.P. Huinink, G.B. Marin, "A Quantitative Analysis of Transient Kinetic Experiments: The Oxidation of CO by O<sub>2</sub> over Pt," *Appl. Catal. A: General* 160 (1997) 139-151.
- [62] M. Sander, R. Imbihl, G. Ertl, "Kinetic Oscillations in Catalytic CO Oxidation on a Cylindrical Pt Single Crystal Surface," *J. Chem. Phys.* 97(7) (1992) 5193-5204.
- [63] A. von Oertzen, A.S. Mikhailov, H.H. Rotermund, G. Ertl, "Subsurface Oxygen in the CO Oxidation Reaction on Pt(110): Experiments and Modeling of Pattern Formation," *J. Phys. Chem. B* 102 (1998) 4966-4981.
- [64] R.K. Grasselli, "Fundamental Principles of Selective Heterogeneous Oxidation Catalysis," *Topics in Catalysis* 21(1-3) (2002) 79-88.
- [65] G. Centi, F. Trifirò, J.R. Ebner, V.M. Franchetti, "Mechanistic Aspects of Maleic Anhydride Synthesis from C<sub>4</sub> Hydrocarbons over Phosphorus Vanadium Oxide," *Chem. Rev.* 88 (1988) 55-80.
- [66] M. Abon, J.-C. Volta, "Vanadium Phosphorus Oxides for n-Butane Oxidation to Maleic Anhydride," *Appl. Catal. A: General* 157 (1997) 173-193.
- [67] Y. Schuurman, J.T. Gleaves, "Activation of Vanadium Phosphorus Oxide Catalysts for Alkane Oxidation. The Influence of the Oxidation State on Catalyst Selectivity," *Ind. Eng. Chem. Res.* 33 (1994) 2935-2941.
- [68] P.L. Mills, H.T. Randall, J.S. McCracken, "Redox Kinetics of VOPO<sub>4</sub> with Butane and Oxygen using the TAP Reactor System," *Chem. Eng. Sci.* 54 (1999) 3709-3721.
- [69] J.R. Ebner, J.T. Gleaves, "Oxygen Complexes and Oxygen Activation by Transition Metals," A.E. Martell, D.T. Sawyer (Eds.), Plenum (1988) 273 pages.
- [70] R. Contractor, J.R. Ebner, M.J. Mummey, *Stud. Surf. Sci. Catal.* 55 (1990) 553.

- [71] Y. Zhang, R.P.A. Sneed, J.C. Volta, "On the Nature of the Active Sites of the VPO Catalysts for n-Butane Oxidation to Maleic Anhydride," *Catal. Today* 16 (1993) 39-49.
- [72] E. Bordes, "Nature of the Active and Selective Sites in Vanadyl Pyrophosphate, Catalyst of Oxidation of n-Butane, Butene and Pentane to Maleic Anhydride," *Catal. Today* 16 (1993) 27-38.
- [73] T.P. Moser, G.L. Schrader, "Stability of Model V-P-O Catalysts for Maleic Anhydride Synthesis," *J. Catal.* 104 (1987) 99-108.
- [74] S.K. Bej, M.S. Rao, "Selective Oxidation of n-Butane to Maleic Anhydride. 1. Optimization Studies," *Ind. Eng. Chem. Res.* 30 (1991) 1819-1824.
- [75] S.O. Shekhtman, G.S. Yablonsky, S. Chen, J.T. Gleaves, "Thin-Zone TAP-Reactor-Theory and Application," *Chem. Eng. Sci.* 54 (1999) 4371-4378.
- [76] P. Phanawadee, S.O. Shekhtman, C. Jarungmanorom, G.S. Yablonsky, J.T. Gleaves, "Uniformity in a Thin-Zone Multi-Pulse TAP Experiment: Numerical Analysis," *Chem. Eng. Sci.* 58 (2003) 2215-2227.
- [77] G.S. Yablonsky, D. Constales, S.O. Shekhtman, J.T. Gleaves, "The Y-Procedure: How to Extract the Chemical Transformation Rate from Reaction-Diffusion Data with No Assumption on the Kinetic Model," *Chem. Eng. Sci.* 62 (2007) 6754-6767.
- [78] J.T. Gleaves, J.R. Ebner, "Method and Apparatus for Carrying Out Catalyzed Chemical Reactions and for Studying Catalysts," U.S. Patent 4,626,412 assigned to Monsanto Company (Dec. 2, 1986).
- [79] J.T. Gleaves, J.R. Ebner, P.L. Mills, "A Novel Catalyst Evaluation System for Temporal Analysis of Reaction Products with Submillisecond Time Resolution," *Studies in Surface Science and Catalysis*, Vol. 38, Elsevier, Amsterdam (1988b).
- [80] J.T. Gleaves, A.G. Sault, R.J. Madix, J.R. Ebner, "Ethylene Oxidation on Silver Powder: A TAP Reactor Study," *J. Catal.* 121 (1990) 202-218.
- [81] G.D. Svoboda, J.T. Gleaves, P.L. Mills, *Studies in Surface Science and Catalysis* 82 (1994) 481.
- [82] J. Libuda, H.-J. Freund, "Molecular Beam Experiments on Model Catalysts," *Surf. Sci. Rep.* 57 (2005) 157-298.



- [83] M. Valden, J. Aaltonen, E. Kuusisto, M. Pessa, C.J. Barnes, "Molecular Beam Studies of CO Oxidation and CO-NO Reactions on a Supported Pd Catalyst," *Surf. Sci.* 307-309 (1994) 193-198.
- [84] M.P. D'Evelyn, R.J. Madix, "Reactive Scattering from Solid Surfaces," *Surf. Sci. Rep.* 3 (1983) 413-495.
- [85] J.A. Barker, D.J. Auerbach, "Gas-Surface Interactions and Dynamics; Thermal Energy Atomic and Molecular Beam Studies," *Surf. Sci. Rep.* 4 (1984) 1-99.
- [86] M.L. Yu, L.A. Delouise, "Surface Chemistry on Semiconductors Studied by Molecular-Beam Reactive Scattering," *Surf. Sci. Rep.* 19 (1994) 285-380.
- [87] A.W. Kleyn, "Molecular Beams and Chemical Dynamics at Surfaces," *Chem. Soc. Rev.* 32 (2003) 87-95.
- [88] C.R. Henry, "Surface Studies of Supported Model Catalysts," *Surf. Sci. Rep.* 31 (1998) 231-325.
- [89] G.S. Yablonsky, M. Olea, G.B. Marin, "Temporal Analysis of Products: Basic Principles, Applications, and Theory," *J. Catal.* 216 (2003) 120-134.
- [90] S.O. Shekhtman, G.S. Yablonsky, J.T. Gleaves, R. Fushimi, "State Defining Experiment in Chemical Kinetics-Primary Characterization of Catalyst Activity in a TAP Experiment," *Chem. Eng. Sci.* 58 (2003) 4843-4859.
- [91] G.S. Yablonskii, S.O. Shekhtman, S. Chen, J.T. Gleaves, "Moment-Based Analysis of Transient Response Catalytic Studies (TAP Experiment)," *Ind. Eng. Chem. Res.* 37 (1998) 2193-2202.
- [92] S.O. Shekhtman, G.S. Yablonsky, J.T. Gleaves, R.R. Fushimi, "Thin-Zone TAP Reactor as a Basis of State-By-State Transient Screening," *Chem. Eng. Sci.* 59 (2004) 5493-5500.
- [93] M. Chareonpanich, A. Nanta-ngern, J. Limtrakul, "Short-Period Synthesis of Ordered Mesoporous Silica SBA-15 using Ultrasonic Technique," *Materials Letters* 61 (2007) 5153-5156.
- [94] T. Witoon, M. Chareonpanich, J. Limtrakul, "Synthesis of Bimodal Porous Silica from Rice Husk Ash via Sol-Gel Process using Chitosan as Template," *Materials Letters* 62 (2008) 1476-1479.

- [95] M.B. Palmer Jr., M.A. Vannice, "The Effect of Preparation Variables on the Dispersion of Supported Platinum Catalysts," *Journal of Chemical Technology and Biotechnology* 30(1) (1980) 205-216.
- [96] R.M. Rioux, H. Song, J.D. Hoefelmeyer, P. Yang, G.A. Somorjai, "High-Surface-Area Catalyst Design: Synthesis, Characterization, and Reaction Studies of Platinum Nanoparticles in Mesoporous SBA-15 Silica," *J. Phys. Chem. B* 109 (2005) 2192-2202.
- [97] M. Chatterjee, T. Iwasaki, Y. Onodera, T. Nagase, "Synthesis of Nanosized Platinum Cluster in Cubic Mesoporous Material via a Direct Introduction Method," *Catalysis Letters* 61(3-4) (1999) 199-202.
- [98] S. Eriksson, U. Nylén, S. Rojas, M. Boutonnet, "Preparation of Catalysts from Microemulsions and Their Applications in Heterogeneous Catalysis," *Appl. Catal. A: General* 265(2) (2004) 207-219.
- [99] G.S. Yablonskii, V.I. Bykov, A.N. Gorban, V.I. Elokhin, "Kinetic Models of Catalytic Reactions," in *Comprehensive Chemical Kinetics* 32, Elsevier (1991) 1-392.
- [100] R. Feres, G.S. Yablonsky, "Knudsen's Cosine Law and Random Billiards," *Chem. Eng. Sci.* 61 (2006) 7864-7883.
- [101] G.E. Uhlenbeck, L.S. Ornstein, "On the Theory of Brownian Motion," *Phys. Rev.* 36 (1930) 823-841.
- [102] R. Feres, G.S. Yablonsky, A. Mueller, A. Baernstein, X. Zheng, J.T. Gleaves, "Probabilistic Analysis of Transport-Reaction Processes over Catalytic Particles: Theory and Experimental Testing," *Chem. Eng. Sci.* 64 (2009) 568-581.
- [103] B. Øksendal, "Stochastic Differential Equations," Springer, Berlin (1998).
- [104] B. Grzybowska-Świerkosz, "Active Centres on Vanadia-Based Catalysts for Selective Oxidation of Hydrocarbons," *Appl. Catal. A: General* 157 (1997) 409-420.
- [105] J.L. Callahan, R.K. Grasselli, "A Selectivity Factor in Vapor-Phase Hydrocarbon Oxidation Catalysis," *AIChE Journal* 9 (1963) 755-760.
- [106] S.O. Shekhtman, "Interrogative Kinetics: A New Methodology for Catalyst Characterization," Doctor of Science Dissertation, Washington University in St. Louis (2003) 1-210.

# Vita

## Xiaolin Zheng

2018 Douglas Drive  
San Angelo, TX 76904  
(512) 659-9847  
LinLin51583@gmail.com

- Date of Birth** May 15, 1983
- Place of Birth** Tianjin, China
- Degrees** B.S. Chemical Engineering, August 2005  
M.S. Chemical Engineering, May 2008  
Ph.D. Energy, Environmental, and Chemical Engineering, August 2009
- Publications** X. Zheng, J.T. Gleaves, G.S. Yablonsky, T. Brownscombe, A. Gaffney, M. Clark, S. Han, Needle in a Haystack Catalysis, *Applied Catalysis A: General* 341 (2008) 86-92.
- R. Fushimi, X. Zheng, J.T. Gleaves, G.S. Yablonsky, A. Gaffney, M. Clark, S. Han, Techniques for Fabricating Nanoscale Catalytic Circuits, *Topics in Catalysis* 49 (2008) 167-177.
- R. Feres. G.S. Yablonsky, A. Mueller, A. Baerstein, X. Zheng, J.T. Gleaves, Probabilistic Analysis of Transport-Reaction Processes over Catalytic Particles: Theory and Experimental Testing, *Chemical Engineering Science* 64 (2009) 568-581.
- J.T. Gleaves, G. Yablonsky, X. Zheng, R. Fushimi, P.L. Mills, Temporal Analysis of Products (TAP) – Recent Advances in Technology for Kinetic Analysis of Multicomponent Catalysts, accepted for publication in *Journal of Molecular Catalysis: A Chemical* (2009) Available Online.

August 2009

**Short Title: Bridging the Catalyst Gap using TAP,**

**Zheng, Ph.D. 2009**